

REMOTE INFRARED SPECTROSCOPY DETECTION OF HIGHLY ENERGETIC MATERIALS

by
John R. Castro Suarez

A dissertation submitted in partial fulfillment of the requirements for the degree of

DOCTOR OF PHILOSOPHY
in
Applied Chemistry

UNIVERSITY OF PUERTO RICO
MAYAGUEZ CAMPUS
December 2015

Approved by:

_____	_____
Samuel P. Hernández-Rivera, Ph.D. President, Graduate Committee	Date
_____	_____
Julio G. Briano-Peralta, Ph.D. Member, Graduate Committee	Date
_____	_____
Nairmen Mina-Camilde, Ph.D. Member, Graduate Committee	Date
_____	_____
Carmen A. Vega-Olivencia, Ph.D. Member, Graduate Committee	Date
_____	_____
Madeline Torres-Lugo, Ph.D. Representative, Graduate Studies	Date
_____	_____
Aidalú Joubert-Castro, Ph.D. Chairperson of the Department	Date

ABSTRACT

The detection, identification, and quantification of threat chemical substances such as high energetic materials (HEM), abuse drugs, and related compounds is a subject that has become a heightened priority in recent years for homeland security, counter-terrorism, and drug dealing prevention applications. Law-enforcement and forensic agencies have interest in promoting research and development for efficient sensing systems than help to detect explosives and abuse drugs at public places, such as airports, maritime, and railway or coach stations. This way terrorist threats and illegal drugs traffic can be minimized or prevented in most cases.

This scientific contribution describes a series of investigations aimed at improving detection capabilities of most used HEM (TNT, PETN, RDX and TATP) present as contamination residues on ideal surfaces (metallic), no-ideal surfaces (wood, baggage and cardboard), and in soil and ambient air. IR vibrational analytical methods were used for identification and classification of HEM, with the assistance of multivariate analyses such as PCA, PLS, and PLS-DA. In addition, synthetic cannabinoids present on vegetable mixes were studied using GC-MS. The contribution specifically deals with:

1. A quantum cascade laser spectrometer used to obtain reflectance spectra of highly energetic materials (HEMs) deposited on non-ideal, low reflectivity substrates such as travel bags (black polyester), cardboard and wood. HEMs used were the nitroaromatic explosive 2,4,6-trinitrotoluene (TNT), the aliphatic nitrate ester pentaerythritol tetranitrate (PETN), and the aliphatic nitramine 1,3,5-trinitroperhydro-1,3,5-triazine (RDX). Chemometrics algorithms were applied to

analyze the recorded spectra. The results demonstrate that the infrared vibrational method described in this study is well suited for rapid screening analysis of HEMs on low reflectivity substrates.

2. The presence of the nitroaromatic HEM 2,4-dinitrotoluene (2,4-DNT) and the cyclic organic peroxide triacetone triperoxide (TATP) in air was detected by chemometrics enhanced vibrational spectroscopy. Several infrared experimental setups were tested using traditional heated sources (Globar), modulated and non-modulated FT-IR and quantum cascade laser (QCL)-based dispersive IR spectroscopy. The QCL based methodology exhibited a better capacity for the discrimination for the detected presence of HEM in air compared to other methodologies.
3. Detection of explosives, such as TNT, 2,4-DNT and PETN and present in soils and other real world complex media using thin layer chromatographic coupled to mid infrared spectroscopy using QCL sources was accomplished. This allows rapid, reproducible, separation and identification of explosives in the field in short time. The results show that TLC-QCL is a useful new tool for separation, identification, and quantification of trace concentrations of explosives as low as 0.39 μg (390 ng)
4. Two remote detection systems were assembled using an infrared telescope coupled to an Open Path Fourier Transform infrared spectrometer (OP/FT-IR), a cryo-cooled MCT detector, and a telescope-coupled mid-infrared (MIR) excitation source. Samples of 2,4,6-trinitrotoluene (TNT) and pentaerythritol tetranitrate (PETN) deposited on aluminum plates were detected at several source-target distances. The effect of the collection angle of the returned IR beams on the signal

to noise ratio (S/N) and vibrational band intensities were evaluated. Partial least squares regression analysis was applied to the obtained spectra. Overall, remote MIR detection in active mode was useful for quantifying HEM deposited on the aluminum plates with high confidence level. Source-target distances were in the range of 1-25 m.

5. Three analytical methods based on a gas chromatography coupled to a mass spectrometer (GC-MS) were developed and tested for abuse-drugs standards of synthetic cannabinoids (SC), THC, cocaine, and heroin. Analytical procedures for extracting synthetic cannabinoids from herbal mixes were implemented. Gas chromatography was used for separation and purification of SC. Electron impact MS was utilized as confirmatory method to identify the SC on the herbal sample. Two SC were found in real-world samples. The results show that the analytical methods developed can be useful to identify SC rarely used such as PB-22 and 5F-PB-22 when these are present in herbal mixtures.

RESUMEN

La detección, identificación y cuantificación de sustancias químicas peligrosas como materiales altamente energéticos (HEM, por sus siglas en inglés), drogas de abuso y compuestos relacionados es un tema que se ha convertido en una prioridad en los últimos años para aplicaciones en seguridad nacional, la lucha contra el terrorismo y la lucha contra el tráfico de drogas. Las agencias gubernamentales de ley y forenses tienen interés en promover la investigación y el desarrollo de sistemas de detección eficientes que ayuden a detectar explosivos y drogas de abuso en lugares públicos, como aeropuertos, terminales marítimos, y estaciones de ferrocarril o de autobuses. De tal manera que los daños y el tráfico ilegal puedan minimizarse o evitarse en el mejor de los casos.

Esta contribución científica describe una serie de investigaciones encaminadas a mejorar la detección de HEM más utilizados: TNT, PETN, RDX, y TATP, presentes en superficies ideales (metal), superficies no ideales (madera, maleta y cartón), aire y suelos. Métodos analíticos vibracionales infrarrojo se utilizaron para la identificación y clasificación de HEM, con la ayuda de análisis multivariado tal como PCA, PLS, y PLS-DA. Además, cannabinoides sintéticos presentes en mezclas vegetales se estudiaron utilizando cromatografía de gases acoplada a espectrometría de masas (GC-MS). La contribución en concreto se trata de:

1. Un espectrómetro Infrarrojo con láser de cascada cuántica (QCL) se utilizó para obtener espectros de reflectancia de HEM depositados sobre sustratos no ideales de baja reflectividad, tales como maletas de viaje (poliéster negro), cartón, y

madera. HEM utilizados fueron el explosivo nitroaromático 2,4,6-trinitrotolueno (TNT), éster de nitrato alifático pentaeritritol tetranitrato (PETN), y la nitramina alifática 1,3,5-trinitroperhydro-1,3,5-triazina (RDX). Algoritmos quimiométricos se utilizaron para analizar los espectros IR. Los resultados demuestran que el método vibracional infrarrojo descrito en este estudio es muy adecuado para el análisis rápido de HEM depositados en superficies de baja reflectividad.

2. La presencia del HEM nitroaromático 2,4-dinitrotolueno (2,4-DNT) y peróxido cíclico orgánico triperóxido triacetona (TATP) en aire se detectó por espectroscopia vibracional realizada por quimiometría. Se probaron varios montajes experimentales infrarrojos utilizando fuentes IR tradicionales (globo), FT-IR modulada y no modulada y espectroscopia IR dispersivo basado QCL. La metodología basada en QCL exhibió una mejor capacidad para la discriminación de la presencia de HEM en aire, en comparación con otras metodologías.
3. Se llevó a cabo la detección de explosivos tales como TNT, 2,4-DNT, y PETN presentes en suelos y otras matrices complejas del mundo real, usando cromatografía de capa fina (TLC, por sus siglas en inglés) acoplada a espectroscopia infrarroja de QCL. Esto permitió una rápida, reproducible, separación e identificación de explosivos en el campo real en corto tiempo. Los resultados muestran que TLC-QCL es una herramienta útil para detectar concentraciones trazas de explosivos tan bajas como 0.39 μg (390 ng).
4. Se ensamblaron dos sistemas de detección a distancia utilizando telescopios de infrarrojo acoplados a un espectrómetro de infrarrojo de transformada de Fourier de paso libre, un detector MCT crio-enfriado y una fuente infrarrojo medio

acoplada a un telescopio. Se detectó muestras de 2,4,6-trinitrotolueno (TNT) y tetranitrato de pentaeritritol (PETN) depositadas sobre láminas de aluminio a varias distancias fuente-blanco. Se evaluó el efecto del ángulo de colección de la luz IR retornante en la intensidad de banda vibracional detectada y la relación del cociente señal a ruido (S/N). Se aplicó análisis de regresión de cuadrados mínimos parciales (PLS) a los espectros obtenidos. En general, la detección a distancia en modo activo fue útil para la cuantificación de HEM depositados sobre láminas de aluminio con un alto nivel de confianza hasta distancias de 1-25 m.

5. Se desarrolló tres métodos analíticos usando GC-MS y se ensayaron utilizando estándares de drogas de abuso como cannabinoides sintéticos (SC), THC, cocaína, y heroína. Se implantaron procedimientos analíticos para la extracción de SC en mezclas vegetales. Se utilizó GC para la separación y purificación de SC. Además, se utilizó espectrometría de masa de impacto con electrones como método de confirmación para identificar los SC en las muestras a base de hierbas. Se encontró dos SC en las muestras del mundo real. Los resultados demuestran que los métodos analíticos desarrollados pueden ser útiles para identificar SC raramente utilizados como PB-22 y 5F-PB-22, cuando están presentes en la mezcla vegetal.

Dedicated to:

God,

My wife Vanessa, my future sons

My parents Betty and Ricardo

My sisters Elena and Monica

© Copyright 2015

John R. Castro Suarez

All rights reserved

This dissertation contains portions that have been published in Advances in Optical Technologies, in the Proceedings of SPIE Defense, Security, and Sensing (proceedings.spiedigitallibrary.org), InTech Open, and in Applied Spectroscopy.

ACKNOWLEDGEMENTS

First, thanks to GOD and My Family.

Thanks to: Dr. Samuel P. Hernández-Rivera for his guidance, his wisdom, and for giving me the opportunity to be part of his excellent research team.

To the University of Puerto Rico-Mayaguez for giving me the opportunity to pursue my graduate studies.

To my lab-partners and the graduate committee for their help and important feedbacks.

To my graduate committee for unconditional support in the research and dissertation.

The U.S. Department of Defense supported this contribution, agreement number: W911NF-11-1-0152. The authors would also like to acknowledge contributions from Dr. Richard T. Hammond of the U.S. Army Research Office, DOD.

The Defense Threat Reduction Agency (DTRA), DOD under grant #DODRIF11-DTRA020-P-0017, also supported the contribution: “IED Sentry Based on Mid-Infrared Laser Arrays” awarded to Eos Photonics, Cambridge, MA. Contributions by Dr. Mark Witinski are also gratefully acknowledged.

Support from the U.S. Department of Homeland Security under Award Number 2013-ST-061-ED0001 is also acknowledged. However, the views and conclusions contained in this document are those of the authors and should not be considered as a representation of the official policies, either expressed or implied, of the U.S. Department of Homeland Security.

I. TABLE OF CONTENTS

II. LIST OF TABLES	xiv
III. LIST OF FIGURES	xv
IV. CHAPTER I BASICS CONCEPTS	1
1.1 INFRARED SPECTROSCOPY	1
1.1.1 Characteristics of infrared spectroscopy	3
1.2 CHEMOMETRICS IN VIBRATIONAL SPECTRAL ANALYSIS	4
1.2 REFERENCES	9
V. CHAPTER II DETECTION OF HIGHLY ENERGETIC MATERIALS ON NON-REFLECTIVE SUBSTRATES USING QUANTUM CASCADE LASER SPECTROSCOPY	11
OVERVIEW	11
2.1 INTRODUCTION	12
2.2 MATERIALS AND METHODS	15
2.2.1 Reagents and Materials	15
2.2.2 Sample preparation	16
2.2.3 Setup	17
2.3 RESULTS	20
2.3.1 Spectral analysis	20
2.3.2 Concentration Profiles and Difference Spectra Identification	24
2.3.3 Target Identification	25
2.3.4 Quantification of HEMs Using PLS Regressions	39
2.4 CONCLUSIONS	41
2.5 ACKNOWLEDGEMENTS	42
2.6 REFERENCES	43
VI. CHAPTER III DETECTION OF NITROAROMATIC AND PEROXIDE EXPLOSIVES IN AIR USING INFRARED SPECTROSCOPY: QCLS AND FT-IR	49
OVERVIEW	49
3.1 INTRODUCTION	50
3.2 EXPERIMENTAL SETUP	53
3.2.1 Materials	53
3.2.2 Synthesis of TATP	53

3.2.3	Instrumentation	54
3.3	MEASUREMENTS AND ANALYSES	55
3.3.1	Experiment	55
3.3.2	Partial Least Squares (PLS) – Discriminant Analysis (DA)	56
3.4	RESULTS AND DISCUSSION	57
3.4.1	Proof of presence of 2,4-DNT and TATP in air at trace levels	62
3.4.2	Limits of Detection	64
3.5	CONCLUSIONS	65
3.6	ACKNOWLEDGMENTS	65
3.7	REFERENCES	66
VII.	CHAPTER IV SEPARATION, IDENTIFICATION AND QUANTIFICATION OF EXPLOSIVES USING THIN LAYER CHROMATOGRAPHY COUPLED TO QUANTUM CASCADE LASER SPECTROSCOPY	70
	OVERVIEW	70
4.1	INTRODUCTION	71
4.2	EXPERIMENTAL	76
4.2.1	Materials and reagents	76
4.2.2	Sample Preparation: TLC	77
4.2.3	Experimental Setup	78
4.3	RESULTS AND DISCUSSION	79
4.3.1	Preparation of ZrO ₂ TLC	79
4.3.2	TLC: TNT and PETN.....	80
4.3.3	Spectral profiles of high explosives on various stationary phase	81
4.3.4	TNT quantification profiles using TLC	85
4.4	CONCLUSIONS	86
4.5	ACKNOWLEDGEMENTS	87
4.6	REFERENCES	87
VIII.	CHAPTER V ACTIVE MODE REMOTE INFRARED SPECTROSCOPY DETECTION OF TRINITROTOLUENE AND PENTAERYTHRITOL TETRANITRATE ON ALUMINUM SUBSTRATES	93
	OVERVIEW	93
5.1	INTRODUCTION	94
5.2	EXPERIMENTAL	97

5.2.1	Reagents	97
5.2.2	Sample Preparation	97
5.2.3	Experimental Setup	98
5.3	RESULTS AND DISCUSSION	100
5.3.1	HEM Standoff Detection	100
5.3.2	HEM Quantification using PLS Regression	108
5.4	CONCLUSIONS	113
5.5	ACKNOWLEDGMENTS	114
5.6	REFERENCES	114
IX.	CHAPTER VI DEVELOPMENT OF GC-MS ANALYSIS METHODS FOR EMERGENT GROUPS OF SYNTHETIC CANNABINOIDS FOUND IN VEGETATIVE SAMPLES	119
	OVERVIEW	119
6.1	INTRODUCTION	119
6.2	MATERIALS AND METHODS	125
6.2.1	Reagents and materials	125
6.2.2	Sample preparation	128
6.2.3	GC-MS Analysis	129
6.3	RESULTS AND DISCUSSION	130
6.3.1	GC-MS Method Development	130
6.3.2	Vegetal samples analyses using GC-MS	134
6.4	CONCLUSIONS	143
6.5	FUTURE WORK	144
6.6	REFERENCES	144

II. LIST OF TABLES

Table 2-1. Values of spectral correlation coefficients (HQI) for spectra of HEM deposited on various substrates.....	29
Table 2-2. Summary of results of PLS-DA of QCLS spectra of HEMs on surfaces obtained for calibration, cross validation (10 groups split in venetian blinds) and prediction set.....	33
Table 2-3. Statistical parameters of PLS calibration models for spectra of HEM deposited on non-ideal, low reflectivity substrates using QCLS. Spectral range: 1000-1600 cm^{-1}	41
Table 3-1. Validation parameters for the various models constructed.	59
Table 3-2. Validation parameters for models in the sub-spectral range: 850-1400 cm^{-1} ..	61
Table 3-3. Mass of 2,4-DNT determined by GC- μ ECD for 2 mL of injected gas.....	63
Table 4-1. R _f values of TNT and PENT mixture on different solvent systems.	80
Table 5-1. PLS calibration parameters for the different analyzed standoff distance. ..	111
Table 5-2. PLS calibration parameters for the different analyzed angle of collection..	111
Table 6-1. Chemical structures and IUPAC name of abuse drugs used.....	127
Table 6-2. GC-MS methods parameter used for analysis of SC present in blend vegetal.....	129
Table 6-3. Retention time for SC standards and other drugs standards using analytical methods show in Table 6-2	131

III. LIST OF FIGURES

Figure 1-1. Simplified scheme for a PCA analysis.....	5
Figure 1-2. Simplified scheme for a PLS transformation.	8
Figure 2-1. Experimental setup. (a) Sample preparation: HEM samples deposited on substrates. (b) In situ QCL spectral measurements. (c) Multivariate statistical analyses.	19
Figure 2-2. QCL spectra of HEM on substrates: (a) Al, (b) CB, (c) wood and (d) TB. Surface concentrations were 15 $\mu\text{g}/\text{cm}^2$. QCL spectra of substrates are included to establish the degree of spectral interference.....	21
Figure 2-3. Comparison of MIR spectra of 2,6-DNT/NaF pellets: (a) QCL and %T FT-IR spectra for thin 2,6-DNT(5%)/NaF pellet; (b) QCL and FT-IR spectra for thick 2,6-DNT(10%)/NaF pellet.	23
Figure 2-4. Surface concentration profiles for. (a) RDX on wood; (b) TNT on CB and (c) PETN on wood; (d) difference spectrum: PETN/CB minus CB and comparison with QCL transmittance spectrum PETN/Al (used as reference).....	25
Figure 5-5. Representation of multivariate analysis (PLS-DA) on spectral data used in this research to identify and classify HEMs deposited on non-ideal, non-reflective substrates.....	30
Figure 2-6. PLS-DA model for discrimination of HEM on TB: (a) class prediction for PETN; (b) class prediction for RDX; (c) class prediction for TNT; (d) scores plot of LV2 vs. LV1 for detection of PETN, RDX and TNT on TB. Preprocessing steps applied were: 1st derive. (15 pt.) and MC. Threshold for discrimination and 95% confidence level for clustering are represented with red dotted lines.	34
Figure 2-7. PLS-DA model for QCL spectra of PETN, RDX, and TNT deposited on TB, CB, and wood substrates. Preprocessing steps applied were 2nd deriv. (17 pts.) + SNV + MC: (a) 2D-Score plot using LV1 and LV2; (b) 3D-Score plot using LV1, LV2 and LV3. 95% confidence level for clustering is represented with red dotted line.	37
Figure 2-8. PLS regression plots of predicted vs. measured surface concentrations for HEM deposited on substrates. (a) RDX on TB, (b) TNT on CB and (c) PETN on wood. Spectral range used: 1000-1600 cm^{-1}	40

Figure 3-1. Schematic diagram of the experimental setup. (a). FT-IR instrument using modulated light source. (b). Open path FT-IR. (c). Quantum cascade scan.	56
Figure 3-2. (a). Histogram for discrimination using modulated source FT-IR. (b). Histogram for discrimination using non-modulated source FT-IR. (c). Histogram for discrimination using QCL.	58
Figure 3-3. (a). First loadings for TATP models for the region (873-1400 cm^{-1}). (b). First loadings for DNT models for the region (873-1400 cm^{-1}). Reference gas phase spectra included.....	62
Figure 3-4. Low pressure spectra in the gas phase with baseline correction of: (a) TATP; (b) DNT.	64
Figure 4-1. Experimental setup: (a) sample preparation, extraction, and separation from matrices; (b) in situ QCLS spectral measurements; (c) spectroscopic analysis.	79
Figure 4-2. Preparation of ZrO_2 TLC using different solvents.	79
Figure 4-3. (a) Spectra from different stationary phases (BaF_2 , CaF_2 , ZrO_2 and silica gel) used to TLC. (b) Spectra of DNT and PETN on silica gel-TLC.....	82
Figure 4-4. Explosives spectra on Silica Gel-TLC. (a) 2,4 DNT spectrum, (b) TNT spectrum. Silica gel was used as background.....	83
Figure 4-5. Explosives spectra on ZrO_2 -TLC. Baseline correction was applied to each spectrum.	84
Figure 4-6. Explosive spectra on CaF_2 -TLC. Baseline correction was applied to each spectrum.	85
Figure 4-7. TNT spectra in different concentrations on silica gel-TLC. Baseline correction and smoothing (25 pt.) was applied to each spectrum.	86
Figure 5-1. FT-IR interferometer configuration; (a) active mode setup for standoff measurements using reflective telescope: 1. IR source; 2. Al plate. (b) Plate mount; 3. Tilting mount. (c) Active mode setup for standoff measurements using refractive telescope.....	98
Figure 5-2. Ratio signal to noise (P-P; principal “y” axis) at various distances for active mode. IR beam spot size (secondary “y” axis) vs. range. Noise levels were measured at 830-870 cm^{-1} and peak heights were measured for signal at 790 cm^{-1}	102

Figure 5-3. (a) Active mode standoff FT-IR spectra of TNT deposited on an Al plate measured at several distances: 8, 20, 30 m and surface concentrations: 400 $\mu\text{g}/\text{cm}^2$ and 50 $\mu\text{g}/\text{cm}^2$; (b) active mode standoff FT-IR spectra of PETN deposited on an Al plate and black painted Al measured at 4 m. 104

Figure 5-4. Vibrational bands intensity and S/N in different angle of collection for PETN (200 $\mu\text{g}/\text{cm}^2$)..... 106

Figure 5-5. (a) Predicted vs. true coverage for TNT explosives on Al plates at different standoff distances: 20 m and 25 m. (b) Predicted vs. true coverage for PETN explosives on Al plates at different angle of collection: 1° and 60°. 110

Figure 5-6. (a) Regression coefficient and loading plot for PLS model of detection of TNT explosives on Al plates at a remote distance 8 m; (b) Regression coefficient and loading plot for PLS model of detection of PETN explosives on Al plates at 1 m standoff distance and angle of collection 1°. 113

Figure 6-1. Experimental Setup for extraction and instrumental analysis of SCs present in vegetal blend. 128

Figure 6-2. Chromatograms using method 1. 132

Figure 6-3. Chromatograms using method 2 described in Table 6-2..... 133

Figure 6-4. Chromatograms using method 3. 134

Figure 6-5. Mass spectra of THC, heroin, cocaine, and JHW-018 standards using method 1. 137

Figure 6-6. Mass Spectra of AM-2201, CP-47,797, XLR-11, MDPV and WIN55,212-2 standards using method 1.. 138

Figure 6-7. MS spectra and GC chromatograms from extract of Sample #1 using method 1. (a) Chromatogram of acetone extract; (b) chromatogram of dichloromethane extract; c) mass spectrum of peak with $R_t = 8.04$ min. 139

Figure 6-8. MS spectrum and GC Chromatograms from extract of sample #1 method 2. a) Chromatogram of acetone extract; (b) mass spectrum of peak with $R_t = 6.98$ min. 140

Figure 6-9. GC Chromatograms from extract of Samples 1 and 2 using method 3. Sample # 1: (a) methanol extract; (b) acetone extract. Sample # 2: (c) methanol extract; (d) acetone extract. 141

Figure 6-10. MS spectrum of SCs present in extracts of Samples 1 and 2 using analytical method 3. (a) Mass spectrum of characteristic peak with $R_t = 6.32$ min shown in Figures 6-9a to 6-9d; (b) Mass spectrum of characteristic peak with $R_t = 7.15$ min shown in Figure 6-9c to 6-9d..... 142

IV. CHAPTER 1

BASICS CONCEPTS

1.1 INFRARED SPECTROSCOPY

When irradiated with infrared light, a molecule absorbs it under certain well-established conditions. The energy of the light quantum or photon ($h\nu$) of the absorbed infrared light is equal to an energy difference between a certain energy level of vibration of the molecule (having an energy E_m) and another energy level of vibration of the molecule (having an energy E_n). In the form of an equation:

$$E_n - E_m = h\nu \quad (1)$$

In other words, absorption of infrared light occurs principally based on a transition between the vibrational energy levels of the molecule. This is why an infrared absorption spectrum is a vibrational spectrum of the molecule.

Satisfying Eq. (1) does not always cause infrared absorption. Transitions are permitted by a *selection rule* (i.e., *allowed transitions*) and others are not allowed by the same rule (i.e., *forbidden transitions*). The principal selection rule with respect to infrared absorption vibrational spectroscopy is based on the symmetry of the vibrational states of the molecule. This selection rule specifies that infrared energy may be absorbed when the electric dipole moment of a molecule changes as a function of the internuclear distance of the two atom bonded that participate in the vibration. The second selection rule states that transitions occur with a change in the vibrational quantum number $\Delta v = \pm 1$.

The two selection rules are developed from quantum-mechanical considerations. According to quantum mechanics, for a molecule to transition from a certain state m to another state n by absorbing or emitting infrared light, it is necessary that the following definite integral:

$$(\mu_x)_{mn} = \int_{-\infty}^{\infty} \Psi_n \mu_x \Psi_m dq \quad (2)$$

or at least one of (μ_y) and (μ_z) which are expressed by a similar equation is not 0, where μ_x denotes an x -component of the electric dipole moment; Ψ denotes the eigenfunction of the molecule in its vibrational state; and Q denotes a *normal coordinate* (i.e., a normal mode of vibration) expressed as a single coordinate.

Considering only (μ_y) , a distribution of electrons in the ground state changes as the coordinate expressing a vibration changes, therefore, the electric dipole moment is a function of the normal coordinate q . Hence, μ_x can be expanded as follows:

$$\mu_x = (\mu_x)_0 + (\partial\mu_x/\partial q)_0 q + \frac{1}{2}(\partial^2\mu_x/\partial Qq^2)_0 Qq^2 + \dots \quad (3)$$

Expressed by a displacement of atoms during the vibration, q has a small value. This allows to omit q^2 and the subsequent terms in the equation above. Substituting the terms up to q of Eq. (3) in Eq. (2)

$$(\mu_x)_{mn} = (\mu_x)_0 \int \Psi_n \Psi_m dq + (\partial\mu_x/\partial q)_0 \int \Psi_n q \Psi_m dq \quad (4)$$

is obtained. Due to the orthogonality of the eigenfunction, the first term of this equation is zero except when $m = n$ holds. The first term denotes the magnitude of the permanent dipole of the molecule. For the second term to have a value other than zero, both $(\partial\mu_x/\partial q)_0 \neq 0$ and $\int \Psi_n q \Psi_m dq \neq 0$ must be satisfied. These two conditions lead to the two selection rules. The nature of the eigenfunction permits the integral to have a value other than zero only when $n = m \pm 1$ holds. Considering q^2 and the subsequent terms of

Eq. (3) as well, it can be proven that even when $n = m \pm 1$ fails to hold, $(\mu_x)_{mn}$ has a value, even though small, other than zero. The second selection rule regarding infrared absorption is thus proved. The other selection rule, which is based upon the symmetry of a molecule, is obtained from $(\partial\mu_x/\partial q)_0 \neq 0$. The relationship $(\partial\mu_x/\partial q)_0 \neq 0$ indicates that infrared absorption occurs only when certain vibration changes the electric dipole moment. The vibration is *infrared active* when $(\partial\mu_x/\partial q)_0 \neq 0$ holds, but is *infrared inactive* when $(\partial\mu_x/\partial q)_0 = 0$ holds.

Since most molecules are in the *ground vibrational state* at room temperature, a transition from the state $v'' = 0$ to the state $v' = 1$ (first excited state) is possible. Absorption corresponding to this transition is called *the fundamental transition*. Although most bands that are observed in infrared absorption spectra arise from fundamental transitions, in some cases one can find bands which correspond to transitions from the state $v'' = 0$ to the state $v' = 2, 3, 4 \dots$ (i.e., *overtone* transitions). However, overtone bands are weak based on the Boltzmann distribution of energy states of a molecule. [1-5]

1.1.1 Characteristics of infrared spectroscopy

Infrared spectroscopy provides detailed information about the vibrations of a molecule. Since molecular vibrations readily reflect chemical features of a molecule, such as an arrangement of nuclei and chemical bonds within the molecule, infrared spectroscopy contributes considerably not only to identification of the molecule but also to study of the molecular structure. Furthermore, an interaction with a surrounding environment also causes a change in molecule vibrations, and hence, infrared spectroscopy is useful in studying the interaction too. Infrared spectroscopy has many uses from basic research to

numerous applications. Why is infrared spectroscopy useful? The answer is simple: it is spectroscopy that probes the vibrations of a functional group. Infrared spectroscopy can be used not only for the identification of a functional group, but also for the investigation of the chemical bond and environment of the functional group. For example, groups of C=O, -C=C-C=O, and -CH₂-CH₂-C=O give rise to different frequencies. Of course, a -C=O group and -C=O...H-O- also yield different frequencies. The specific characteristics of infrared spectroscopy can be summarized as follows:

1. Using an electromagnetic wave of low energy, such as in infrared spectroscopy (IRS), rarely damages a sample. Thus, IRS may be used for non-destructive analysis of a sample.
2. IRS is applicable to samples in various physical states, e.g., solids, crystals, films, liquids, solutions, and gases and vapors. Furthermore, measurements of infrared spectra of a sample in a solution and in its solid state, allows comparing its structure in the solution with respect to that of the solid.
3. IRS includes IR absorption, but also IR reflection, emission, photoacoustic, and other types of spectroscopies as well.
4. Connection with an optical microscope, a gas chromatograph, a liquid chromatograph, or other instruments is relatively easy. This allows doing hyphenated analysis. [6-8]

1.2 CHEMOMETRICS IN VIBRATIONAL SPECTRAL ANALYSIS

The automation and computerization of laboratories have been carried out with various important consequences. One of them is the rapid acquisition of large amounts of data.

However, it is well known that acquiring such a large amount of data is far from providing appropriate answers quicker. Obtaining vibrational spectroscopy multivariate data is not synonymous with possessing vibrational information. The latter must be interpreted and placed in context to convert it into useful information for the user. Chemometrics is the field of chemistry that provides the user with the required tools to enable that capability. A great deal of chemometrics tools have been developed and tested. However, the most used of these tools to identify, quantify, and classify data sets are those that make use of principal components analysis (PCA), partial least squares (PLS), discriminant analysis (DA), and their combined usage: PLS-DA and hierarchical cluster analysis (HCA). PCA transforms a set of variables into fewer variables (called factors, rank, dimensions, principal components, or components) which contain most of the information (variance) of the initial data set [9-12].

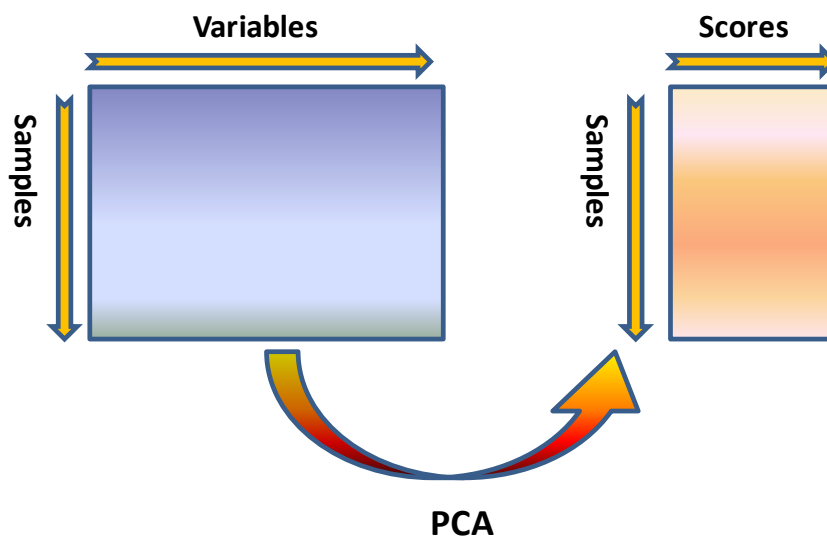


Figure 1-1. Simplified scheme for a PCA analysis.

The PCA algorithm seeks to save the information from a large number of variables in a

small number of uncorrelated components, with minimal loss of information. The main reasons for performing PCA are reduction of the number of variables to fewer dimensions that contain as much information as possible and to have uncorrelated dimensions (used to avoid multi-collinearity in multiple regressions, among other things). An important method for qualitative analysis of spectral data is principal component analysis. PCA is a method for the investigation of the variation within a multivariable data set. The first step in PCA is to subtract the average value or spectrum from the entire data set, this is called mean centering. The largest source of variation in the data set is called principal component # 1 (PC-1). The second largest source of variation in the data, which is independent of PC-1, is called PC-2. Principal components form a set of orthogonal vectors. For each one of the data points, the projection of the data point onto the P1 or P2 vector is called a score value. Plots of sample score values for different principal components, typically P1 versus P2 are called score plots. Score plots provide important information about how different samples are related to each other. Principal component plots, also called loading plots, provide information about how different variables are related to each other. In practical cases, PCA uses a single X matrix, which is represented by the infrared spectra. PCA is a purely qualitative analysis (does not give a quantitative value that establishes how different are a spectral dataset) to visualize if there is variability between a set of infrared spectra. PCA can thus also be used to detect the presence of outliers. Figure 1-8 shows a simplified scheme for a PCA [9-10].

Partial least squares (PLS) regression is a quantitative spectral decomposition technique that is closely related to PCA regression. The importance of PLS is that it is used to design and build robust calibration models for multivariate quantitative analysis. PLS actually

uses the concentration information during the decomposition process. This causes spectra containing higher constituent concentrations to be weighted heavier than those with lower concentrations. The main idea of PLS is to get as much concentration information as possible into the first few loading vectors (number of component, factors, ranks or principal components). PLS regression consists of two fundamental steps. The first step is to transform the **X** predictive matrix (spectra) of order $n \times p$ (n = number of samples and p = number of variables: cm^{-1} or nm), into a matrix of components or latent variables uncorrelated, **T** = (T_1, \dots, T_p) of order $n \times p$, called PLS components. Using the **Y** response vector (concentrations) of order $n \times 1$ contrasts with the principal component analysis in which the components are obtained using only the **X** predictive matrix. The second step is to calculate the estimated regression model using the **Y** response original vector as predictive, PLS components. The dimensionality reduction can be applied directly on the components, as they are orthogonal. The number of components required for the regression analysis must be much smaller than the number of predictors. There is a number of ways of expressing these, a convenient one being (equations 9 and 10) [12]:

$$\mathbf{X} = \mathbf{T} \cdot \mathbf{P} + \mathbf{E} \quad (9)$$

$$\mathbf{c} = \mathbf{T} \cdot \mathbf{q} + \mathbf{f} \quad (10)$$

Figure 1-8 illustrates a simplified scheme for PLS: **X** represents the experimental measurements (e.g. spectra) and **c** (or **Y**) the concentrations. The first equation above appears similar to that of PCA, but the scores matrix also models the concentrations, and the vector **q** has some analogy to a loadings vector. The matrix **T** is common to both equations. **E** is an error matrix for the **X** block and **f** an error vector for the **C** block. The scores are orthogonal, but the loadings (**P**) are not orthogonal, unlike in PCA, and usually

they are not normalized.

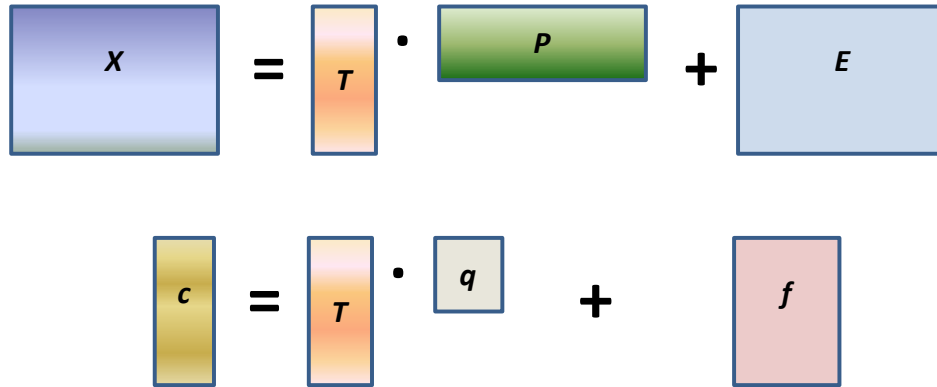


Figure 1-2. Simplified scheme for a PLS transformation.

Various preprocessing methods such as vector normalization (VN), mean centering (MC), auto scaling (AS), multiple scattering correction (MSC), standard normal variate (SNV), and first and second derivatives have been developed to improve a good multivariate quantification. The performance of the final PLS and DA-PLS models are evaluated according to the root mean square error of cross-validation (RMSECV), a leave-one-sample-out cross-validation method and the predictive ability of models were assessed by the root mean square error of prediction (RMSEP) and the correlation coefficient (R) in prediction set. In general, for PLS models the values of RMSECV can be calculated as follows:

$$RMSECV = \sqrt{\frac{\sum_{i=1}^{n_{cal}} (c_p - c_i)^2}{n_{cal}}} \quad (3)$$

Where c_i and c_p are the experimental and predicted concentration, respectively, of the i^{th} calibration sample when situated in a left out segment, n_{cal} is the number of calibration samples in the training set. The number of PLS components included in the model is

selected according to the lowest RMSECV. This procedure is repeated for each of the preprocessed spectra. For the test set, the root mean square error of prediction (RMSEP) is calculated as follows:

$$RMSEP = \sqrt{\frac{\sum_{i=1}^{n_{test}} (c_i - c_p)^2}{n_{test}}} \quad (4)$$

The best model with the overall lowest RMSECV will be selected as final model. Correlation coefficients between the predicted and the true concentration are calculated for both the calibration and the test set, which are calculated as follows Equation 11, where \bar{c}_i is the mean of the experimental measurement results for all samples in the train and test sets.

$$R = \sqrt{1 - \frac{\sum_{i=1}^n (c_p - c_i)^2}{\sum_{i=1}^n (c_i - \bar{c}_i)^2}} \quad (11)$$

1.2 REFERENCES

- [1] B. C. Smith, *Fundamentals of Fourier Transform Infrared Spectroscopy*, 2011. CRC Press, Boca Raton, Florida. 2nd Edition.
- [2] P. Griffiths, J. de Haseth, *Fourier Transform Infrared Spectrometry*, 2007. Wiley, New York, New York. 2nd Edition.
- [3] J. M. Hollas, *Modern Spectroscopy*, 1996. Wiley, New York, New York, 3rd Edition.
- [4] B. C. Smith, *Quantitative Spectroscopy: Theory and Practice*, 2002. Academic Press, Boston, Massachusetts.
- [5] B. C. Smith, *Infrared Spectral Interpretation: A Systematic Approach*, 1999. CRC Press, Boca Raton, Florida.

- [6] N. Colthup, L. Daly and S. Wiberley, *Introduction to Infrared and Raman Spectroscopy*, 1990. Academic Press, Boston, Massachusetts.
- [7] D. Lin-Vien, N. Colthup, W. Fateley and J. Graselli, *The Handbook of Infrared and Raman Characteristic Frequencies of Organic Molecules*, 1991. Academic Press, Boston, Massachusetts.
- [8] G. Socrates, *Infrared and Raman Characteristic Group Frequencies: Tables and Charts*, 2001. John Wiley, Boston, Massachusetts.
- [9] K. R. Beebe, R. J. Pell and M. B. Seasholtz, *Chemometrics: A Practical Guide*, 1998. John Wiley & Sons, New York, NY.
- [10] R.G. Brereton, *Applied Chemometrics for Scientists*, 2007. The Atrium, Southern Gate, John Wiley & Sons Ltd. Chichester.
- [11] D. L. Massart, B. G. M. Vandeginste and L. M. C. Buydens, *Data Handling in Science and Technology Handbook of Chemometrics and Qualimetrics Part B*, 1997. The Netherlands: Elsevier Science B.V.
- [12] D. L. Massart, B. G. M. Vandeginste and L. M. C. Buydens L, *Handling in Science and Technology Handbook of Chemometrics and Qualimetrics Part A*, 1997. The Netherlands: Elsevier Science, B.V.

V. CHAPTER 2

DETECTION OF HIGHLY ENERGETIC MATERIALS ON NON-REFLECTIVE SUBSTRATES USING QUANTUM CASCADE LASER SPECTROSCOPY

OVERVIEW

A quantum cascade laser spectrometer was used to obtain reflectance spectra of highly energetic materials (HEMs). These were deposited on non-ideal, low reflectivity substrates such as travel bags (polyester), cardboard and wood. Various deposition methods were used to prepare the standards and samples used in the study. HEMs used were the nitroaromatic explosive 2,4,6-trinitrotoluene (TNT), the aliphatic nitrate ester pentaerythritol tetranitrate (PETN), and the aliphatic nitramine 1,3,5-trinitroperhydro-1,3,5-triazine (RDX). Chemometrics algorithms were applied to analyze the recorded spectra. Partial least squares (PLS) regression analysis was used to find the best correlation between the infrared signals and the surface concentrations of the samples and PLS combined with discriminant analysis (PLS-DA) was used to discriminate, classify and identify similarities in the spectral data sets. Several preprocessing steps were applied to prepare the mid-infrared spectra of HEMs deposited on the target substrates. The results demonstrate that the infrared vibrational method described in this study is well suited for rapid screening analysis of HEMs on low reflectivity substrates when a

supervised model has been previously constructed or when a reference spectrum of the neat substrate can be acquired to be subtracted from the HEM/substrate spectrum.

2.1 INTRODUCTION

The detection and identification of hazardous chemical compounds on substrates, such as highly energetic materials (HEMs), is of great interest to defense and security agencies and is of importance in forensic applications. When detonated, HEMs have the potential to destroy public and private buildings and may jeopardize the lives of, first responders, of law enforcement employees and of civilians. Over the past few years, vibrational spectroscopy techniques, such as Raman and infrared spectroscopies, have frequently been used to deter possible terrorist threats by providing the basis for the required countermeasures to prevent explosive terrorist events [1-5].

Mid-infrared (MIR) electromagnetic radiation is located in the spectral region from approximately 350 to 4000 cm^{-1} . In this region, molecules have characteristic vibrational energy states that can be populated upon interaction with photons from an appropriate excitation source, enabling the detection of trace amounts of compounds by measuring the intensities of absorbed, reflected, or transmitted MIR light. [6] Fourier transform infrared (FT-IR) spectroscopy has been extensively used in both active and passive modalities in the MIR region in many defense and security applications [1,2,7-10]. Active mode FT-IR spectroscopy has been used for the post-blast detection of energetic materials using infrared radiation produced from both global and synchrotron sources. Reports have also validated FT-IR spectroscopy as a useful tool for forensic science applications [7,8]. Emission (passive mode) and absorption MIR spectroscopies have

recently been used as vibrational techniques for the standoff detection of explosives and other chemical agents deposited on metallic surfaces [2,9,10].

The need to develop more powerful IR sources that would enable detection at longer distances when a target is deposited on substrates at trace levels suggests the use of collimated, coherent, and polarized sources. These sources were first developed in 1994 at Bell Labs with the invention of quantum cascade lasers (QCLs). [11] A QCL is a unipolar semiconductor injection laser based on sub-interband transitions in a multiple quantum-well heterostructure. As a semiconductor laser that has the ability to produce varying wavelengths and to operate at various temperatures, this type of laser has various advantages over other types of lasers [11,12]. QCLs are capable of producing from a few tens to hundreds of milliwatts of continuous mode or pulsed power under ambient conditions, are commercially available, and have enabled the development of ruggedized systems for the detection of hazardous chemical compounds. Recent developments in QCL technology include size reduction, which have enabled the transition from tabletop laboratory instruments to easy-to-handle, small instrument designs, and portable units that can be used by first responders and military personnel outside the confinement of a sample compartment. Moreover, the increase in output power has enabled the use of QCL-based spectrometers in long-distance (range) applications, making the detection of chemical and biological threat agents possible at tens of meters from the source [13,14]. Furthermore, QCLs can be operated in field conditions, allowing for the sensitive detection of homemade explosives such as triacetone triperoxide (TATP), of aliphatic nitrate esters such as pentaerythritol tetranitrate (PETN), of aliphatic nitramines as 1,3,5-trinitroperhydro-1,3,5-triazine (RDX) and of nitroaromatic HEMs as 2,4-dinitrotoluene

(2,4-DNT) and 2,4,6-trinitrotoluene (TNT) in the vapor phase using photoacoustic spectroscopy [15-17]. The detection of TATP and TNT in the vapor phase has also been achieved using infrared absorption spectroscopy with satisfactory results [3,18]. Moreover, the use of QCL sources has been useful for remote detection of HEMs deposited on surfaces using photoacoustic and traditional infrared absorption spectroscopies [19-23]. Thundat's group recently reported that nanomechanical infrared spectroscopy provides high selectivity for the detection of TNT, RDX and PETN without the use of chemoselective interfaces by measuring the photothermal effect of the adsorbed molecules on a thermally sensitive microcantilever [23]. However, the majority of previous investigations focused on the detection of HEMs deposited on nearly ideal, highly reflective substrates (such as metallic surfaces), and there are few published reports on the effects of non-ideal, low reflectivity substrates on the spectra of the analyzed target HEMs.

In this study, non-contact detection experiments using QCL spectroscopy (QCLS) were performed. The experiments were conducted using an active mode QCL source to excite the MIR molecular vibrations from the investigated HEMs. Two chemometrics routines were applied to analyze the characteristics of the recorded spectra using QCLS: partial least squares (PLS) regression analysis, which assisted in finding the best correlation between the MIR signals and the analyte surface concentrations, and partial least squares coupled with discriminant analysis (PLS-DA), which was used to discriminate, classify and identify similarities between the spectral data. Several preprocessing steps were applied prior to the multivariate analyses protocols employed. The results indicate that the QCL based methodology described in this study could be used for rapid screening

analysis of HEMs on low reflectivity substrates such as travel bags materials, cardboard and wood when a supervised model has been previously constructed or when a reference spectrum of the neat substrate can be acquired prior to acquiring the HEM/substrate spectrum.

2.2 MATERIALS AND METHODS

2.2.1 Reagents and Materials

The reagents and materials used in this study included HEMs, solvents, and substrates. 2,6-Dinitrotoluene (2,6-DNT) and TNT were acquired as a crystalline solids (99% min.; 30% min. water content; standard grade) from Chem Service, Inc. (West Chester, PA, USA). PETN and RDX were synthesized and purified in the laboratory according to the methods described by Ledgard [24]. Methanol (99.9%, HPLC grade), dichloromethane (CH_2Cl_2 , HPLC grade), acetone (99.5%, GC grade) were purchased from Sigma-Aldrich (Milwaukee, WI, USA) and were used as obtained as solvents to deposit HEM samples at various surface concentrations onto test substrates. Sodium fluoride (NaF, ACS reagent, $\geq 99\%$) was purchased from Sigma-Aldrich (Milwaukee, WI, USA) and was used to make pellets with 2,6-DNT. The substrates used were travel bag fabric (TB; black polyester), cardboard (CB; corrugated single-wall) and wood (grade C-C, plugged soft 3-ply spruce plywood). Aluminum (Al; highly polished) plates were used as reference substrates of high reflectivity. The substrates were acquired from local suppliers. These were cut into square pieces of approximately 31 mm x 31 mm, gently cleaned using acetone or methanol and stored in Dry Keeper™ desiccator cabinets to stabilize their weights by controlling their moisture contents. Attempts to stabilize the weights of the

substrates were only successful for TB substrates. Because the humidity levels in the laboratory varied on a daily basis, the wood and CB substrates did not attained stable weights, and deposition methods that did not depend on the weight of the substrates had to be used employed.

2.2.2 Sample preparation

Sample preparation is a fundamental step in this type of experiments. To obtain calibration models that resulted in good predictions of the validation samples, methods that allowed for the proper transfer of the target HEMs to the test substrates had to be used. This was required to achieve reliable and consistent analyte surface concentrations (mass/area), thereby allowing validation of the experimental methodology. Various deposition methods were tested, including sample smearing, spin coating, spray deposition, and partial immersion. Results of HEMs samples transfers to solid matrices have previously been reported [21]. In summary, sample smearing and spin coating based methodologies for sample transfer onto substrates work well for flat, non-porous surfaces such as polished metals, glass, silicon and others of the like. For rough, not-flat, highly porous substrates, such as CB, wood, and TB, partial immersion provided the means of devising the optimum sample transfer protocol. When using this method, the sample loss was negligible, a good homogeneity was attained, and no substrate preparation was required. A spectrophotometric (UV-Vis) methodology was used to validate this deposition method.

Eleven to fourteen surface concentrations for each HEM, ranging from 0.1 to 14 $\mu\text{g}/\text{cm}^2$ were prepared, including zero concentration (substrates without HEM) and distributed as

follows: 11 surface concentrations each for PETN on TB, PETN on wood, TNT on CB, and TNT on wood; 12 surface concentrations for TNT on TB, RDX on TB, PETN on CB and RDX on wood; and 14 surface concentrations for RDX on CB. For PLS analysis, 4 spectra were acquired, resulting in 424 independent measurements. For PLS-DA analysis, twelve additional spectra from each clean substrate (36 total QCL spectra without HEM) were added to the data used in PLS, totalizing 460 independent measurements.

In order to characterize the spectral features of HEMs when reflection/transmission experiments were carried out, 2,6-DNT spectra for two optical sample thicknesses of 1 cm (diam.) pellets of 2,6-DNT in NaF were prepared: an optically thin pellet of 1% 2,6-DNT/NaF (~ 0.5 mm thick) and an optically thick pellet with 10% 2,6-DNT/NaF (~ 3 mm thick). Both reflection and transmission spectra were recorded using an evacuable bench FT-IR interferometer (IFS-66/S/v, Bruker Optics, Billerica, MA, USA) using 62 scans at 4 cm^{-1} resolution. The reflectance spectra were measured at 80° with respect to the surface normal.

2.2.3 Setup

Figure 2-1 shows a diagram that illustrates the experimental setup: (a) sample preparation using the aerosol spray and partial immersion deposition methods; (b) non-contact detection of the target chemicals; (c) chemometrics multivariate analyses. The detection of PETN, RDX and TNT deposited on non-ideal, low reflectivity substrates was performed using a QCL based spectroscopic system acquired from Block Engineering (LaserScan™, 6-10 μm , Marlborough, MA, USA). The specifications for the spectroscopic

system and laser source used were the following: nearly continuous wavenumber coverage; laser pulse modulation: 200 kHz; collimated elliptical beam: 4 mm x 2 mm; beam divergence: < 5 mrad; internal coupling to a thermoelectrically cooled Hg-Cd-Te (MCT) detector. The system was designed to operate in back reflection mode (at zero or a small angle with respect to the surface normal, as shown in Figure 2-1b. No attempt was made to separate the specular component from the diffusely reflected light. The solid angle of collection for the 2 in. diam. zinc selenide lens leading to the detector was 0.086 sr. QCL measurements obtained in this configuration for the samples prepared as part of the study can be described as transflection (or double pass) mode. MIR spectra were recorded at a distance of 6 in. from the substrates at 4 cm^{-1} resolution. The acquisition time for one spectrum (3 acquisitions, averaged) was ~ 3 s. For the data included, two spectra were co-added (6 acquisitions, averaged) for a total acquisition time per co-added spectra of approximately 9 s. However, it was found that the signal to noise ratio increased only slightly with two co-adds.

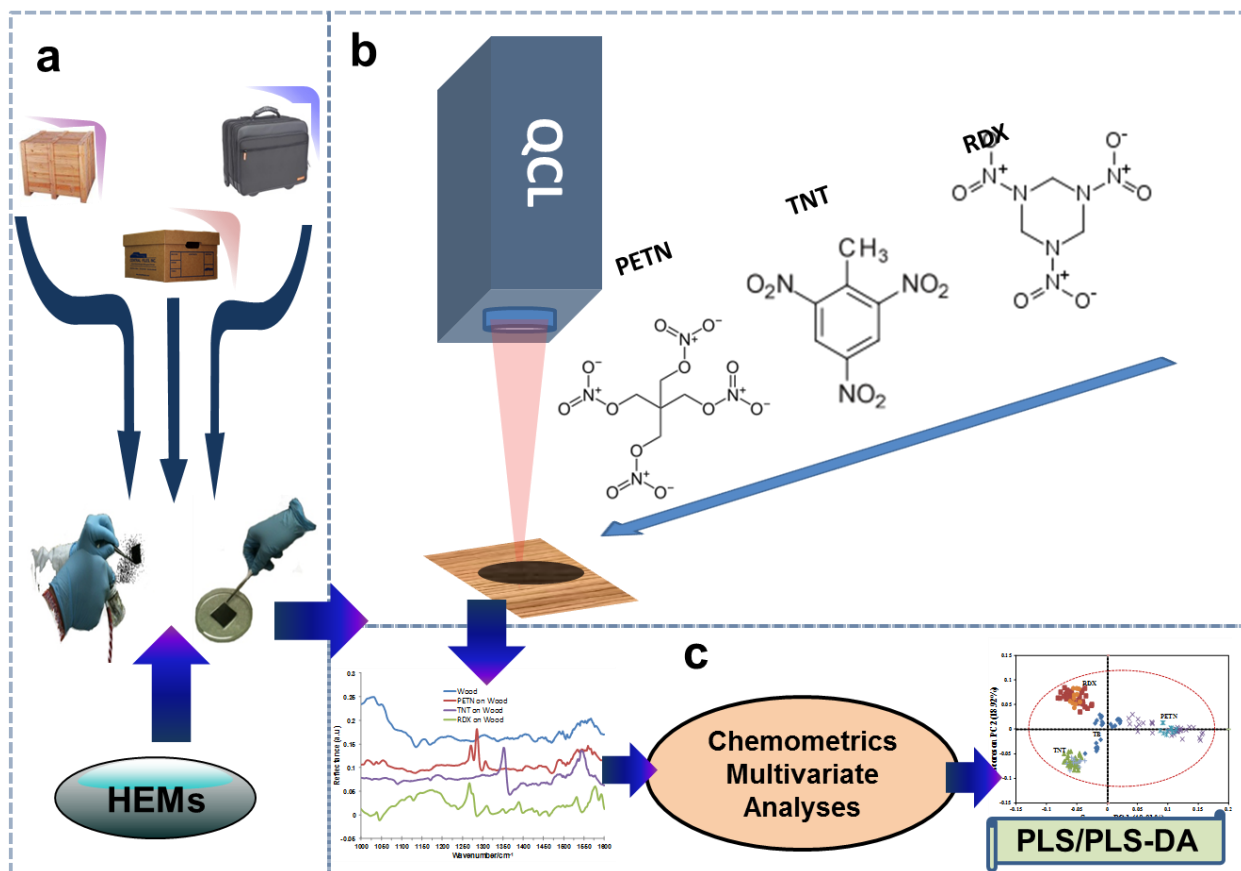


Figure 2-1. Experimental setup. (a) Sample preparation: HEM samples deposited on substrates. (b) In situ QCL spectral measurements. (c) Multivariate statistical analyses.

All spectra were stored in Thermo-Galactic™ SPC format (Thermo-Fisher Scientific, Inc., Waltham, MA, USA) and analyzed using PLS and PLS-DA chemometrics models with PLS Toolbox™, v. 6.5 (Eigenvector Research Inc., Wenatchee, WA, USA) for MatLab™ (The MathWorks, Inc., Natick, MA, USA). The reference (library) spectra were obtained using flat, non-porous Al substrates (31 mm x 31 mm). Surface HEMs concentrations were 15 $\mu\text{g}/\text{cm}^2$ (nominally) prepared using sample smearing protocol as deposition method.

2.3 RESULTS

2.3.1 Spectral analysis

MIR vibrational spectra of TNT, RDX, and PETN deposited on Al, TB, CB and wood substrates were obtained using a QCL spectrometer. The spectra were recorded in the spectral region of 1000-1600 cm^{-1} , where the symmetric and asymmetric nitro group vibrations of the HEMs occur. Figure 2-2 shows the QCL reflectance mode spectra of TNT, PETN and RDX deposited on Al, CB, wood and TB. The spectra on Al are included as references to assist in identifying the obtained MIR vibrational bands of QCL spectra of HEMs deposited on nonmetallic substrates. As shown in Figure 2-2a, the form of the vibrational bands of the HEMs clearly confirm the highly reflective nature of the Al substrate. These spectra have the appearance of “double pass” transmission-reflection (transflectance) spectra. Transflection experiments are usually made by placing a thin analyte sample on a non-IR absorbing, reflective substrate such as a polished metal surface, focusing an IR beam onto a region of interest, and collecting the radiation that is reflected to the collection optics. The technique is termed transflection because most of the signal intensity collected is a transmission signal as the beam passes through the sample, reflects off the substrate, passing through the sample again to the detector. [25,26] Some of the vibrational bands that were tentatively assigned to TNT were 1024 cm^{-1} (CH_3 - deformation), 1086 cm^{-1} (C-H ring in-plane bending), 1350 cm^{-1} (symmetric stretching of nitro groups) and 1551 cm^{-1} (asymmetric NO_2 stretching) [27]. For PETN, some of the important signatures appeared at 1003 cm^{-1} (CO stretching), 1038 cm^{-1} (NO_2 rocking), 1272 cm^{-1} (ONO_2 rocking), 1285 cm^{-1} (NO_2 stretching) and 1306 cm^{-1} (NO_2 rocking) [28]. Finally, important markers for RDX were detected at 997 cm^{-1} (N-N and ring

stretching), 1220 cm^{-1} (C-N stretching), 1270 cm^{-1} (NO_2 stretching), 1310 cm^{-1} (N-N stretching), 1420 and 1445 cm^{-1} (H-C-N asymmetric bending) and 1570 cm^{-1} (N-O asymmetric stretching) [29,30].

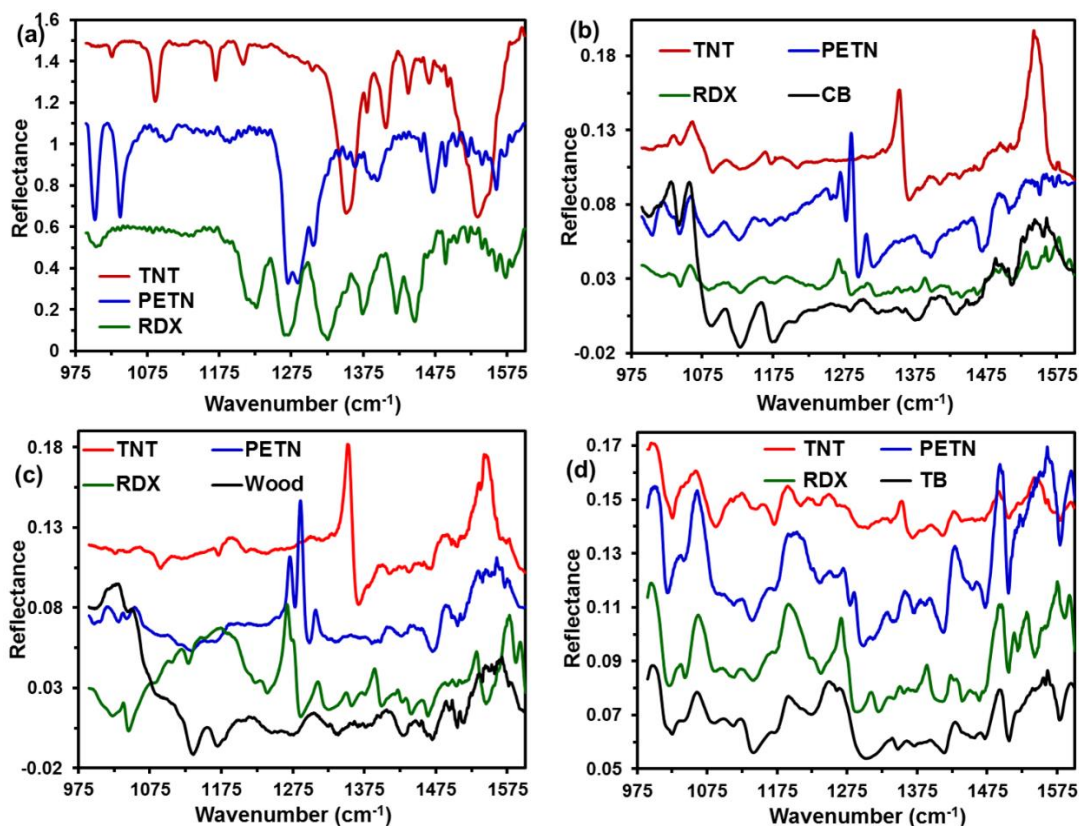


Figure 2-2. QCL spectra of HEM on substrates: (a) Al, (b) CB, (c) wood, and (d) TB. Surface concentrations were $15 \mu\text{g}/\text{cm}^2$. QCL spectra of substrates are included to establish the degree of spectral interference.

Typical spectra of the HEMs deposited on CB, wood and TB are shown in Figures 2b-2d. In addition to the HEM signatures, vibrational bands from the substrates were also observed. However, providing details about the signals from the substrates that give rise to these infrared bands is beyond of the scope of this contribution. The focus of this work is the analysis of the interferences produced by the substrate contributions and the effects of these interferences on the ability to detect and discriminate HEMs deposited on the

investigated substrates. The spectral profiles of each HEM were similar when deposited on CB and wood (Figures 2b and 2c). The prominent MIR signatures of the HEMs on CB and wood were the NO₂ bands at approximately 1270 cm⁻¹ for the aliphatic explosives PETN and RDX and at 1350 cm⁻¹ for the aromatic explosive TNT. The infrared bands of the HEMs on TB are shown in Figure 2-2d.

QCL spectra of HEM shown in Figure 2-2 evidence the effects of sensing for explosives deposited on surfaces with different reflectivities. The spectra were acquired in reflection mode. Two different spectral profiles of HEM are shown in Figure 2-2: those when substrates used have high reflectivities, in this case a polished Al plate, and those where substrates have low reflectivities (such as CB, TB, and wood). These spectral patterns can be understood by taking into account that in a transflection experiment IR radiation reaching the detector passes through the sample and is reflected off the front surface of a highly reflective substrate. However, part of the intensity detected originates from IR light reflected from the sample itself. Consequently, the recorded transflection spectra are a weighted sum of the transmission and reflection characteristics of the samples and substrates. As demonstrated by Bassan et al. [26] in samples where the optical density (thickness) is low and high reflectivity substrates are used the weighting is such that the transmission signal dominates and the reflection signal is negligible, producing spectra closely resembling that of a transmission spectrum. However, if the transmission signal is weak or extinct, the reflection signal will dominate and a reflectance spectrum is obtained. As shown in Figure 2-3, the profile of a transflection spectrum for 2,6-DNT depends of the optical thickness of the sample. For optically thin samples, contributions from transmission are higher than those from reflection, producing a spectrum similar to

the transmission mode (Figure 2-3a). On the other hand, for optically thick samples the contributions by transmission are negligible or nonexistent producing a spectrum similar to the reflection mode as in Figure 2-3b.

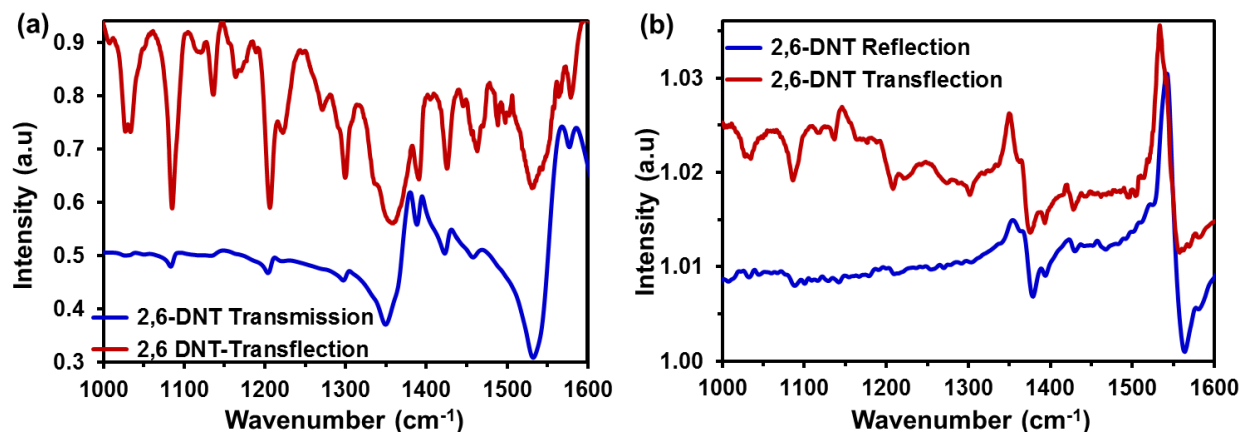


Figure 2-3. Comparison of MIR spectra of 2,6-DNT/NaF pellets: (a) QCL and %T FT-IR spectra for thin 2,6-DNT(5%)/NaF pellet; (b) QCL and FT-IR spectra for thick 2,6-DNT(10%)/NaF pellet.

Reference spectra of investigated HEM are shown in Figure 2-2a. Surface concentrations of 15 $\mu\text{g}/\text{cm}^2$ were deposited on Al reflective plates and used to measure the reference QCL spectra. As can be observed, the transmission component dominates the QCL transflection spectra, producing a spectral profile similar to that of a transmission FT-IR spectrum (Figure 2-3a). However, when HEM spectra were acquired from non-reflective substrates (Figure 2-2b to 2d) the reflectance component of the QCL transflection spectra stood out more prominently, producing reflectance spectra with profiles similar those with anomalous dispersions [31,32]. These spectral features are usually observed when sample refractive index decreases to the high-wavenumber side of the absorption band maximum, returning to the normal value at the absorption band center, then increasing to

the lower-wavenumber side, before returning again to the normal values [25,31]. In other words, these distortions usually result in asymmetric bands with negative intensity contributions at the high wavenumber side of the band, accompanied by a shift towards lower wavenumbers, and distorted band shapes and inconsistent intensities [32]. These spectral features are well appreciated in the nitro group vibrational bands of HEM at 1350 and 1551 cm^{-1} for TNT, 1285 and 1306 cm^{-1} for PETN and 1270 cm^{-1} for RDX, in which the transfection spectra become significantly distorted exhibiting skewed lineshapes when low reflectivity materials (CB, TB, and wood) were used substrates. It is clear that the spectral distortions in this study are not anomalies but rather spectral profiles dominated by the reflectance of the HEM samples as demonstrated by Bassan and confirmed by the results shown in Figures 3a and 3b for 2,6-DNT [26].

2.3.2 Concentration Profiles and Difference Spectra Identification.

Figures 4a to 4c show some of the spectra used for the surface concentration profiles constructed in preparation to perform quantitative multivariate analyses runs. A total of 9 surface concentration profiles: 3-HEM x 3-substrates (plus 3 replicas of each combination) was assembled. QCL spectra of clean Al substrates were used as backgrounds. Figure 2-4a shows some of the RDX spectra recorded on wood substrates; Figure 2-4b shows spectra for TNT on CB at various surface concentrations; and Figure 2-4c shows measured QCL reflectance spectra for PETN on wood. However, the QCL methodology used for detection of explosives on non-reflective substrates does not require the use of multivariate analyses for identification of HEM, but rather, as illustrated in Figure 2-4d, a single acquisition (3 s) of CB was subtracted from the corresponding

QCL spectrum of PETN on CB to obtain the difference spectrum of PETN. Comparison with the QCL transfectance spectrum of PETN on Al demonstrates that several of the aliphatic nitrate ester signature bands can be readily assigned by comparison with the reference QCL spectrum. The only requirement for this type of remote detection experiment is be able to acquire a QCL spectrum of a non-contaminated (non-dosed) segment of the substrate.

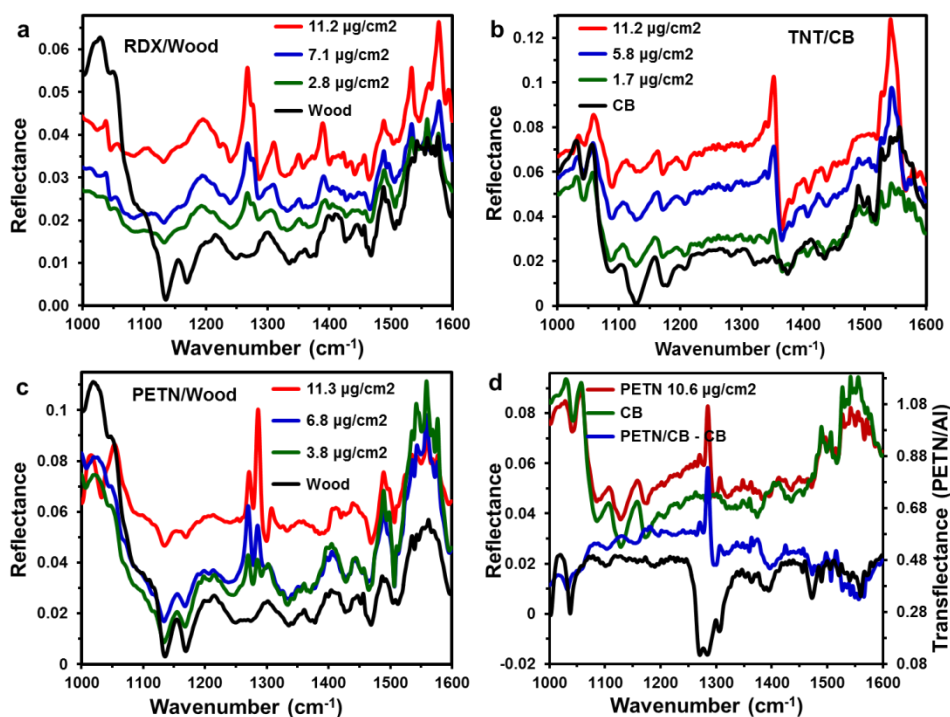


Figure 2-4. Surface concentration profiles for: (a) RDX on wood; (b) TNT on CB; (c) PETN on wood; and (d) difference spectrum: PETN/CB minus CB and comparison with QCL transfectance spectrum PETN/Al (used as reference).

2.3.3 Target Identification

Target identification with typical routines used in portable IR and Raman systems for remote detection were applied for the HEMs studied on the substrates used. First, a spectral search was applied to each spectrum with the purpose identifying the detected

HEM. The simplest spectral search is based on the calculation of the hit quality index (HQI) values [33]. The HQI is a numerical quantity that indicates the correlation between two spectra and has been widely used in spectroscopy to indicate the degree of spectral matching in library searches [8,34-38]. In the protocol, a spectrum of an unknown sample is compared with all spectra of known samples in a library, and the best match is determined based on the calculated HQI values. Routines for calculating the HQI are available in most commercial portable spectrometers to facilitate the identification of unknown compounds in the field. HQI values can be calculated using various algorithms, but the two most commonly used are the Euclidean distance and spectral correlation algorithms. In the Euclidean distance algorithm, the HQI values are calculated from the square root of the sum of the squares of the difference between the vectors for the unknown spectrum and each library spectrum [33,38]. In contrast, the spectral correlation algorithm utilizes the Pearson product-moment correlation coefficient, r_{xy} , which is a measure of the strength and direction of the linear relationship between two variables. This parameter is defined as the covariance of the variables divided by the product of their standard deviations. In this case, the spectral correlation algorithm is applied between two spectra: a reference (or library of spectra) and an unknown spectrum to be identified [34-37]. The r_{xy} values were calculated using Eq. 1:

$$r_{xy} = \frac{\sum x_i y_i - \frac{1}{n}(\sum x_i)(\sum y_i)}{\left[\left\{ \sum x_i^2 - \frac{1}{n}(\sum x_i)^2 \right\} \left\{ \sum y_i^2 - \frac{1}{n}(\sum y_i)^2 \right\} \right]^{1/2}} \quad (1)$$

where x and y represent the spectral responses of the reference spectrum and of an unknown spectrum, respectively, measured at the i^{th} wavenumber for a set of n corresponding wavenumber points. In the present case, the HQI assumes values between +1 and -1. A HQI value of +1 is obtained when the spectral similarities are

maximum (the unknown spectrum is identical to a library spectrum), -1 when the spectral similarities are inverted (the unknown spectrum is identical to a library spectrum but with peaks inverted with respect to the library spectrum) and zero when there is no spectral similarity. Often, the values are rescaled to values between 0 and 1, where values between -1 and 0 are equated to zero and a value of 1 indicates maximum spectral similarity.⁸ Another possibility is to rescale the square of r (r^2) to yield positive values between 0 and 1 [36-37]. However, in this investigation, the rescaling step was not applied such that the effects of the contributions of complex substrates on the transfection spectra (analyte + substrate) could be evaluated when HQI algorithms were used to identify unknown spectra from a spectral library or from reference spectra.

Table 2-1 presents the spectral correlation coefficients for unknown spectra on the various types of substrates tested. Before calculating the r values, a spectral normalization was performed on the entire spectral range of 1000-1600 cm^{-1} for both the unknown (measured) and library spectra (measured on Al substrates). The normalization of a spectrum for library searching is a two-step process, as recommended by ASTM E2310-04 (2009): "Standard Guide for Use of Spectral Searching by Curve Matching Algorithms with Data Recorded Using MIR Spectroscopy" [33]. First, the minimum spectral response value in the selected spectral range is subtracted from the entire spectral response in the same range. The resulting values are then scaled by dividing by the maximum value in that range. The net result is a spectrum in which the minimum intensity value is zero (0) and the maximum value is one (1). The values of the spectral correlation coefficients for the HEMs shown in Table 2-1 are severely influenced by the type of substrate used, which can be confirmed when metal substrates such as Al were

used, resulting in high values of r . When non-metallic substrates were used, such as TB, CB and wood, low values of r were obtained. It is generally acceptable to consider a spectrum of an unknown compound to be similar to one of the library when the spectral correlation coefficient is greater than ~ 0.85 . Given this restriction, spectra measured on only Al substrates were correctly identified when QCLS coupled with spectral correlation algorithms were used. All of the spectral correlation coefficients for unknown spectra of HEMs deposited on CB, wood and TB were well below the minimum accepted r value (0.85). In some cases, the r values were negative (i.e., some unknown spectra had peaks inverted with respect to the library spectra). These results highlight two factors. First, low r values were obtained when the QCL spectra of HEMs deposited on low reflectivity, complex substrates were measured. Second, negative r values were obtained due to the effect of such substrates, resulting in spectra with inverted peaks.

The QCL methodology used for detection of explosives on non-reflective substrates does not necessarily require the use of multivariate analyses for identification of HEM. As illustrated in Figure 2-4d, a single acquisition (3 s) of CB was subtracted from the corresponding QCL spectrum of PETN on CB (PETN/CB) to obtain the difference spectrum of PETN. Comparison with the QCL transmittance spectrum of PETN on Al demonstrates that several of the aliphatic nitrate ester signature bands can be readily assigned by comparison with the reference QCL spectrum. The only requirement for this type of remote detection experiment is to be able to acquire a QCL spectrum of a neat part of the substrate that does not contain HEM residues.

Table 2-1. Values of spectral correlation coefficients (HQI) for spectra of HEM deposited on various substrates.

HQI / Spectral Correlation												
Spectra Queried												
library spectra	HEM spectra on Al			HEM spectra on CB			HEM spectra on wood			HEM spectra on TB		
	PETN	RDX	TNT	PETN	RDX	TNT	PETN	RDX	TNT	PETN	RDX	TNT
PETN	0.95	0.39	0.07	0.06	0.00	-0.03	-0.39	0.13	-0.10	0.20	0.21	0.12
RDX	0.39	0.94	0.09	0.15	0.30	0.25	-0.05	0.14	0.07	0.34	0.36	0.40
TNT	0.10	0.14	0.96	-0.03	-0.09	-0.55	-0.22	0.22	-0.60	-0.10	0.11	0.14

Because the spectral correlation coefficients were not efficient for the identification and classification of HEMs when they were deposited on non-ideal, low reflectivity substrates (such as CB, TB, and wood) for direct field detection applications, multivariate analysis methods, such as PLS and PLS-DA, were applied for robust spectral identification, classification and quantification. PLS Toolbox™ version 6.5 for MATLAB™ was used to analyze the data. Figure 2-1c illustrates the use of chemometrics multivariate statistical analysis applied to the data. PLS-DA is one of the most widely used chemometrics tools, particularly when the goal is to discriminate, classify and identify spectral similarities in a multivariate data set. PLS-DA is a supervised pattern recognition method. A detailed explanation on the numerous applications of PLS-DA and on how it works are not included in this paper. Excellent in-depth mathematical support and various applications in natural sciences and engineering are available in the literature [39-41]. PLS-DA is a linear classification method that combines the properties of PLS regression with the discrimination power of a classification technique. PLS-DA is based on the PLS regression algorithm, which searches for latent variables with a maximum covariance

between a descriptor matrix X and a response matrix Y (containing the membership of samples to the G classes expressed with a binary code: 1 or 0). The primary advantage of PLS-DA is that the relevant sources of data variability are modeled by the so-called latent variables (LVs), which are linear combinations of the original variables, and consequently, allowing graphical visualization and understanding of the different data patterns and relations by LV scores and loadings. The scores represent the coordinates of the samples in the LV projection hyperspace [40,41].

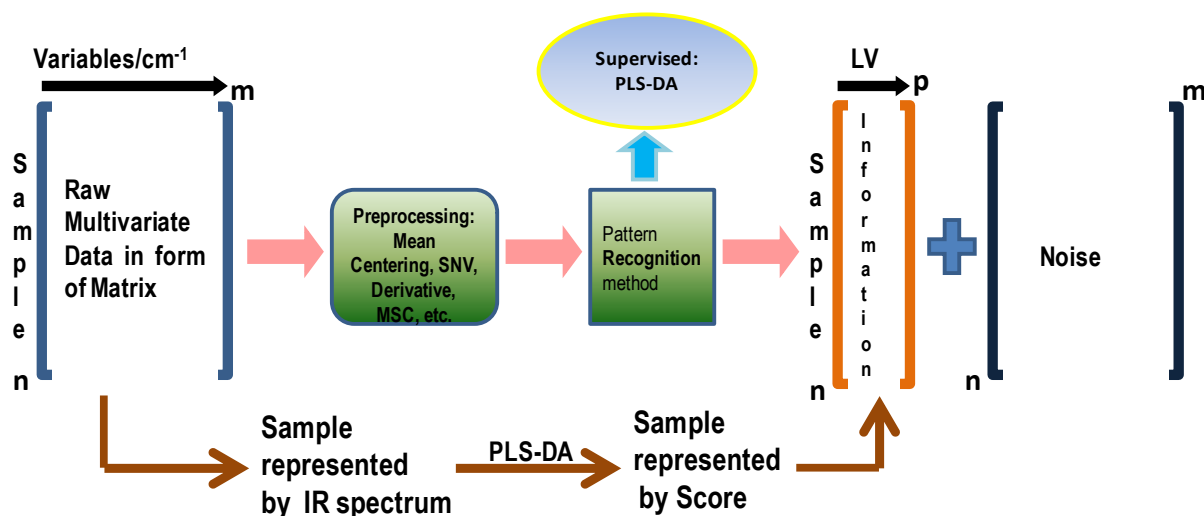


Figure 5-5. Representation of multivariate analysis (PLS-DA) on spectral data used in this research to identify and classify HEMs deposited on non-ideal, non-reflective substrates.

The data were divided into two groups for each model: a calibration set and a prediction or test set. The calibration set contained approximately 70% of the data, and the prediction set contained the remainder of the data. PLS-DA was applied to the spectral data to discriminate, classify, or group all spectra by HEM type and to discriminate between clean substrates and the substrates with HEMs. An overview of the performance

of PLS-DA on the spectral data (matrix \mathbf{X}) is presented in Figure 2-5. The first step was intended to arrange the spectral data in a matrix with dimensions of “ $n \times m$ ” (n rows and m columns), where n represents the number of samples used in the calibration set, and m represents the number of spectral variables in the study. In this work, the matrix dimensions were 104×3056 for the calibration set of each type of substrate tested. The second step was to apply the required preprocessing handling of the data. The purpose of preprocessing the data was to remove or to decrease the effect of the interferences from the background/substrate, thereby enhancing the vibrational signatures of the HEMs. PLS-DA was able to decompose the original matrix into two new matrices: one that has most of the relevant information containing the largest variability in the data and another that contains information that is not as relevant to the data, generally termed noise. The matrix that contains the information of interest has dimensions of “ $n \times p$ ”, where p is a new column matrix called the latent variable (LV), which is the product of the transformation from the original variables. LVs are orthogonal vectors that are linear combinations of the original data. In general, two or three LVs are sufficient to capture the majority of the variability in the data. In the LVs, each sample that was initially represented by an IR spectrum is now represented by only one value, termed the “score” of the sample. These scores describe how the samples are related to each other. Score plots are obtained by graphing LV2 vs. LV1. These plots provide important information regarding how different samples are related to each other. Finally, the original matrix with dimensions of 104×3056 for the calibration set of each substrate tested was reduced to a matrix with dimensions of 104×3 using three LVs.

In PLS-DA, the optimal number of LVs that provided the best classification for the calibration set was determined using cross validation procedures. The Venetian blinds procedure with 10 group splits was used to divide the calibration set into cross validation groups. Several preprocessing steps were applied to the data with the objective of generating multivariate models capable of discriminating and clustering the spectra based on chemical similarities, i.e., PETN, RDX, TNT and clean substrates (TB, CB, and wood). The preprocessing steps used were auto scaling (AS), mean centering (MC), standard normal variate (SNV), 1st / 2nd derivatives and their combinations. For all the multivariate models generated, the ones that performed best were those that used the full spectral range (1000-1600 cm⁻¹).

For PLS-DA, classification parameters, such as sensitivity and specificity, derived from the confusion matrix from the calibration, cross validation and prediction sets were used to evaluate the performances of the classification models. The sensitivity (SEN) describes the model's ability to correctly recognize samples that belong to that class and the specificity (ξ) describes the model's ability to reject samples of all other classes and can be calculated as follows:

$$\text{SEN} = \frac{\text{TP}}{(\text{TP}+\text{FN})} ; \quad \xi = \frac{\text{TN}}{(\text{TN}+\text{FP})} \quad (2)$$

where TP = true positive, TN = true negative, FP = false positive, and FN = false negative.

When dealing with two classes A and B, A: positive (a specific HEM) and B: negative (the other HEM or the clean substrates), TP is the number of members of class A that have been correctly classified, FP (false positive) is the number of members of class B that have been incorrectly predicted as class A, TN is the number of members of class B that have been correctly classified and the number of members of class A that have been

incorrectly predicted as class B. Both SEN and ξ take values between 0 and 1, where 1 is the desired result [40]. Table 2-2 presents a summary of the results obtained from applying PLS-DA to the QCLS spectra of the HEMs on the investigated surfaces for the calibration, cross validation and prediction sets.

Table 2-2. Summary of results of PLS-DA of QCLS spectra of HEMs on surfaces obtained for calibration, cross validation (10 groups split in venetian blinds) and prediction set.

	HEM spectra on TB			HEM Spectra on CB			HEM spectra on Wood		
	PETN	RDX	TNT	PETN	RDX	TNT	PETN	RDX	TNT
SEN (Cal)	1	1	1	1	1	1	1	1	1
ξ (Cal)	1	1	1	1	1	1	1	1	1
SEN (CV)	1	1	1	1	1	1	1	1	1
ξ (CV)	1	1	1	1	1	0.991	1	1	1
SEN (Pred)	1	1	1	1	1	1	1	1	1
ξ (Pred)	1	1	1	1	1	1	1	1	1
Class. Err. (Cal)	0	0	0	0	0	0	0	0	0
Class. Err. (CV)	0	0	0	0	0	0.005	0	0	0
Class. Err. (Pred)	0	0	0	0	0	0	0	0	0
RMSEC	0.136	0.137	0.123	0.086	0.101	0.124	0.112	0.151	0.072
RMSECV	0.149	0.142	0.132	0.089	0.104	0.130	0.127	0.176	0.078
RMSEP	0.109	0.104	0.100	0.098	0.087	0.089	0.191	0.228	0.076
LV	4	4	4	4	4	4	5	5	5
Variance Captured (%)	87.8	87.8	87.8	91.5	91.5	91.5	92.3	92.3	92.3

The score plots, which allow visualization of the clustering of the spectral data, resulting from the PLS-DA runs are shown in Figures 6 and 7. These plots demonstrate that the best results were obtained for the various generated models after the preprocessing steps mentioned above had been applied. For the multivariate analysis of the MIR vibrations of the HEMs deposited on TB and CB, taking the first derivative (15 pts.) and applying MC

were sufficient to obtain the best chemometrics models. Using derivatives in spectroscopy facilitates the identification of the wavenumber location of the maxima/minima of poorly resolved spectral features in complex spectra. Taking derivatives can also be used as a background correction technique to reduce the effect of spectral background interferences in quantitative analytical methods [42]. MC was used to decrease the dimensionality of the spectral data.

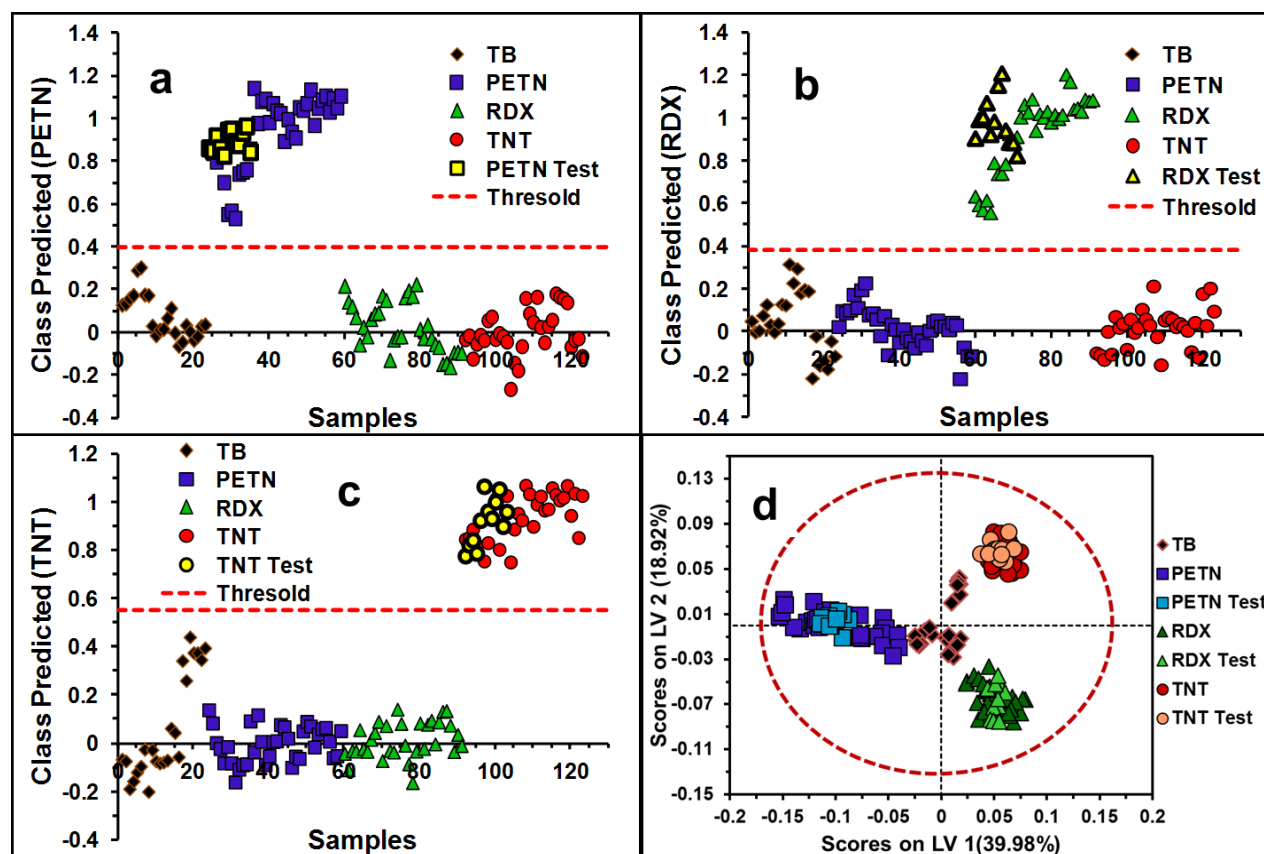


Figure 2-6. PLS-DA model for discrimination of HEM on TB: (a) class prediction for PETN; (b) class prediction for RDX; (c) class prediction for TNT; (d) scores plot of LV2 vs. LV1 for detection of PETN, RDX and TNT on TB. Preprocessing steps applied were: 1st derive. (15 pt.) and MC. Threshold for discrimination and 95% confidence level for clustering are represented with red dotted lines.

The PLS-DA models resulting from the discrimination of each HEM from the others and from the neat substrate for TB are shown in Figure 2-6. The class predictions of PETN, RDX, and TNT on TB from the cross validation are shown in Figures 6a-6c. Four LVs were required to obtain the best multivariate classification model with SEN and ξ equal to 1 (see Table 2-2) for the HEMs tested from the calibration, cross validation and prediction data sets. The variance captured from matrix \mathbf{Y} was 87.8%, which is sufficient for a good classification of the predicted spectra set on TB. For the multivariate (clustering) analysis of the HEMs on TB, a total of six LVs were necessary to capture 80% of the total variance in the spectral data. As shown in the scores plot in Figure 2-6d, two latent variables with 60% of the spectral variance were sufficient to obtain an excellent classification according to the type of HEM deposited and to discriminate from the TB substrate. In this model, spectra from the prediction set (RDX Test, TNT Test, and PETN Test) were well grouped according to chemical characteristics with spectra from the calibration sets.

Class predictions of PETN, RDX, and TNT on CB from the cross validation required four LVs were to obtain the best classification model allowing SEN and ξ to equal 1 (see Table 2-2) for the HEMs tested for the calibration, cross validation and prediction data sets. The variance captured from matrix \mathbf{Y} was 91.5%, which is sufficient for a good classification of the predicted spectra set on CB. In the PLS-DA clustering analysis for the QCL spectra of the HEMs on CB, five LVs were required to capture 80% of the total variance in the spectral data using the first derivative (15 pts.) and MC as preprocessing steps. Two LVs corresponding to 63% of the variance were sufficient to obtain excellent spectral classification according to the type of explosive deposited and to discriminate from the substrate. Using this model, spectra from the validation set (RDX Test; TNT Test; PETN

Test) were grouped reasonably well with spectra from the calibration set according to vibrational signatures.

Class predictions of HEMs on wood from the cross validation required five LVs to obtain the best multivariate classification model that allowed SEN and ξ to equal 1 (see Table 2-2) for the HEMs tested from the calibration, cross validation and prediction data sets. The variance captured from matrix **Y** was 92.3%, which is sufficient for a good classification of the prediction spectra set on wood. For the multivariate analysis of the MIR vibrations of the HEMs deposited on wood, preprocessing of the data using the first derivative (15 pts.), SNV transformation and MC was necessary to obtain the best chemometrics results. The first derivative was used to eliminate spectral differences on the baseline and to smooth the spectra. SNV transformation and MC were used to normalize and center the data. In the PLS-DA clustering model of the HEMs on wood, six LVs were required to capture 80% of the total variance in the spectral data. Two LVs accounting for 61% of the spectral variance were sufficient to obtain a good spectral classification according to the type of HEM deposited and to discriminate from the wood substrate. Spectra from the prediction set were precisely grouped with the spectra from the calibration set according to chemical similarities.

The much more challenging problem of obtaining discriminating functions for three spectroscopically different HEMs: a nitroaromatic explosive (TNT), an aliphatic nitramine (RDX) and an aliphatic nitrate ester (PETN) on three markedly different substrates: CB which is mainly cellulose; TB made from black polyester fabric and wood made also from cellulose but also containing lignin can result in a more complex problem to handle. Initially the problem to discriminate among the three HEMs requires addressing α -

substitution effects: NO₂- linked directly to C (TNT) vs. linked directly to O (PETN or to N (RDX). These different α -substitutions lead to spectroscopic markers that can be used for spectroscopic discriminating among the HEMs. Addition of contributions of substrates MIR absorptions results in a formidable problem in which one clearly does not expect neat boundaries separating the 12 groups in a 2-dimensional space (2 LVs) or even in 3-dimensions (or 3 LVs).

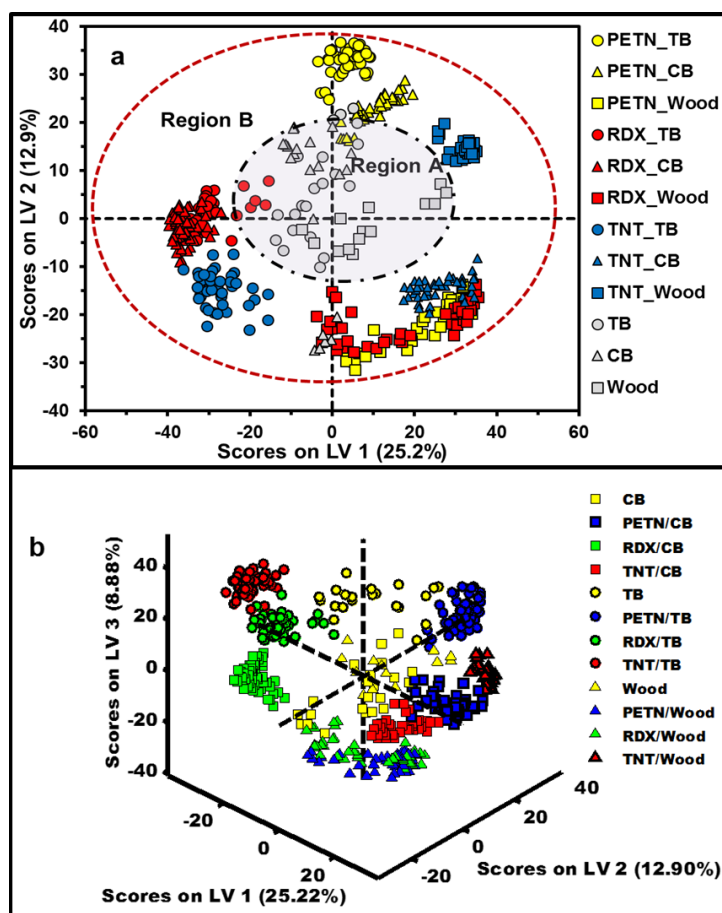


Figure 2-7. PLS-DA model for QCL spectra of PETN, RDX, and TNT deposited on TB, CB, and wood substrates. Preprocessing steps applied were 2nd deriv. (17 pts.) + SNV + MC: (a) 2D-Score plot using LV1 and LV2; (b) 3D-Score plot using LV1, LV2 and LV3. 95% confidence level for clustering is represented with red dotted line.

A more general model based on QCL spectral data for the three HEMs on the three substrate types was generated using PLS-DA. In the multivariate analysis, preprocessing of the data required applying the second derivative (17 pts.), as well as using SNV transformation and MC. In this analysis, twelve LVs were required to capture 80% of the total variance in the spectral data. Results are represented in Figure 2-7a in a 2-LV representation. The PLS-DA model generated using the three HEMs deposited on three non-ideal, low reflectivity substrates was capable of differentiating substrates without HEMs (Region A, Figure 2-7a) from surfaces with HEMs (Region B, Figure 2-7a). In the model representation, there are a few outliers: substrate spectra classified as spectra of substrates with HEMs, and vice versa, which is a consequence of the plot representation using only 2 LVs.

In the 3-dimensional representation (3-LVs) shown in Figure 2-7b, the first three LVs explained 47% of the spectral variance (Figure 2-7b) according to the type of HEM. The general trend established for the 2-LVs representation is maintained: substrates are grouped close to the center of the 3-axes figure while HEMs/substrates are projected further out from the origin. QCL spectra for TB and TNT/TB, PETN/TB and RDX/TB have been neatly grouped in the octant between LV-1(-) and LV-2(+). This fact in itself can be attributed to the distinct spectroscopic properties of the substrate: black polyester fabric. Spectra for CB and PETN/CB and TNT/CB have been projected to the octants LV-2(+)/LV-1(+) and LV-1(+)/LV-2(-); RDX/CB was projected to the LV-2(-)/LV-1(-) octant. A similar result was obtained for QCL spectra of wood and HEM/wood: PETN/wood and TNT/wood were projected to the LV-1(+)/LV-2(-) octant together with some of the neat wood QCL spectra. Most of the rest of the wood QCL spectra and RDX/wood spectra

were projected onto the LV-1(+)/LV-2(+) octant. Neater separations would have to be illustrated in higher dimensional LV spaces, however, in general, the ambitious task of grouping HEMs deposited on non-ideal substrates based on spectral similarities and discriminating the spectral features of the HEMs from those of the substrates was largely achieved.

2.3.4 Quantification of HEMs Using PLS Regressions

PLS regressions were used to analyze the spectral data and to find the best correlation between the multivariate spectral information and the HEM surface concentrations. The main concept of PLS is to obtain the most information possible concentrated in the first few loading vectors or latent variables (LV) [39-41]. PLS regressions were used to generate models for all the HEMs deposited on the investigated substrates. In addition, the root mean square error of cross validation (RMSECV), root mean square error of prediction (RMSEP), coefficient of determination from cross validation (R^2 -CV) and coefficient of determination from prediction (R^2 -Pred) were calculated and used as indications of the quality of the obtained spectral correlations. Chemometrics models based on PLS regressions were obtained using the complete spectral range measured (1000 to 1600 cm^{-1}). The sample concentrations were the same as those in the PLS-DA analyses. MC was applied to each spectrum from the spectral data set as a preprocessing step. Figure 2-8 shows some of the PLS regression plots obtained for the predicted concentration vs. measured concentrations for each HEM deposited on each substrate. Figure 2-8a shows a PLS model for RDX on TB, Figure 2-8b displays a PLS model representing TNT on CB, and Figure 2-8c presents a PLS model for PETN on wood.

The best results for RMSECV, RMSEP, R^2 -CV, and R^2 -Pred, including the number of LVs required in the PLS model, are shown in Table 2-3. Eight LVs were required to obtain the best PLS models, resulting in determination coefficients higher than 0.99, with the exception of TNT on wood, in which 9 LVs were required. Higher values of RMSECV and RMSEP were found for TNT in the three substrates tested. These results can be attributed to the higher vapor pressure of the nitroaromatic HEM when compared to PETN and RDX, leading to mass losses via sample sublimation during the course of the experiments. Based on the obtained results, it can be concluded that the PLS-based models were highly successful in correlating the surface concentrations of HEMs on the investigated substrates.

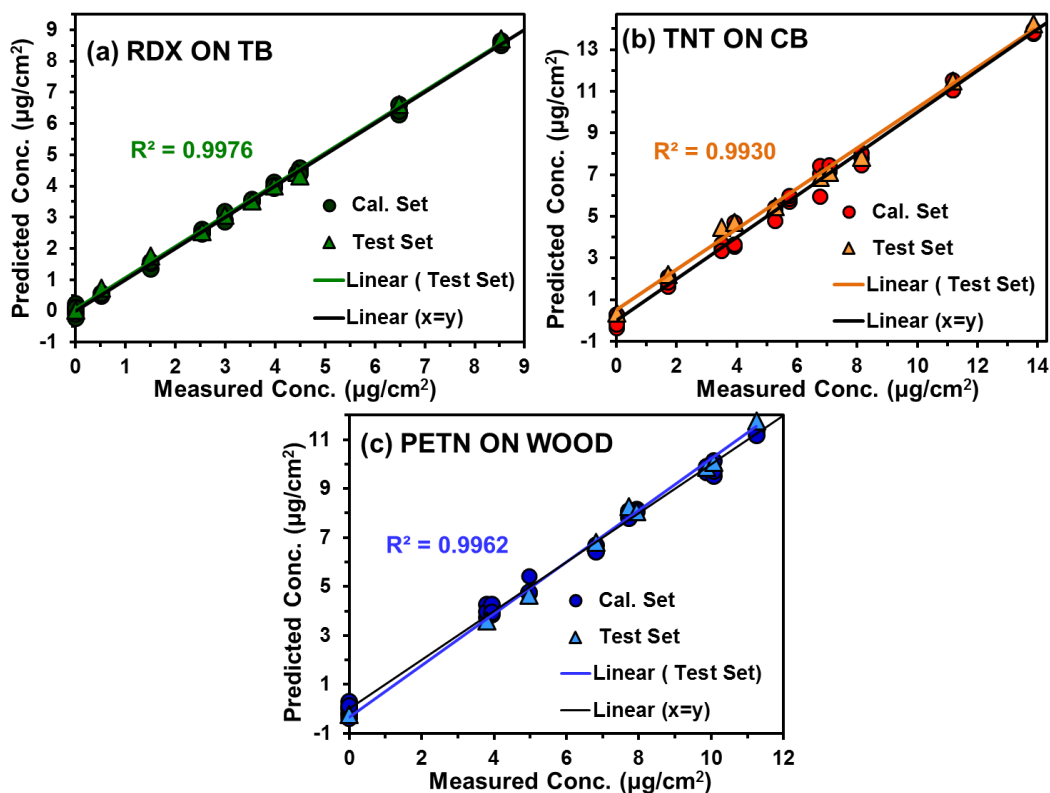


Figure 2-8. PLS regression plots of predicted vs. measured surface concentrations for HEM deposited on substrates. (a) RDX on TB, (b) TNT on CB and (c) PETN on wood. Spectral range used: 1000-1600 cm^{-1} .

Table 2-3. Statistical parameters of PLS calibration models for spectra of HEM deposited on non-ideal, low reflectivity substrates using QCLS. Spectral range: 1000-1600 cm^{-1} .

Substrate	Explosive	LV	R ² CV	R ² Pred	RMSECV ($\mu\text{g}/\text{cm}^2$)	RMSEP ($\mu\text{g}/\text{cm}^2$)
TB	PETN	8	0.998	0.999	0.12	0.09
	RDX	8	0.996	0.998	0.17	0.13
	TNT	8	0.973	0.971	0.48	0.41
CB	PETN	7	0.980	0.985	0.56	0.41
	RDX	8	0.980	0.987	0.61	0.40
	TNT	8	0.945	0.993	1.06	0.47
Wood	PETN	5	0.989	0.996	0.43	0.29
	RDX	8	0.984	0.985	0.46	0.39
	TNT	9	0.918	0.982	1.03	0.45

2.4 CONCLUSIONS

A QCL-based spectroscopy system allowed for the detection of HEMs deposited at low surface concentrations on three types of non-ideal, low reflectivity substrates: travel bag fabric (TB), cardboard (CB) and wood. Spectral profiles of HEM on transflection experiments depend on the reflectivity of the substrate. For highly reflective substrates such as Al the transflection spectra are similar to transmission spectra. For low reflectivity substrates such as TB, CB, and wood the transflection spectra are similar to reflection spectra, where nitro group bands prevail. Spectral identification using spectral correlation algorithms was not sufficiently efficient for identifying the HEMs when present on non-ideal, low reflectivity, strong mid-infrared-absorbing substrates. However, multivariate analyses were sufficiently efficient to attain the goals of this investigation. The chemometrics-based multivariate analyses used to detect the target HEMs deposited on TB and CB substrates only required first derivative and mean centering as preprocessing

steps. Generating efficient PLS-DA models for wood substrates was a greater challenge, and a third preprocessing step (SNV transformation) was required to achieve the desired discrimination on these substrates. Moreover, classifications according to the type of HEM were achieved. PLS-DA models for the investigated HEMs on the three substrates tested (general PLS-DA model) allowed for discrimination even in the presence of highly interfering and complex substrates, although the model required 12 LVs to account for 80% of the variance.

In general, QCL spectroscopy was demonstrated to be useful for developing a rapid screening methodology for detection and discrimination of HEMs from non-ideal, low reflectivity, highly interfering substrates when coupled with chemometrics tools such as PLS and PLS-DA analyses. When a reference spectrum of the neat substrate can be acquired prior to acquiring the HEM/substrate spectrum, the HEM can be readily identified from a single quick measurement. Multivariate analysis can be used to render the methodology in a more statistically robust one. Finally, PLS models demonstrated the capability of predicting the surface concentrations of HEMs on the substrates tested using a maximum of 8 LVs to obtain R^2 values higher than 0.9.

2.5 ACKNOWLEDGEMENTS

This contribution was supported by the U.S. Department of Defense, Agreement Number: W911NF-11-1-0152. The authors would also like to acknowledge contributions from Dr. Richard T. Hammond of the U.S. Army Research Office, DOD.

The contribution was also supported by the Defense Threat Reduction Agency (DTRA), DOD under grant # DODRIF11-DTRA020-P-0017: "IED Sentry Based on Mid-Infrared

Laser Arrays” awarded to Eos Photonics, Cambridge, MA. Contributions by Dr. Mark Witinski are also gratefully acknowledged.

Support from the U.S. Department of Homeland Security under Award Number 2013-ST-061-ED0001 is also acknowledged. However, the views and conclusions contained in this document are those of the authors and should not be considered as a representation of the official policies, either expressed or implied, of the U.S. Department of Homeland Security.

2.6 REFERENCES

- [1]. D.S. Moore, *Instrumentation for Trace Detection of High Explosives*. Review of Scientific Instruments, 2004. **75**(8): p. 2499-2512.
- [2]. J.R. Castro-Suarez, L.C. Pacheco-Londoño, M. Vélez-Reyes, M. Diem, T.J. Tague and S.P. Hernández-Rivera, *FT-IR Standoff Detection of Thermally Excited Emissions of Trinitrotoluene (TNT) Deposited on Aluminum Substrates*. Applied Spectroscopy, 2013. **67**(2): p. 181-186.
- [3]. L.C. Pacheco-Londoño, J.R. Castro-Suarez and S.P. Hernández-Rivera, *Detection of Nitroaromatic and Peroxide Explosives in Air Using Infrared Spectroscopy: QCL and FTIR*. Advances in Optical Technologies, 2013. **2013**: p. 1-8 pages.
- [4]. G. Mogilevsky, L. Borland, M. Brickhouse and A.W. Fountain III, *Raman Spectroscopy for Homeland Security Applications*. International Journal of Spectroscopy, 2012. **2012**: p.1-12.
- [5]. W. Ortiz-Rivera, L.C. Pacheco-Londoño and S.P. Hernández-Rivera, *Remote Continuous Wave and Pulsed Laser Raman Detection of Chemical Warfare Agents*

- Simulants and Toxic Industrial Compounds*. Sensing and Imaging: An International Journal, 2010. **11**(3): p. 131-145.
- [6]. H. Gunzler and H.-U. Gremlich, *IR Spectroscopy: an Introduction*. Weinheim, Germany: Wiley-VCH, 2002.
- [7]. A. Banas, K. Banas, M. Bahou, H. O. Moser, L. Wen, P. Yang, Z. J. Li, M. Cholewa, S. K. Lim and Ch. H. Lim, *Post-blast Detection of Traces of Explosives by Means of Fourier Transform Infrared Spectroscopy*. *Vibrational Spectroscopy*, 2009. **51**(2): p. 168–176.
- [8]. K. Banas, A. Banas, H.O. Moser, M. Bahou, W. Li, P. Yang, M. Cholewa and S.K. Lim, *Multivariate Analysis Techniques in the Forensics Investigation of the Postblast Residues by Means of Fourier Transform-Infrared Spectroscopy*. *Analytical Chemistry*, 2010. **82**(7): p. 3038-3044.
- [9]. L.C. Pacheco-Londoño, W. Ortiz-Rivera, O.M. Primera-Pedrozo and S.P. Hernández-Rivera, *Vibrational Spectroscopy Standoff Detection of Explosives*. *Analytical and Bioanalytical Chemistry*, 2009. **395**(2): p. 323-335.
- [10]. J.R. Castro-Suarez, L.C. Pacheco-Londoño, W. Ortiz-Rivera, M. Vélez-Reyes, M. Diem and S.P. Hernández-Rivera, *Open Path FTIR Detection of Threat Chemicals in Air and on Surfaces*. *Proc. SPIE*, 2011. **8012**: p.801209-801209.
- [11]. J. Faist, F. Capasso, D.L. Sivco, C. Sirtori, A.L. Hutchinson and A.Y. Cho, *Quantum Cascade Laser*. *Science*, 1994. **264**(5158): p. 553-556.
- [12]. J. Faist, F. Capasso, C. Sirtori, D.L. Sivco, J.N. Baillargeon, A.L. Hutchinson, S.G. Chu and A.Y. Cho, *High Power Mid-Infrared ($\lambda \sim 5 \mu\text{m}$) Quantum Cascade Lasers*

- Operating above Room Temperature*. Applied Physics Letters, 1996. **68**(26): p. 3680-3682.
- [13]. C.W. Van Neste, L.R. Senesac and T. Thundat. *Standoff Spectroscopy of Surface Adsorbed Chemicals*. Analytical Chemistry, 2009. **81**(5): p. 1952–1956.
- [14]. A.C. Padilla-Jiménez, W. Ortiz-Rivera, C. Ríos-Velázquez, I. Vázquez-Ayala and S.P. Hernández-Rivera, *Detection and Discrimination of Microorganisms on Various Substrates with QCL Spectroscopy*, Optical Engineering, 2014. **53**(6): p. 061611-1 – 061611-10.
- [15]. M.B. Pushkarsky, I.G. Dunayevskiy, M. Prasanna, A.G. Tsekoun, R. Go and C.K.N. Patel, *High-Sensitivity Detection of TNT*. Proceedings of the National Academy of Sciences, 2006. **103**(52): p. 19630–19634.
- [16]. C.K.N. Patel, *Laser Based In-Situ and Standoff Detection of Chemical Warfare Agents and Explosives*. Proc. SPIE. 2009. **7484**: p. 748402-748402.
- [17]. C. Bauer, U. Willer and W. Schade, *Use of Quantum Cascade Lasers for Detection of Explosives: Progress and Challenges*. Optical Engineering, 2010. **49**(11): p. 111126-111126-7.
- [18]. J. Hildebrand, J. Herbst, J. Wöllenstein, A. Lambrecht. “Explosive Detection Using Infrared Laser Spectroscopy”. Proc. SPIE. 2009. 7222: 72220B.
- [19]. F. Fuchs, S. Hugger, M. Kinzer, R. Aidam, W. Bronner, R. Losch and Q. Yang, *Imaging Standoff Detection of Explosives Using Widely Tunable Mid Infrared Quantum Cascade Lasers*. Optical Engineering, 2010. **49**(11): p. 111127-111127-8.

- [20]. J.D. Suter, B. Bernacki, M.C. Phillips, *Spectral and Angular Dependence of Mid-Infrared Diffuse Scattering From Explosives Residues for Standoff Detection Using External Cavity Quantum Cascade Lasers*. Appl. Phys. B, 2012. **108**(4): p. 965–974.
- [21]. J.R. Castro-Suarez, Y.S. Pollock and S.P. Hernández-Rivera, *Explosives Detection Using Quantum Cascade Laser Spectroscopy*. Proc. SPIE, 2013. **8710**: p. 871010-871010.
- [22]. E.R. Deutsch, P. Kotidis, N. Zhu, A.K. Goyal, J. Ye, A. Mazurenko, M. Norman, K. Zafiriou, M. Baier and R. Connors, *Active and Passive Infrared Spectroscopy for the Detection of Environmental Threats*. Proc. SPIE, 2014. **9106**: p. 91060A-9-91060A-9.
- [23]. S. Kim, D. Lee, X. Liu, C. Van Neste, S. Jeon and T. Thundat, *Molecular Recognition Using Receptor-Free Nanomechanical Infrared Spectroscopy Based on a Quantum Cascade Laser*. Scientific reports, 2013. **3**: Article number 1111.
- [24]. J. Ledgard, *The Preparatory Manual of Explosives*. 2007. 3rd Ed.
- [25]. J.M. Chalmers, *Mid-Infrared Spectroscopy: Anomalies, Artifacts and Common Errors*. In Handbook of vibrational spectroscopy, 2006. J.M. Chalmers and P.R. Griffiths, Eds. Chichester, John Wiley and Sons, vol. 3.
- [26]. P. Bassan, H.J. Byrne, J. Lee, F. Bonnier, C. Clarke, P. Dumas, E. Gazi, M.D. Brown, N.W. Clarke, and P. Gardner, *Reflection Contributions to the Dispersion Artefact in FTIR Spectra of Single Biological Cells*. Analyst 2009. **134**(6): p. 1171-1175.
- [27]. J. Clarkson, W.E. Smith, D.N. Batchelder, D.A. Smith and A.M. Coats, *A Theoretical Study of the Structure and Vibrations of 2,4,6-Trinitrotoluene*. Journal of Molecular Structure, 2003. **648**(3): p. 203–214.

- [28]. W.F. Perger, J. Zhao, J.M. Winey and Y.M. Gupta, *First-Principles Study of Pentaerythritol Tetranitrate Single Crystals under High Pressure: Vibrational Properties*. Chemical physics letters, 2006. **428**(4): p. 394–399.
- [29]. R.L. Prasad, R. Prasad, G.C. Bhar and S.N. Thakur, *Photoacoustic Spectra and Modes of Vibration of TNT and RDX at CO₂ Laser Wavelengths*. Spectrochimica Acta, Part A, 2002. **58**(14): p. 3093-3102.
- [30]. R.J. Karpowicz and T.B. Brill, *Comparison of the Molecular Structure of Hexahydro-1,3,5-Trinitro-s-Triazine in the Vapor, Solution, and Solid Phases*. The Journal of Physical Chemistry, 1984. **88**(3): p. 348–352.
- [31]. D.M. Hembree and H.R. Smyrl, *Anomalous Dispersion Effects in Diffuse Reflectance Infrared Fourier Transform Spectroscopy: A Study of Optical Geometries*. Applied Spectroscopy, 1989. **43**(2): p. 267-274.
- [32]. M. Miljković, B. Bird and M. Diem, *Line Shape Distortion Effects in Infrared Spectroscopy*. Analyst, 2012. **137**(17): p. 3954-3964.
- [33]. ASTM E2310 - 04(2009), *Standard Guide for Use of Spectral Searching by Curve Matching Algorithms with Data Recorded Using Mid-Infrared Spectroscopy*. 2009
- [34]. J.C. Reid and E.C. Wong, *Data-Reduction and Search System for Digital Absorbance Spectra*. Applied Spectroscopy, 1966. **20**(5): p. 320-325.
- [35]. K. Tanabe and S. Saeki, *Computer Retrieval of Infrared Spectra by a Correlation Coefficient Method*. Analytical Chemistry, 1975. **47**(1): p. 118-122.
- [36]. J.D Rodriguez, B.J Westenberger, L.F. Buhse and J.F. Kauffman, *Quantitative Evaluation of the Sensitivity of Library-Based Raman Spectral Correlation Methods*. Analytical Chemistry, 2011. **83**(11): p. 4061-4067.

- [37]. S. Lee, H. Lee and H. Chung, *New Discrimination Method Combining Hit Quality Index Based Spectral Matching and Voting*. *Analytica Chimica Acta*, 2013. **758**(3): p. 58–65.
- [38]. M. Boruta, *FT-IR Search Algorithm – Assessing the Quality of a Match*. *Spectroscopy*, 2012. **27**(8): p. s26-s33.
- [39]. M. Barker and W. Rayens, *Partial Least Squares for Discrimination*. *Journal of Chemometrics*, 2003. **17**(3): p. 166-173.
- [40]. R.G. Brereton, *Chemometrics for Pattern Recognition*, 2009. Chichester, England. The Atrium, Southern Gate: John Wiley & Sons Ltd.
- [41]. D. Ballabio and V. Consonni, *Classification Tools in Chemistry. Part 1: Linear Models. PLS-DA*. *Analytical Methods*, 2013. **5**(16): p. 3790-3798.
- [42]. T.C. O'Haver, A.F. Fell, G. Smith, P. Gans, J. Sneddon, L. Bezur, R.G. Michel, J.M. Ottaway, J.N. Miller, T.A. Ahmad, B.P. Chadburn and C.T. Cottrell, *Derivative Spectroscopy and its Applications in Analysis*. *Analytical Proceedings*, 1982. **19**(1): p. 22-46.

VI. CHAPTER 3

DETECTION OF NITROAROMATIC AND PEROXIDE EXPLOSIVES IN AIR USING INFRARED SPECTROSCOPY: QCLS AND FT-IR

OVERVIEW

A methodology for processing spectroscopic information using a chemometrics based analysis was designed and implemented in the detection of highly energetic materials (HEMs) in the gas phase at trace levels. The presence of the nitroaromatic HEM 2,4-dinitrotoluene (2,4-DNT) and the cyclic organic peroxide triacetone triperoxide (TATP) in air was detected by chemometrics enhanced vibrational spectroscopy. Several infrared experimental setups were tested using traditional heated sources (Globar), modulated and non-modulated FT-IR and quantum cascade laser (QCL)-based dispersive IR spectroscopy. The data obtained from the gas phase absorption experiments in the mid-infrared (MIR) region were used for building the chemometrics models. Partial least squares-discriminant analysis (PLS-DA) was used to generate pattern recognition schemes for trace amounts of explosives in air. The QCL based methodology exhibited a better capacity for the discrimination for the detected presence of HEM in air compared to other methodologies.

3.1 INTRODUCTION

The detection of highly energetic materials (HEMs) at trace levels in air remains a subject of great importance to national defense and security. In the past few years, most of the published reports have focused on the detection of these important chemical compounds. However, the majority of them require some type of sampling [1, 2]. Obtaining samples in the field is the principal disadvantage of most explosive detection devices because the person doing the sampling is at risk.

Most of the analytical techniques employed for development of methodologies for HEM detection are based on spectroscopic and chromatographic techniques [1, 2]. Trace amounts of 2,4-dinitrofluorene (2,4-DNF) in air have been detected and discriminated by surface enhanced Raman spectroscopy (SERS) using a gold surface sensor [3]. These sensors generate a response in the presence or absence of 2,4-DNF and other volatile nitroaromatic HEMs in air. In this case, the sample vapor was introduced to the sensor with a fan. High-speed fluorescence spectroscopy is another method for detection for nitroaromatic HEM in the air. This method employs silica microspheres coated with a highly sensitive fluorescent polymer that responds by quenching the fluorescence when HEM molecules attach to the polymer [1,2,5-8]. 2,4-DNF can also be detected and quantified by measuring the IR acoustic wave in polymer coated surfaces [9]. In this method, the presence of 2,4-DNF generates a change in the frequency of the acoustic wave on the surface, and this change is used for detection and quantification.

Air sampling with a solid-phase extraction cartridge to collect a toluene/methyl-tertbutyl ether analyte using a modified supercritical fluid extraction apparatus followed by separation and measurement of the extracted analyte by GC has also been used for the

analysis of nitroaromatic HEM [10]. The detection of nitroaromatic HEM in air can also be performed by extraction with C-18 solid-phase membranes. In this case, the analyte is desorbed directly in a chromatographic mobile phase [11]. The detection of triacetone triperoxide (TATP) in air has been reported using a gas-washing sampling technique [12]. HPLC with post-column UV irradiation and photometric detection following photochemical degradation of TATP has also been used for detection [12,13].

The use of chemometrics (multivariate analysis) with spectroscopic data in HEM detection has been very valuable because it has allowed for the exploration of very complex ambient matrices [14,15]. Many chemometrics tools have been developed and tested. However, the most commonly used tools employed to identify, quantify and classify data sets are those that make use of principal components analysis (PCA), partial least squares (PLS), discriminant analysis (DA), as well as their combined usage in PLS-DA, and hierarchical cluster analysis (HCA). PCA transforms a set of variables into fewer variables (called dimensions, principal components, or components) that contain most of the information (variance) from the initial data set. The PCA algorithm seeks to save the information from a large number of variables in a small number of uncorrelated components with minimal loss of information. One of the main reasons for performing a PCA is to reduce the number of variables to a few uncorrelated dimensions that contain as much information as possible (used to avoid multi-collinearity in multiple regressions, among other things) [15]. PLS is a linear analysis routine that is used to design and build robust calibration models for quantitative analysis. PLS regression analysis is a quantitative spectral decomposition technique that is closely related to PCA regression [16]. PLS uses the concentration information during the decomposition process, which

causes the spectra containing higher constituent concentrations to be weighted more heavily than those with lower concentrations. The main idea of PLS is to obtain as much information about the concentration as possible into the first few latent variables (number of components) [17]. Linear discriminant analysis (LDA or DA) is a multivariate technique that allows for the differentiation of separate objects from distinct populations and allocates new objects into populations previously defined [18]. The usefulness of this methodology is to determine a relationship of belonging or not belonging to a previously defined group.

The application of pattern recognition to infrared spectroscopy can be found in the current literature. PCA was used to analyze the FTIR spectra of mixtures of two monomers [19]. Discrimination between mayonnaise samples that contained different vegetable oils was achieved by PLS-DA of near infrared spectral data [20]. PLS-LDA has also been used in other areas of science and engineering, including biomedical studies such as the classification of tumors [21], early detection of diabetes related to changes in the skin [22] and fault diagnosis in chemical processes [23].

Detection and discrimination of HEM are important in applications for national defense and security. Being able to detect and prevent a chemical/biological threat long before any damage to civilians, military personnel and private or public property is a goal of agencies in charge of public security and national defense. To a large extent, remote detection modalities will benefit from chemometrics enhanced spectroscopic detection.

In this report, infrared vibrational detection of highly energetic materials, such as 2,4-DNT and TATP, present in the gas phase in air was performed. The detection experiments were performed in the active mode using two source types including a traditional globar

IR source for detection using FT-IR spectrometers (for both, modulated and unmodulated light) and a quantum cascade laser (QCL) IR source for detection with a dispersive spectrometer. PLS-DA was used to generate pattern recognition schemes for trace amounts of explosives in air from the obtained IR spectra. Classificatory capacities from different models based on PLS-DA were used to establish the best experimental setup for the detection and classification of these explosives in the gas phase.

3.2 EXPERIMENTAL SETUP

3.2.1 Materials

The reagents used in this investigation included acetone (CH_3COCH_3 , 98% w/w, Sigma-Aldrich Chemical Co., Milwaukee, WI, USA), hydrogen peroxide (H_2O_2 , 50% in water, Sigma-Aldrich), hydrochloric acid (HCl, 12 M, Merck, VWR, Inc., West Chester, PA, USA), sulfuric acid (H_2SO_4 , 18 M, Merck) and dimethyl ether (CH_3OCH_3 , Sigma-Aldrich). Standard solutions of 2,4-DNT 1000 parts per million (ppm) GC/MS primary standards were obtained from Restek Corp. (Bellefonte, PA) and from Chem Service, Inc. (West Chester, PA). Crystalline samples of 2,4-DNT were purchased from Chem Service, Inc. (West Chester, PA).

3.2.2 Synthesis of TATP

TATP cannot be purchased from chemical reagents suppliers. Therefore, it was prepared in small quantities as needed due to the high thermal instability of this powerful explosive. A white crystalline precipitate was obtained using a conventional synthesis method. The

crystals were filtered and washed using distilled water followed by re-crystallization from methyl ether.

3.2.3 Instrumentation

A Fourier transform IR (FT-IR) interferometer model IFS 66v/S (Bruker Optics, Billerica, MA, USA) was used for the experiments. This system had an evacuable bench equipped with several sources, detectors, beam splitters and other accessories to perform experiments on solid, liquid and gas samples from the far IR region (to 50 cm^{-1}) to the near IR region (as high as 7500 cm^{-1}). For the experiments described, the system was equipped with a deuterated triglycine sulfate (DTGS) detector and a potassium bromide (KBr) beam splitter. An EM-27 open path (OP) FT-IR interferometer (Bruker Optics) was used to obtain the IR spectral information from the TATP samples with a thermoelectrically (TE) cooled mercury-cadmium telluride (MCT) detector. A pre-dispersive IR spectrometer equipped with a quantum cascade laser (QCL) source and a thermoelectrically (TE) cooled MCT detector (model LaserTune™; Block Engineering, Marlborough, MA) was employed to obtain spectral information of the TATP samples. An Agilent 6890 gas chromatograph (GC) coupled to an Agilent 5893 mass selective detector (MSD) was used for qualitative analyses. An Agilent Technologies model 6890N, Network GC system with micro cell, ^{63}Ni Electron Capture Detector ($\mu\text{-ECD}$) was also used for the quantitative analyses. A capillary column: HP-5 MS 5% phenyl methyl siloxane: 30 m, 250 μm in diameter and 0.25 μm of film thickness was used.

3.3 MEASUREMENTS AND ANALYSES

3.3.1 Experiment

Figure 3-1 shows the schematic diagram of the experimental setup used in the investigation. Three types of experiments were performed. The setup for the first experiment is shown in Figure 3-1a. The HEM samples were placed on the bottom of 500 mL Erlenmeyer flasks. A flow of dry air (1-16 mL/s) at several temperatures (0-38°C) was used. The temperature was regulated by either scanning in the range of temperature or by using point-by-point fixed temperature measurements. Trace amounts of explosives in the gas phase were dragged from the surface by the air flow and transported to an IR gas cell for detection. Spectra were recorded using the instrument at 4 cm^{-1} of resolution and 25 scans. The spectral range was from 400-4000 cm^{-1} .

The number of spectra obtained was: 799 for 2,4-DNT/air; 120 for TATP/air; and 1881 spectra of ambient air. Figure 3-1b shows a schematic representation of the EM-27 interferometer setup employed to collect absorption spectra excited by a Globar source. All of the active mode experiments were performed at ambient temperature (25°C) at 30 scans and 4 cm^{-1} resolution. Sets of 100 air spectra, air with TATP and air with DNT with a spectral range of 650-4000 cm^{-1} were collected.

A third experiment was performed using a quantum cascade laser (QCL) as the source with the Block Engineering LaserTune™ spectrometer. All of the active mode experiments were performed at the lab temperature of 20°C with 1 scan at 4 cm^{-1} resolution. The spectral range was from 830 to 1430 cm^{-1} . Forty-four spectra of air with 2,4-DNT, 25 spectra of air with TATP and 37 spectra of air were obtained. The presence of TATP in the air was determined by GC-MS, and the concentration of 2,4-DNT in the

air for different fluid conditions were calculated using a calibration curve from GC- μ ECD, which was only performed for the first experiment.

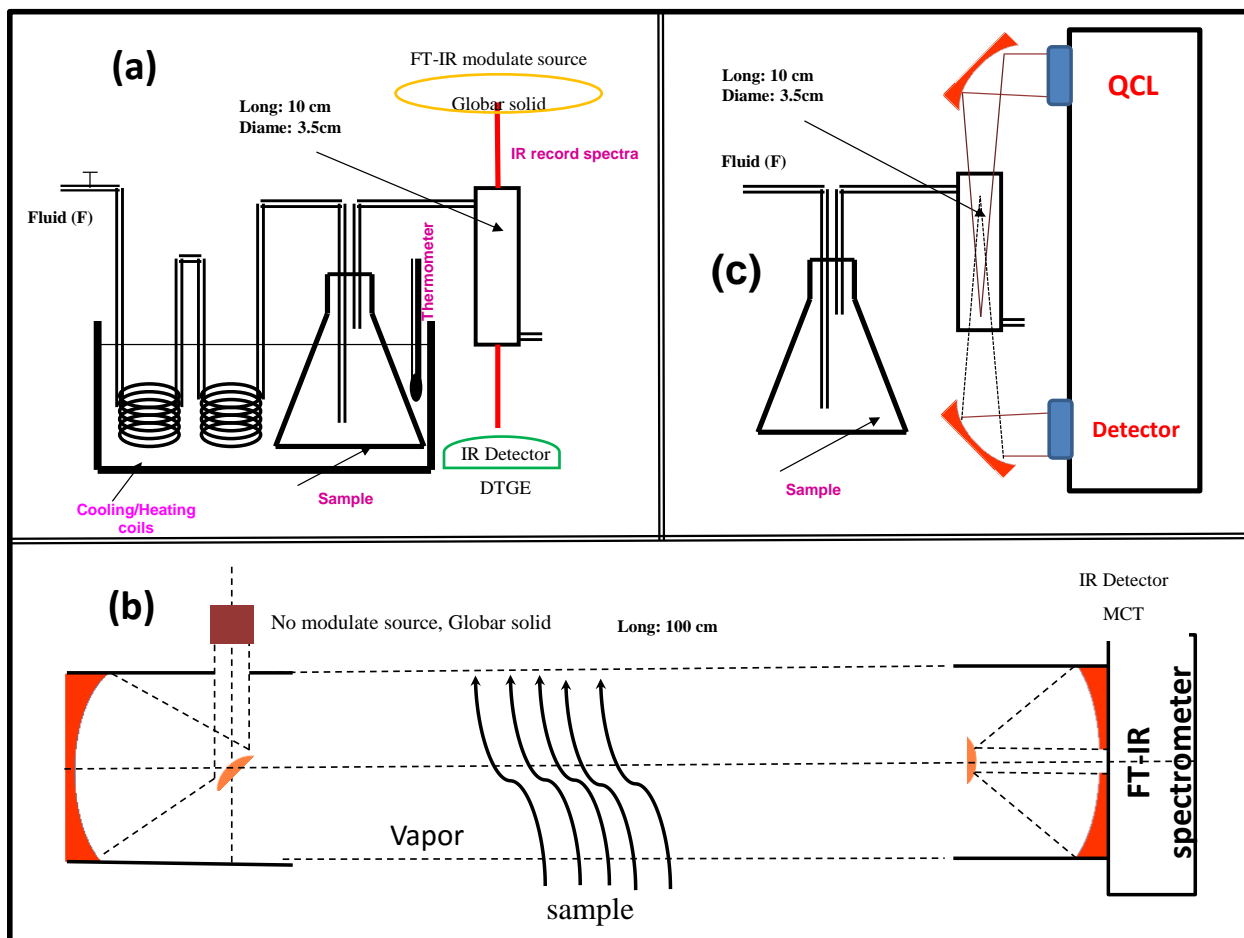


Figure 3-1. Schematic diagram of the experimental setup. (a). FT-IR instrument using modulated light source. (b). Open path FT-IR. (c). Quantum cascade scan.

3.3.2 Partial Least Squares (PLS) – Discriminant Analysis (DA)

PLS-DA runs were performed using the OPUS™ 6.0 software (Bruker Optics) combined with the Statgraphics Plus™ v. 15.2 (Statpoint Technologies, Inc., Warrenton, VA, USA) statistical analysis software. The models were evaluated using internal validation,

statistical significance (**p**) and the percentage of cases correctly classified (**PCCC**). For internal validation, each spectrum was successively removed from the data set and discriminated from a new model built from the remaining spectra. This procedure was performed for each of the spectra in the data set, and the predicted discrimination was compared with the experimental observations. The generated percentage of cases correctly classified is called the cross-percentage of cases correctly classified (**PCCCC**) or the leave-one-out cross-validation (LOOCV or CV) procedure. The other statistical indicators that were used included the Wilks' lambda and canonical correlation.

3.4 RESULTS AND DISCUSSION

Figure 3-2 shows the frequency distribution for the CV of air with TATP and DNT. The solid line represents the data for air with the analyte of interest, and the dotted line represents the data for clean air and air with other analytes. Good discrimination was obtained in all of the statistical experiments. The evaluation is shown in Table 3-1. The PCCC for all of the models was 100.0%, and complete classification is observed. However, the cross-validation PCCCC was not 100.0% for DNT samples.

In the FT-IR model with a modulated Globar source, the PCCCC for TATP was 100% but was lower for 2,4-DNT. This result can be attributed to the fact that pure air was only analyzed at 25°C whereas 2,4-DNT was analyzed from 0°C to 38°C. In this model for 2,4-DNT, 0.25% of the sample was not correctly classified. These data missed the detection of or indicated a false negative for air with 2,4-DNT at low temperatures where the sublimation of DNT is very small. For this model of 2,4-DNT, the sensitivity was 100.00%, the specificity was 99.75% and the false alarm rate was 0.00%.

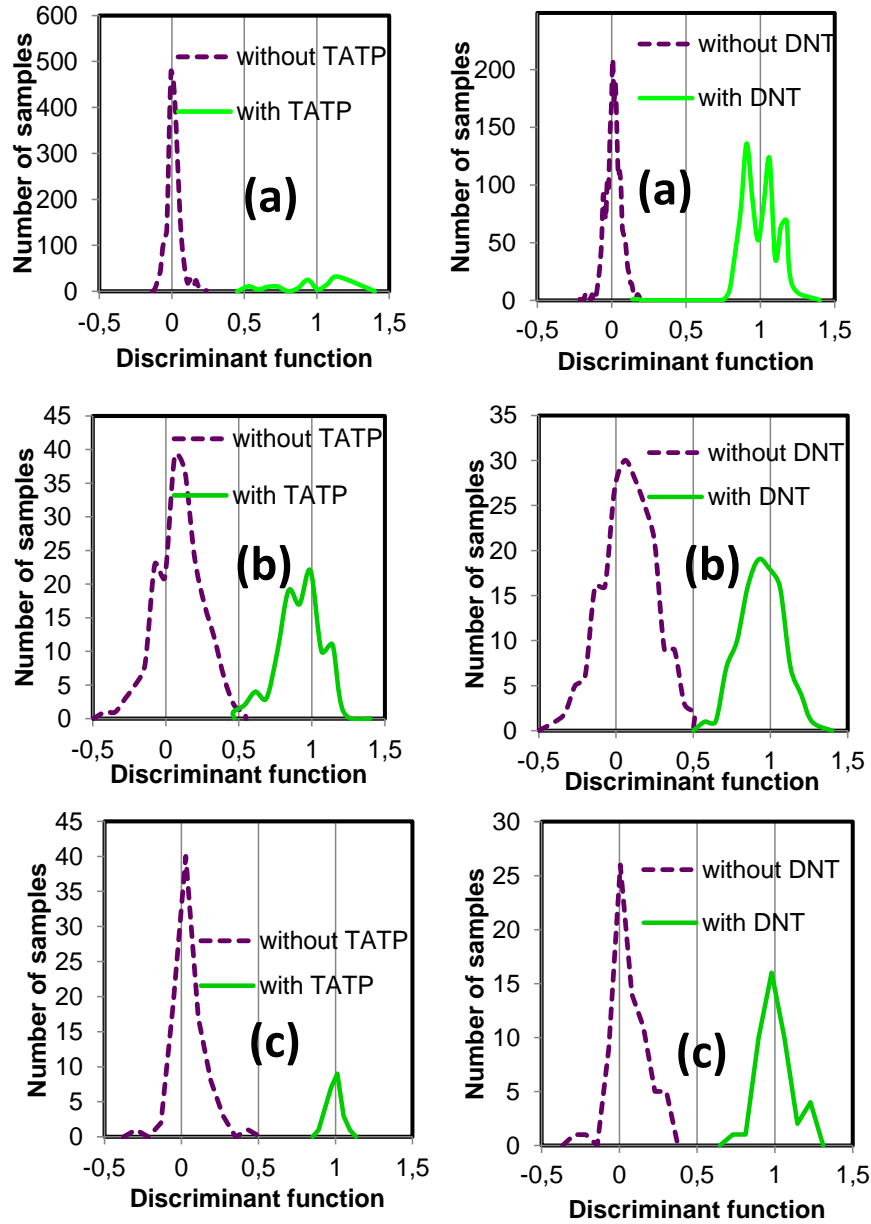


Figure 3-2. (a). Histogram for discrimination using modulated source FT-IR. (b). Histogram for discrimination using non-modulated source FT-IR. (c). Histogram for discrimination using QCL.

In the second model (unmodulated FT-IR), the PCCC for all of the models constructed were also 100.0%, but the PCCC for 2,4-DNT was 99.67%. In these cases, the false alarm rates were 0.50%, and the sensitivities were 99.50%. This result is an indication

that samples of air or air with TATP were discriminated better than air with 2,4-DNT. In these cases, one of the air samples was poorly discriminated because this experiment was open to the surroundings resulting in possible contamination in the lab. In this setup interferences from ambient water vapor and CO₂ were high. Therefore, in the model using the entire IR spectral region measured (600-4000 cm⁻¹), it was necessary to eliminate the sub-spectral regions of 4000-3541, 2384-2295 and 1758-1490 cm⁻¹, resulting in improvement of the model, as summarized in Table 3-1.

In the third model (QCL scan), all of the samples were correctly classified. However, the number of samples analyzed must be considered, and the number of variables in this experiment is lower compared to the other experiments. The experimental conditions are not fully comparable because the intensity of this source is much higher than those of the other experiments and the sampling path is smaller for this system.

For the models to have highly significant statistical merit according to the canonical correlation coefficient ($p < 0.0001$), the functions must have an excellent ability to determine the group differences. Wilks' Lambda value indicates how many times the variance is not explained by group differences. Because these values were small, highly correlated differences were established.

Table 3-1. Validation parameters for the various models constructed.

Parameter	modulated FTIR (model 1)		unmodulated FTIR (model 2)		QCL scan (model 3)	
	TATP	DNT	TATP	DNT	TATP	DNT
Wilks' lambda	0.12	0.03	0.09	0.11	0.05	0.06

Canonical correlatio	0.94	0.98	0.96	0.94	0.98	0.97
PCCC	100.00%	100.00%	100.00%	100.00%	100.00%	100.00%
PCCCC	100.00%	99.94%	100.00%	99.97%	100.00%	100.00%
Sensibility	100.00%	100.00%	100.00%	99.50%	100.00%	100.00%
Specificity	100.00%	99.75%	100.00%	100.00%	100.00%	100.00%
False alarm	0.00%	0.00%	0.00%	0.50%	0.00%	0.00%
Missed detection	0.00%	0.25%	0.00%	0.00%	0.00%	0.00%
Loadings	7	7	10	10	5	5
Samples (N)	3079	3079	300	300	106	106
p-value	< 0.0001	< 0.0001	< 0.0001	< 0.0001	< 0.0001	< 0.0001

Other models were generated using only the region of 873-1400 cm^{-1} or the region of emission of the QCL to compare the technique with the FT-IR based experiments. The QCL-based experiments were better than the modulated source FT-IR setup, which, in turn, were better than the non-modulated source FT-IR setup. The validation information is shown in Table 3-2. A high significance ($p < 0.0001$, equivalent to $> 99.99\%$ confidence level) for all of the models were found, indicating that the resulting parameters are highly reliable and the comparison between techniques is highly dependable. The high power QCL scan produces a high sensitivity for trace level detection in air but the modulated source FT-IR is close in performance to the QCL-based methodology. This result indicates that the modulation of light (using an interferometer) before reaching the sample increases the sensitivity [24] compared to a non-modulated source FT-IR where the light first interacts with the sample prior to entering the interferometer.

Table 3-2. Validation parameters for models in the sub-spectral range: 850-1400 cm⁻¹

Parameter	modulated FTIR (model 1)		unmodulated FTIR (model 2)		QCL scan (model 3)	
	TATP	DNT	TATP	DNT	TATP	DNT
Wilks' lambda	0.15	0.04	0.55	0.54	0.05	0.06
Canonical correlation	0.92	0.98	0.67	0.65	0.98	0.97
PCCC	99.74%	99.98%	92.00%	93.33%	100.00%	100.00%
PCCCC	99.73%	99.97%	82.00%	78.33%	100.00%	100.00%
Sensibility	100.00%	100.00%	81.00%	77.00%	100.00%	100.00%
Specificity	93.33%	99.87%	84.00%	81.00%	100.00%	100.00%
False alarm	0.00%	0.00%	16.00%	19.00%	0.00%	0.00%
Missed detection	6.67%	0.13%	19.00%	23.00%	0.00%	0.00%
Loadings	10	10	10	10	5	5
p-value	< 0.0001	< 0.0001	< 0.0001	< 0.0001	< 0.0001	< 0.0001

The loading for models of the region (870-1400 cm⁻¹) are shown in Figure 3-3. The band observed for TATP at 1200 cm⁻¹ that was tentatively assigned to C-O stretching [25, 26] is the largest contributor to the loadings calculated by the models for modulated source FT-IR and QCL source. However, in the unmodulated source FT-IR experiments, the same result was not found: the first loading has the spectral information shifted. Other bands that contribute occur at 890 cm⁻¹ and 939 cm⁻¹ which are tentatively assigned to O-O stretching [25, 26]. The same analysis applies for all of the other loadings (data not

shown). This indicates that the discrimination is generated by a combination of all of the loadings. The QCL model requires only 5 loadings; FT-IR based models require 7 (full spectrum) or 10 (spectral width) loadings.

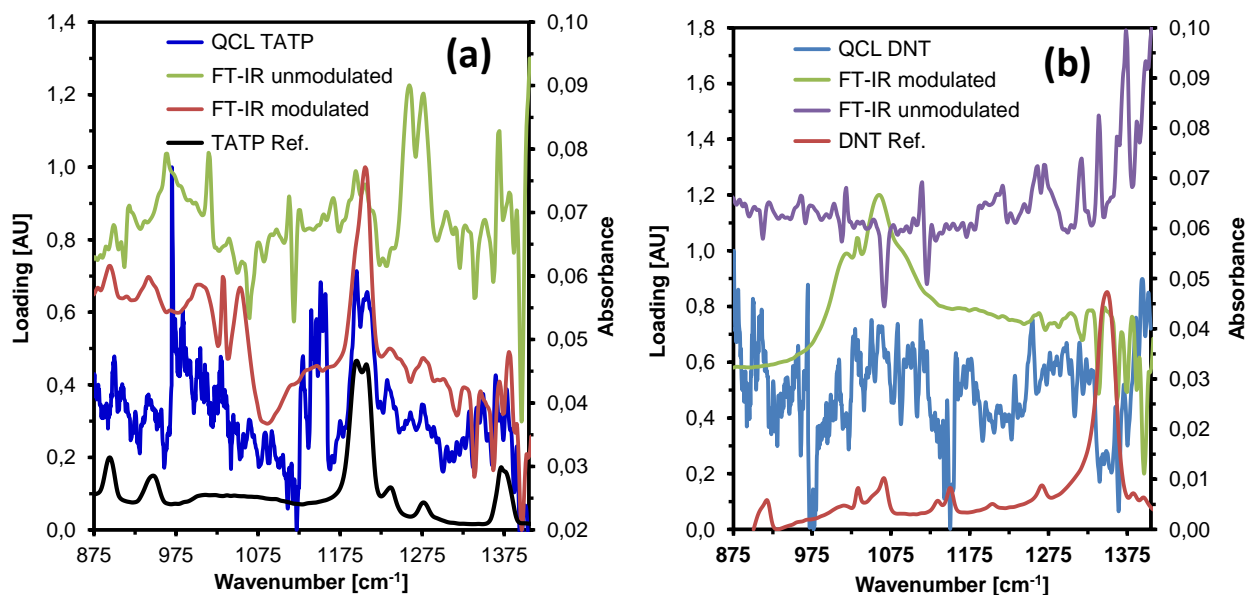


Figure 3-3. (a). First loadings for TATP models for the region (873-1400 cm^{-1}). (b). First loadings for DNT models for the region (873-1400 cm^{-1}). Reference gas phase spectra included.

3.4.1 Proof of presence of 2,4-DNT and TATP in air at trace levels

The concentration of 2,4-DNT in air for different flow conditions and temperatures was calculated via a calibration curve obtained by GC- μ ECD (Table 3-3). The presence of TATP was also established using GC-MS. To demonstrate the presence of the infrared signal in air, a small amount of TATP or 2,4-DNT (0.1 μg) was deposited on a plate and introduced into a gas cell of 38.7 cm^3 at a pressure of 0.0001 mBar. This procedure generated a density of 2538 pg/mL (in the worst case) when all of the explosive material

sublimed and negligible amounts were suctioned by the vacuum pump. This suggests that the concentration in the cell for the gas was $\ll 2538$ pg/mL. Spectra for the trace amounts of explosive were recorded to confirm that the detector was able to detect at this concentration level (Figure 3-4). This experiment was performed using the modulated source FT-IR system.

Table 3-3. Mass of 2,4-DNT determined by GC- μ ECD for 2 mL of injected gas.

T (°C)	F (mL/s)	Peak Area	Mass (pg)	pg/mL ($\mu\text{g}/\text{m}^3$)
20	1.6	7.564.E+03	98	49
20	7.8	3.314.E+03	48	25
20	15.7	3.078.E+03	46	23
26	1.6	1.030.E+05	1202	601
26	7.8	6.650.E+04	779	390
26	15.7	5.720.E+04	672	336
38	1.6	3.800.E+05	4407	2203
15	15.7	2.793.E+03	42	21

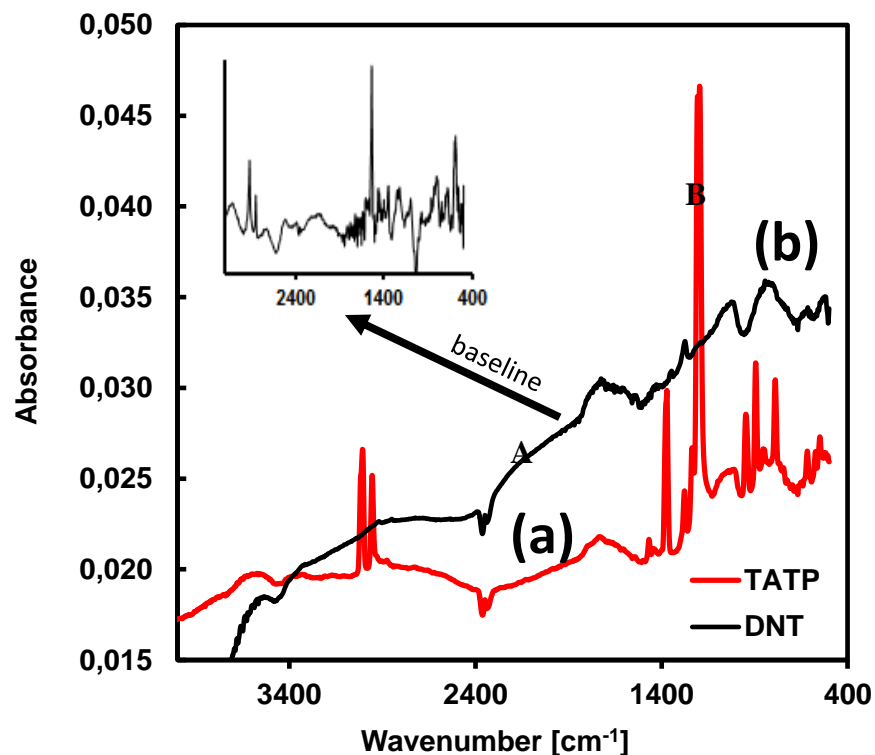


Figure 3-4. Low pressure spectra in the gas phase with baseline correction of: (a) TATP; (b) DNT.

3.4.2 Limits of Detection

The low limits of detection (LOD) have been estimated for the two better performing techniques and their corresponding models: modulated source FT-IR and mid IR (QC) laser source. In the case of the homemade explosive, TATP, LOD values were estimated as 800 pg/m³ and 300 pg/m³ for modulated FT-IR and QCL based detection, respectively. For the nitroaromatic military explosive 2,4-DNT LOD values were even lower: 31 pg/m³ and 0.7 pg/m³ for modulated source FT-IR and QCL source, respectively.

3.5 CONCLUSIONS

The results obtained in this research show that it is possible to determine the presence of peroxide-based explosives, such as TATP, and high sublimation pressure nitro compounds when they are in the gas phase mixed with air using PLS-DA regression analysis of infrared spectral data. The QCL-based results exhibited a better capacity for discrimination or detection of the presence of explosives in air compared to other techniques. This result is due to the high power and collimation of the laser source increasing the sensitivity at trace level in air. It was also demonstrated that when the light is modulated an increase of sensitivity is obtained. Possible synergies between QCL sources, which are inherently modulated, and detection schemes could generate higher sensitivity techniques for gas phase sensing of hazardous chemicals. However, technical problems related to QCL scanning generated high noise levels. This resulted in unsuccessful efforts to modulate this source. A possible solution is to stop the QCL in a wavenumber range corresponding to emission bands within the target chemicals and then modulate the source and acquire the spectra at this position; next move the QCL to another wavenumber central position close to the previous band and acquire the spectrum, and so on until the whole range of the QCL is scanned. This would provide the required sensitivity for the analysis at trace level.

3.6 ACKNOWLEDGMENTS

This contribution was supported by the U.S. Department of Defense, Agreement Number: W911NF-11-1-0152. The authors would also like to acknowledge contributions from Dr. Richard T. Hammond of the U.S. Army Research Office, DOD.

Support from the U.S. Department of Homeland Security under Award Number 2013-ST-061-ED0001 is also acknowledged. However, the views and conclusions contained in this document are those of the authors and should not be considered as a representation of the official policies, either expressed or implied, of the U.S. Department of Homeland Security.

We gratefully acknowledge contributions by Dr. Fred Haibach from Block Engineering in setting up the experimental part of the QCL based experiments involving the LaserTune™ (Block Eng., Marlborough, MA) and for his enlightening discussions.

3.7 REFERENCES

- [1]. D.S. Moore, *Instrumentation for trace detection of high explosives*. Review of scientific instruments, 2004. **75**: p. 2499-2512.
- [2]. D.S. Moore, *Recent Advances in Trace Explosives Detection Instrumentation*. Sensing and Imaging: An International Journal, 2007. **8**(1): p. 9-38.
- [3]. J.M. Sylvia, et al., *Surface-Enhanced Raman Detection of 2,4-Dinitrotoluene Impurity Vapor as a Marker To Locate Landmines*. Analytical Chemistry, 2000. **72**(23): p. 5834-5840.
- [4]. K. H. S. Chang, and V.V. Tsukruk, *Porous Substrates for Label-Free Molecular Level Detection of Nonresonant Organic Molecules*. ACS Nano, 2008. **3**(1): p. 181-188.
- [5]. K.J. Albert and D.R. Walt, *High-Speed Fluorescence Detection of Explosives-like Vapors*. Analytical Chemistry, 2000. **72**(9): p. 1947-1955.

- [6]. E.R. Menzel, L.W. Menzel, J.R. Schwierking, *A photoluminescence-based field method for detection of traces of explosives*. The Scientific World Journal, 2004. **4**: p. 725-35.
- [7]. Y. Salinas, et al., *Optical chemosensors and reagents to detect explosives*. Chemical Society reviews, 2012. **41**(3): p. 1261-96.
- [8]. Y. Salinas, et al., *Fluorogenic detection of Tetryl and TNT explosives using nanoscopic-capped mesoporous hybrid materials*. Journal of Materials Chemistry A, 2013. **1**(11): p. 3561-3564.
- [9]. G.K. Kannan, et al., *Adsorption studies of carbowax coated surface acoustic wave (SAW) sensor for 2,4-dinitro toluene (DNT) vapour detection*. Sensors and Actuators B: Chemical, 2004. **101**(3): p. 328-334.
- [10]. R. Batlle, et al., *Enhanced Detection of Nitroaromatic Explosive Vapors Combining Solid-Phase Extraction-Air Sampling, Supercritical Fluid Extraction, and Large-Volume Injection-GC*. Analytical Chemistry, 2003. **75**(13): p. 3137-3144.
- [11]. C. Sánchez, et al., *Determination of Nitroaromatic Compounds in Air Samples at Femtogram Level Using C18 Membrane Sampling and On-Line Extraction with LC-MS*. Analytical Chemistry, 2003. **75**(17): p. 4639-4645.
- [12]. R. Schulte-Ladbeck, and U. Karst, *Determination of triacetone triperoxide in ambient air*. Analytica Chimica Acta, 2003. **482**(2): p. 183-188.
- [13]. J.I. Steinfeld and J. Wormhoudt, *Explosives Detection: A Challenge for Physical Chemistry*. Annual Review of Physical Chemistry, 1998. **49**: p. 203-32.

- [14]. J. J. Perez, et al., *Classification of smokeless powders using laser electrospray mass spectrometry and offline multivariate statistical analysis*. Analytical Chemistry, 2013. **85**(1): p. 296-302.
- [15]. Jr. F.C De Lucia and J.L. Gottfried, *Influence of variable selection on partial least squares discriminant analysis models for explosive residue classification*. Spectrochimica Acta Part B: Atomic Spectroscopy, 2011. **66**(2): p. 122-128.
- [16]. J.K.V. Mardia, J.T. Kent and J.M. Biby, *Chemometrics: Statistic and Computer Application in Analytical Chemistry*, 1980, London: Academic Press.
- [17]. K.R. Beebe, R.J. Pell, and M.B. Seasholtz, *Chemometrics. A Practical Guide*, 1998, New York: John Wiley & Sons, Inc.
- [18]. C.J. Huberty, *Applied Discriminant Analysis*, 1994, New Jersey: Wiley-Interscience.
- [19]. Y. M. Kim, J.F. MacGregor, and L.K. Kostanski, *Principal component analysis of FT-IR spectra for cationic photopolymerization of mixtures of two monomers*. Chemometrics and Intelligent Laboratory Systems, 2005. **75**(1): p. 77-90.
- [20]. U.G. Indahl, et al., *Multivariate strategies for classification based on NIR-spectra— with application to mayonnaise*. Chemometrics and Intelligent Laboratory Systems, 1999. **49**(1): p. 19-31.
- [21]. Y. Tan, et al., *Multi-class tumor classification by discriminant partial least squares using microarray gene expression data and assessment of classification models*. Computational Biology and Chemistry, 2004. **28**(3): p. 235-243.
- [22]. B. Lindholm-Sethson, et al., *Multivariate analysis of skin impedance data in long-term type 1 diabetic patients*. Chemometrics and Intelligent Laboratory Systems, 1998. **44**(1–2): p. 381-394.

- [23]. Q.P. He, S.J. Qin, and J. Wang, *A new fault diagnosis method using fault directions in Fisher discriminant analysis*. AIChE Journal, 2005. **51**(2): p. 555-571.
- [24]. L.C. Pacheco-Londoño, O.M. Primera-Pedrozo, and S.P. Hernandez-Rivera, *Vibrational spectroscopy standoff detection of explosives*. Analytical and Bioanalytical Chemistry, 2009. **395**(2): p. 323-335.
- [25]. G.A. Buttigieg, et al., *Characterization of the explosive triacetone triperoxide and detection by ion mobility spectrometry*. Forensic Science International, 2003. **135**(1): p. 53-59.
- [26]. B. Brauer, et al., *Vibrational spectroscopy of triacetone triperoxide (TATP): Anharmonic fundamentals, overtones and combination bands*. Spectrochimica Acta - Part A: Molecular and Biomolecular Spectroscopy, 2008. **71**(4): p. 1438-1445.

VII. CHAPTER 4

SEPARATION, IDENTIFICATION AND QUANTIFICATION OF EXPLOSIVES USING THIN LAYER CHROMATOGRAPHY COUPLED TO QUANTUM CASCADE LASER SPECTROSCOPY

OVERVIEW

The need for instrumentation and methods for rapid detection and identification of chemical and biological threat agents in military and homeland defense settings has become an ever more important issue in modern society. Many of the samples collected for the sensing of explosives are contained in soil matrices. Other common substrates that can be targets for detection of explosives are metals, plastic, wood, cardboard, fabrics, debris, etc. This study focuses on chemical analysis of explosives, such as TNT, 2,4-DNT and PETN present in soils and other real world complex media using thin layer chromatography (TLC) coupled to mid-infrared (MIR) quantum cascade laser spectroscopy (QCLS) that allows rapid, reproducible, separation and identification of explosives in the field in short time.

The retention factor (R_f) values for TNT and PETN were determined for different solvents or solvent mixtures, using silica plates as stationary phase. The position and spot diameter of the sample on the plate of silica before and after the chromatographic run were measured and compared. The best mobile phase to separate TNT ($R_f = 0.75 \pm 0.05$) and PETN ($R_f = 0.63 \pm 0.06$) was the mixture 1:4 hexane:toluene. The spot diameters

before and after the chromatographic run, in most cases the change in size was approximately 0.5 cm.

4.1 INTRODUCTION

Modern society faces an ever increasing need for rapid methods and instrumentation for detection and identification of chemical and biological threat agents. From security anti-terrorist personnel, to first responders and law enforcement employees, such as forensic science, police officers, airport screeners, and border patrol personnel, to the Navy, Army, Air Force, and National Guard workforces, the threat of coming in contact with explosive agents is highly pervasive.

Many of the samples collected for sensing of explosives come from complex matrices containing dirt and soil. Soils can be contaminated with explosives in a number of different human activities, such as: use of explosives in training ranges, impact areas and firing ranges, explosives syntheses sites, as result of wars between nations, from used waters and wastes in clandestine laboratories, as result of terrorist events, controlled demolitions, mining, and others. These types of explosives containing samples display a broad spectrum of compounds, which are heterogeneously distributed in their matrices. Other common substrates that can be targets for detection of explosives are debris, metals, plastic, wood, cardboard, fabric, etc. Hexahydro-1,3,5-trinitro-1,3,5-triazine (RDX) is the primary explosive found in training ranges, but other munitions constituents such as 2,4,6-trinitrotoluene (TNT), 2,6-dinitrotoluene (2,4-DNT) and pentaerythritol tetranitrate (PETN) are also present in soils of military ranges.

Most of the studies that have been published on detection of explosives are based on spectroscopic and chromatographic methodologies [1-6], obtaining very low limits of detection. However, the use of chromatographic techniques in field applications has been very limited, mainly because of the lack of portability of the instrumentation. On the other hand, spectroscopic techniques have the advantage of being tested in field applications, facilitating the acquisition of data and information very fast, leading to prompt decisions based on the results obtained, thus saving numerous lives and reducing casualties. Vibrational spectroscopy has demonstrated to be valuable for detection of high explosives, homemade explosive and toxic industrial compounds [2, 8-16]. In particular, infrared spectroscopy (IRS), in various modalities, has played unique roles in detection of threat compounds [9-16]. IRS is commonly employed for detection explosives and chemical warfare agents, as well as other chemical and biological threats in military environments, in government buildings and other public safety places. The MIR spectral region comprises the spectral window from approximately 350 to 4000 cm^{-1} . In this range, all molecules have characteristic vibrational signals that can be excited upon interaction with photons from the excitation source, enabling the detection of trace amounts of compounds [17]. Fourier transform infrared (FT-IR) spectroscopy has been extensively used in both active and passive modalities for explosives detection. Active mode FT-IR spectroscopy has been used for post-blast detection of energetic materials using both globar and synchrotron infrared radiation, validating FT-IR spectroscopy as a useful tool for forensic applications [10, 12]. Emission (passive mode) and absorption MIR spectroscopy have been used recently as vibrational techniques for the standoff detection of explosives and other chemical agents deposited on metallic substrates [9, 11, 13-16].

On the other end, TLC provides a streamlined sampling and testing protocol that allows rapid, reproducible, separation and identification of drugs, explosives and precursors, with extended use to a wide range of hazardous materials obtained from substrates, liquids and solids for laboratory and field operations. The use of IRS as a detection/identification technique arises from the need to identify, in a reliable way, the components separated by TLC. IRS has a high discrimination capability and therefore in principle is a powerful identification method. If reference spectra are available, almost all analytes, including structural isomers, can nearly be unambiguously identified based on their IR spectrum. Thus TLC-IRS technique changes from a presumptive analysis (when TLC alone is used) to a confirmatory analysis when hyphenated to IRS. When reference spectra are absent, valuable information about the molecular structure of the analyzed compounds may still be obtained by spectral interpretation.

Up to now, the combination of TLC and IRS has been approached in two ways. In the first approach FT-IR measurement is performed *in situ*, that is, the separated compounds are analyzed directly on the TLC plate upon transferring to the sample compartment of a FT-IR. Using this method, spectral interferences can be expected as almost all TLC stationary phases have intense absorption bands in the MIR region. The second approach is usually more laborious and involves the transfer of analyte from the TLC plate to an IR-transparent substrate prior to FT-IR measurements. Over the years, research has shown that *in situ* as well as transfer methods can be effective and useful, each having specific advantages and limitations [18].

The first *in situ* FT-IR detection of spots on a plate was demonstrated by Percival and Griffiths [19]. A thin layer (depth: 100 μm) of adsorbent on an IR transparent support

(AgCl) allowed IR transmission measurements of dyes and amino acids at the 1-10 μg levels. In later studies, detection limits were improved by application of mulling oil to TLC plates to reduce IR scattering [20, 21]. In 1978 Fuller and Griffiths [22] demonstrated the viability of diffuse reflectance IRS (DRIRS) in measurements of methylene blue on a silica plate. Since then, DRIRS has become the most commonly used method for performing *in situ* TLC detection with FT-IR. Several studies have been performed to explore the potential of TLC-DRIRS analysis [23-26]. These studies, extensively reviewed by Brown and Beauchemin [27], revealed that various conventional TLC phases, such as silica, alumina, cellulose and reversed-phase materials can be used in combination with DRIRS yielding minimum identifiable quantities (identification limits) down to about 1 μg . The main difficulty encountered in using DRIRS as an *in situ* detection method for TLC is the strong absorption background of the adsorbent material, which causes serious interferences in particular spectral regions. For example, silica gel absorbs strongly in the regions from 3100 to 3700 cm^{-1} and from 1600 to 800 cm^{-1} , obscuring possible analyte absorptions at these frequencies. Consequently, the DRIRS spectrum of a TLC spot is divided into main parts: spectral areas where sensitivity is high and appropriate to obtain analyte information and spectral regions where the signal-to-noise ratio is poor and only minimal information can be extracted.

Danielson et al. reported on the use of a zirconium oxide as TLC stationary phase in combination with DRIRS analysis [28, 29]. Zirconia showed significantly higher IR reflectivity than silica or alumina resulting in only moderate background interferences. Zirconia has relatively much lower absorption over the range 4000 – 1100 cm^{-1} than either silica or alumina, and thus larger coverage of the MIR region is available for observing

adsorbate bands. When TLC was performed in zirconia-packed microchannels, small analyte spots were obtained and subsequent use of microscopic DRIRS analysis yielded detection limits in the 1 to 10 ng range for several dyes [29].

The development of more powerful IR sources gave rise to collimated, coherent and polarized sources. These sources were first developed at Bells Labs in 1994 with the invention of quantum cascade lasers (QCLs) [30, 31]. QCLs are commercially available and portable setup allowing detection of chemical and biological threat compounds in the field like explosives such as TATP, PENT, RDX, and TNT [32-36]. Coupling with chromatographic techniques, such as thin layer chromatography (TLC) with QCL spectroscopy to sense for explosives in the field has not been reported before. This justifies the usefulness of coupling thin layer chromatography (TLC) techniques with QCL spectroscopy (QCLS) to sense for explosives in the field.

TLC-QCLS, as a portable hyphenated technique for explosives analysis, will be most commonly used in two situations: (1) post-blast examination, (2) identification of suspected explosive material (pre-blast analyses on bulk material). In a post-blast situation, preliminary results can lend support to the link between multiple incidents or between a terrorist incident and the organization potentially responsible for the incident. This portable hyphenated technique can provide critical information in the identification of suspected explosive material. In these situations, portable instrumentation has a two-fold advantage: (1) the speed with which results can be obtained and (2) removing the need to transport potentially dangerous materials back to a central laboratory. Identification at a scene enables informed decisions to be made concerning render-safe procedures and the transportation of materials. This is of particular importance when extremely sensitive

explosives, such as organic peroxides, are suspected. When portable instruments are utilized at searches authorized by search warrants, preliminary results can be used to indicate areas where more efforts should be directed. Preliminary results can also give advanced warning of which types of explosives may be encountered at a scene and hence enable searchers to be better informed about the safety risks at a particular scene. In this study, a methodology that allows explosives detection, such as TNT present in real world soils and in complex substrates using TLC-QCLS is used. The methodology tested allow rapid and reproducible separation and identification of targeted explosives at near trace level ($\sim ng$) in the field in short time. The results show to TLC-QCLS as a hyphenated technique for chemical analysis.

4.2 EXPERIMENTAL

4.2.1 Materials and reagents

Reagents used were explosive materials known as PETN, RDX, and TNT. PETN was prepared in the laboratory. Methanol (99.9%, HPLC grade), dichloromethane (CH_2Cl_2 , HPLC grade), acetone (99.5%, GC grade) were purchased from Sigma-Aldrich (Milwaukee, WI, USA) and were used as solvents to prepare standard solutions of explosive. All solvent used as mobile phase (reactive grade) like acetone, hexane, cyclohexene, ethyl acetate, toluene, methanol, petroleum ether, dichloromethane used were purchased from Sigma-Aldrich (Milwaukee, WI, USA). Silica gel plates Aluminum TLC plates (Merck, TLC Silica gel 60 F254) was used for chromatographic runs. ZrO_2 and CaF_2 , used as stationary phases, were purchased from Sigma-Aldrich.

4.2.2 Sample Preparation: TLC

The developing chamber for TLC was a jar with a lid, to which the solvent (or mix solvents, 5 mL) was added to a depth of just less than 0.5 cm. The jar was allowed to stand for the saturation of the TLC chamber with solvent vapors while the silica gel plate was prepared. TLC plates used were cut to a convenient size of 2 cm width x 9 cm tall and were carefully managed to avoid damage or contamination of the adsorbent layer. Then a line was drawn across the plate TLC plate 1.5 cm from the bottom using a graphite pencil. Then 10 μL of the explosive material dissolved in methanol were placed at the center of the marked line by then gently touching the TLC plate and the methanol was allowed to evaporate. The prepared TLC plate was placed in the developing chamber and covered. The TLC plate was allowed to develop until the solvent was about 0.5 cm centimeter below the top of the plate. Then the plate was immediately removed from the developing chamber, and the solvent front was marked with the graphite pencil and allowed dry. If there were any colored spots, these were circled lightly with the graphite pencil. If the samples are not colored (target explosives) these were visualized using a UV lamp ($\lambda = 254 \text{ nm}$) and then marked with circles. The distances traveled by the solvent and the explosive materials (spots) were measured and R_f values determined. The spot diameter of the sample on the plate of silica before and after the chromatographic run were measured and compared.

ZrO_2 and CaF_2 powder were deposited on metal supports. TLC using ZrO_2 and CaF_2 transferred to mini channels ($w = 5 \text{ mm}$; $d = 0.2 \text{ mm}$; $l = 700 \text{ mm}$) made on aluminum plates of dimensions 250 mm x 5 mm x 700 mm on which stationary phases were

deposited using aqueous/organic suspensions. Then, a similar approach as used silica gel TLC was employed to prepare the ZrO_2 and CaF_2 plates.

4.2.3 Experimental Setup

Explosives solutions containing from 0.39 μg to 100 μg were transferred as already discussed using micropipettes to perform their respective chromatographic runs, and spots were identified using the UV lamp. Finally, each spot was interrogated using QCLS to obtain diffuse reflectance MIR spectra and to identify its characteristic vibrational signatures. Figure 4-1 shows an overview of the experiment setup used. Taking into consideration the setup illustrated in Figure 4-1b, the configuration used to record vibrational spectra was operated in transreflectance mode, since the matrix that contains the samples (separated explosives) is a dielectric material with lower reflectivity than metals.

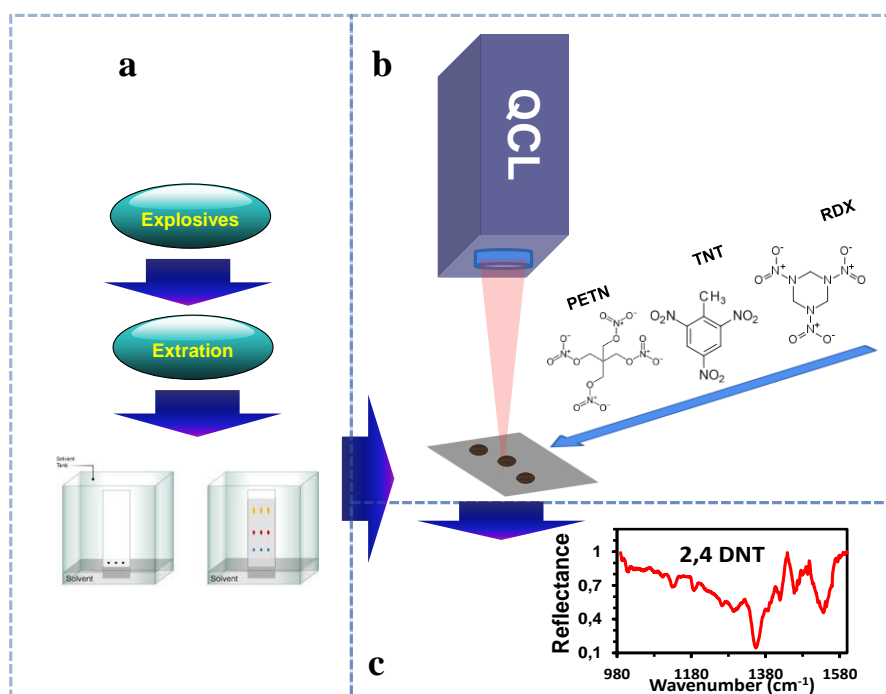


Figure 4-1. Experimental setup: (a) sample preparation, extraction, and separation from matrices; (b) *in situ* QCLS spectral measurements; (c) spectroscopic analysis.

4.3 RESULTS AND DISCUSSION

4.3.1 Preparation of ZrO₂ TLC

For the preparation of ZrO₂, different amount ZrO₂ wer added to 1 mL of solvent. The solvents used were water and methanol. The amount of ZrO₂ were varied from 0.1 to 0.3 g by mL of solvent. When methanol was used, non-homogeneous layers of ZrO₂ were obtained. When water was used, segregated layers of the materials were obtained. However when a water/methanol mix of solvents was used, homogeneous ZrO₂ layers were obtained. Figure 4-2 shows some results of preparation of ZrO₂ using different solvents.

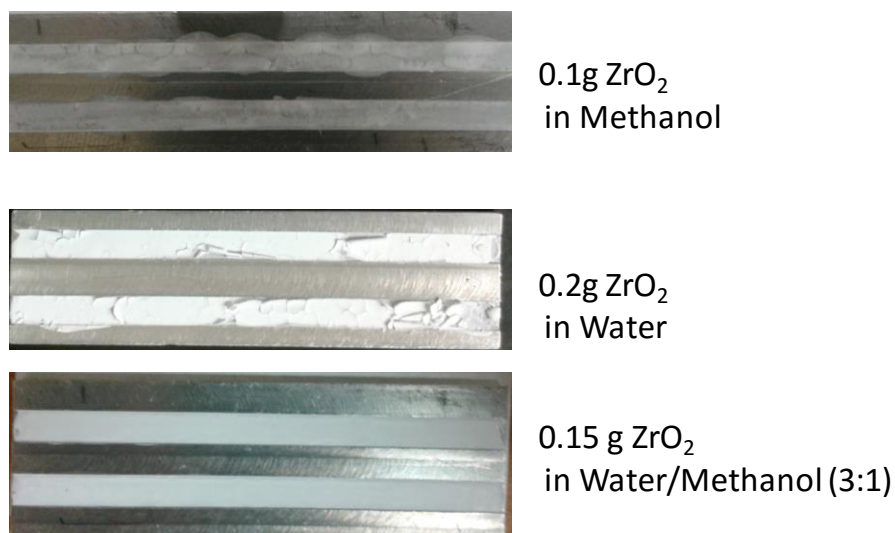


Figure 4-2. Preparation of ZrO₂ TLC using different solvents.

4.3.2 TLC: TNT and PETN

The best mobile phase to separate TNT ($R_f = 0.75 \pm 0.05$) and PETN ($R_f = 0.63 \pm 0.06$) was the mixture hexane:toluene (1:4). Toluene demonstrated to be a good mobile phase to separate both explosives: TNT ($R_f = 0.9$) and PETN ($R_f = 0.76$). The mobile phases dichloromethane, hexane:toluene (2:3), methanol:toluene (4:1), hexane:acetone (2:3), hexane:acetone (1:4), toluene:acetone (1:1), hexane:ethyl acetate (1:1) and hexane:acetone (1:1) showed the same affinity for both explosives (TNT and PETN), so they are not suitable as mobile phases for separation of these compounds by TLC. Table 4-1 shows the results for R_f values for TNT and PETN in some mobile phases used.

Table 4-1. R_f values of TNT and PENT mixture on different solvent systems.

Solvents (Mobile phase)	R_f value	
	TNT	PETN
Dichloromethane	0.87	0.87
Toluene	0.90	0.76
Hexane:Toluene (1:1)	0.45	0.30
Hexane:Toluene (1:4) (n=6)	0.81 – 0.81	0.68 – 0.72
	0.72 – 0.73	0.61 – 0.61
	0.70 – 0.70	0.58 – 0.58
Hexane:Toluene (2:3)	0.50	0.50
Methanol:Toluene (1:1)	0.66	0.70
Methanol:Toluene (4:1)	0.83	0.83
Hexane:Acetone (4:1)	0.26	0.16
Hexane:Acetone (2:3)	0.96	0.96
Hexane:Acetone (1:4)	1.00	1.00
Toluene:Acetone (1:1)	0.98	0.98
Hexane:Acetone (1:1)	0.63	0.63
Hexane:Ethyl acetate (1:1)	0.85	0.85

4.3.3 Spectral profiles of high explosives on various stationary phase

Figure 4-3a shows the infrared spectra of the substrates used as stationary phases (BaF_2 , CaF_2 , ZrO_2 and silica gel) using a bench FT-IR (IFS/66v, Bruker Optics, Billerica, MA) and KBr pellet. Silica gel is the most used stationary phase in TLC separations. However when infrared measurements are made directly on the stationary phase, silica gel has a strong absorption in the range $900\text{-}1400\text{ cm}^{-1}$ spectral range where explosives have strong bands. When QCLS spectra of explosives deposited and on silica gel, many of the vibrational bands of the explosives were masked by the strong MIR absorption of silica. Figure 4-3b show the effect of the silica gel on the vibrational bands of PETN and DNT present around 1300 cm^{-1} for PETN and 1350 cm^{-1} for DNT when KBr is used as background.

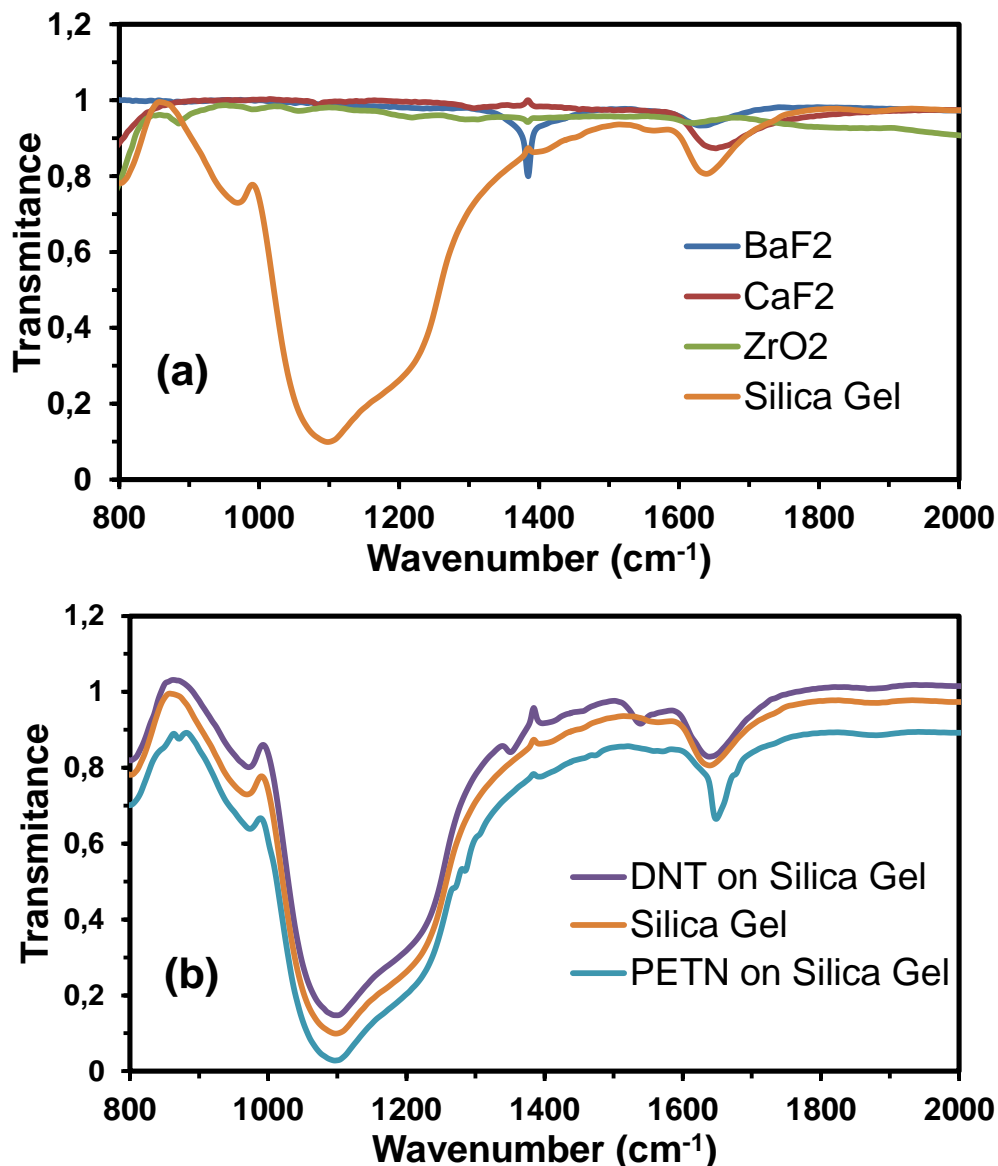


Figure 4-3. (a) Spectra from different stationary phases (BaF₂, CaF₂, ZrO₂ and silica gel) used to TLC. (b) Spectra of DNT and PETN on silica gel-TLC.

The spectra shown in Figures 4-4 to 4-6 demonstrate that TLC-QCLS method can be applied successfully for the identification of explosives. Spectra of 2,4-DNT and TNT on silica gel TLC are illustrated in Figure 4-4, in which characteristic bands at ~ 1350 cm⁻¹ and ~ 1530 cm⁻¹ can be clearly observed.

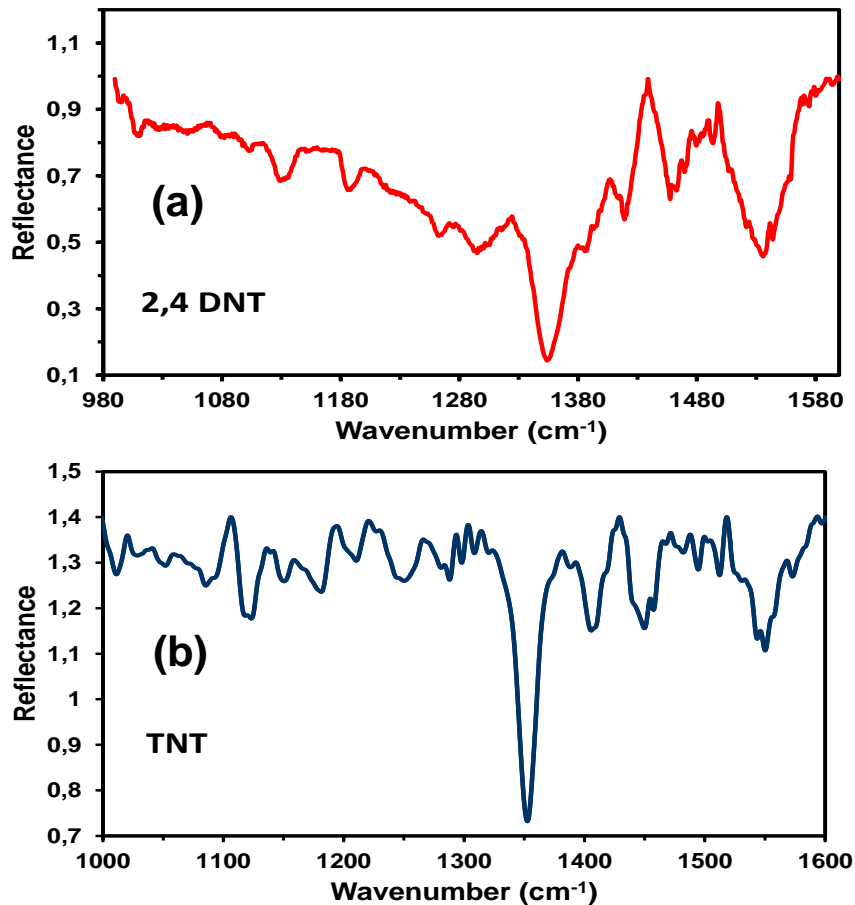


Figure 4-4. Explosives spectra on Silica Gel-TLC. (a) 2,4 DNT spectrum, (b) TNT spectrum. Silica gel was used as background.

Taking into account the disadvantages of silica gel due to its strong IR absorption in the spectral range of interest, other substrates were explored as stationary phases. The candidates selected were CaF₂ and ZrO₂. These compounds do not show IR interfering vibrational bands in the spectral region where explosives materials have strong IR absorption bands. Figure 4-3a shows the spectra for CaF₂ and ZrO₂ which have no IR vibrational information in spectral range of analytical interest.

Figures 4-5 shows the IR spectra of TNT, DNT PETN and urea nitrate (UN) after these were analyzed using ZrO_2 as stationary phase. Figure 4-6 shows the IR spectra of PETN and 2,4-DNT when these were analyzed using CaF_2 as stationary phase. In both cases the stationary phases did not present highly interfering IR bands from the inorganic substrates.

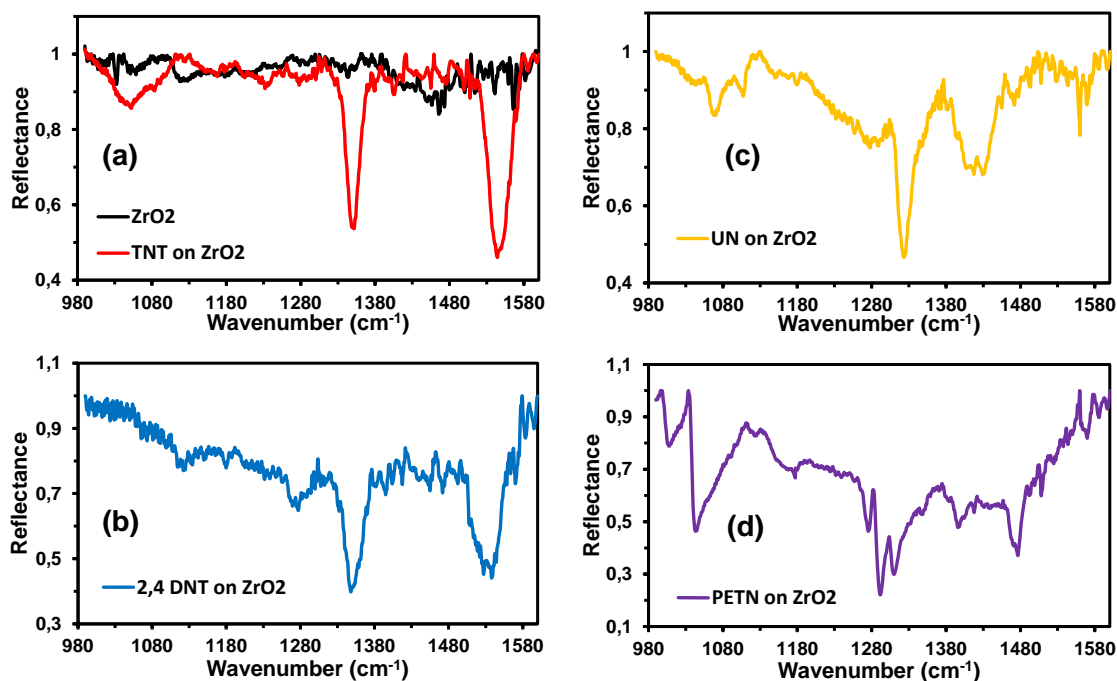


Figure 4-5. Explosives spectra on ZrO_2 -TLC. Baseline correction was applied to each spectrum.

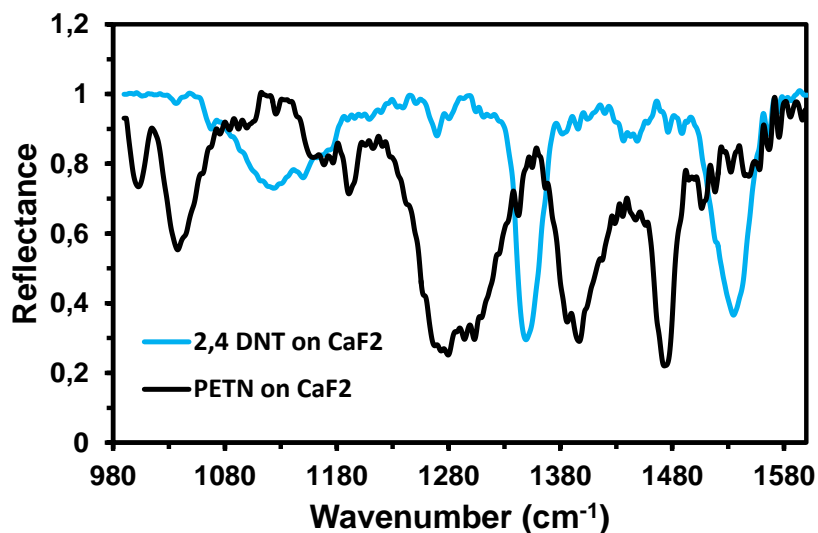


Figure 4-6. Explosive spectra on CaF₂-TLC. Baseline correction was applied to each spectrum.

4.3.4 TNT quantification profiles using TLC

The spectra shown in Figure 4-7 demonstrate that TLC-QCLS can serve as an excellent platform to devise analytical methods useful for identification and quantification of chemical targets. QCL spectra of TLC runs of TNT at various concentrations (0.39 to 12.5 μg / spot) were very similar TNT reference spectrum obtained from the literature. Characteristic bands of TNT at 1350 cm^{-1} and 1530 cm^{-1} were tentatively assigned. Even at low concentrations as 0.39 μg (390 ng), TNT prominent IR bands at 1350 cm^{-1} can be clearly appreciated.

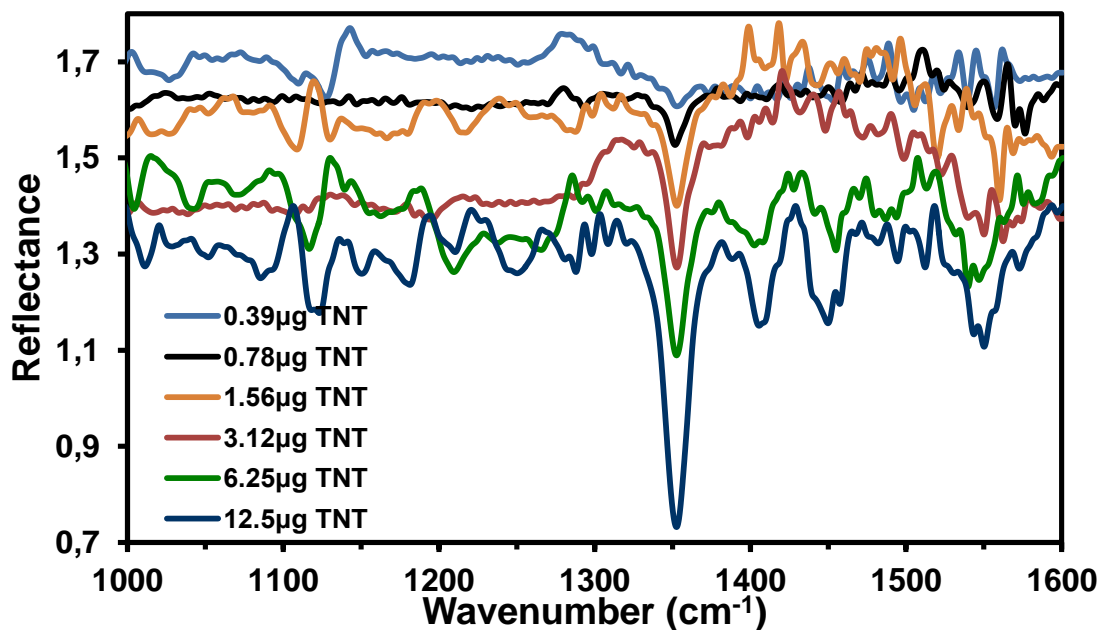


Figure 4-7. TNT spectra in different concentrations on silica gel-TLC. Baseline correction and smoothing (25 pt.) was applied to each spectrum.

4.4 CONCLUSIONS

TLC can be employed for rapid separation and identification of low levels of explosive materials complex samples. It can be utilized with various explosive materials, including home-made explosive materials, military explosives, and propellant stabilizers. The best mobile phase to separate TNT ($R_f = 0.75 \pm 0.05$) and PETN ($R_f = 0.63 \pm 0.06$) was the mixture hexane:toluene (1:4). The spot diameters before and after the chromatographic run, in most cases were approximately ~ 0.5 cm. The results show that TLC-QCLS is a useful tool to detect trace concentrations of explosives as low as $0.39 \mu\text{g}$ (390 ng).

4.5 ACKNOWLEDGEMENTS

Support from the U.S. Department of Homeland Security under Award Number 2013-ST-061-ED0001 is also acknowledged. However, the views and conclusions contained in this document are those of the authors and should not be considered as a representation of the official policies, either expressed or implied, of the U.S. Department of Homeland Security.

4.6 REFERENCES

- [1]. M.L. Ramirez, N. Gaensbauer, H. Felix, W. Ortiz-Rivera, L. C. Pacheco-Londoño and S. P. Hernandez-Rivera, *Fiber Optic Coupled Raman Based Detection of Hazardous Liquids Concealed in Commercial Products*. International Journal of Spectroscopy, 2012; **1**: p. 1-7.
- [2]. T. Caron, M. Guillemot, P. Montméat, F. Veignal, F. Perraut, P. Prené, F. Serein-Spirau, *Ultra-trace detection of explosives in air: Development of a portable fluorescent detector*. Talanta, 2010; **81**(1-2): 543-548.
- [3]. A. Hilmi, J. Luong, *Micromachined Electrophoresis Chips with Electrochemical Detectors for Analysis of Explosive Compounds in Soil and Groundwater*. Environmental science & technology, 2000. **34**(14): p. 3046-3050.
- [4]. J. Yinon, *Trace analysis of explosives in water by gas chromatography-mass spectrometry with a temperature-programmed injector*, Journal of Chromatography A, 1996. **742**(1-2): p. 205-209.

- [5]. C. Szakal and T. M. Brewer, *Analysis and mechanisms of cyclotrimethylenetrinitramine ion formation in desorption electrospray ionization*. Analytical Chemistry, 2009. **81**(13): p. 5257- 5266.
- [6]. C.J. Miller and T. S. Yoder, *Explosive Contamination from Substrate Surfaces: Differences and Similarities in Contamination Techniques Using RDX and C-4*. Sensing and Imaging: An International Journal, 2010. **11**(2): p. 77-87.
- [7]. W. Ortiz-Rivera, L. C. Pacheco-Londoño and S. P. Hernandez-Rivera, *Remote Continuous Wave and Pulsed Laser Raman Detection of Chemical Warfare Agents Simulants and Toxic Industrial Compounds*. Sensing and Imaging: An International Journal, 2010. **11**(3): p. 131-145.
- [8]. W. Ortiz, L. C. Pacheco, J. R. Castro, H. Felix and S. P. Hernandez-Rivera, *Vibrational spectroscopy standoff detection of threat chemicals*. Proc. SPIE, 2011. **8031**: 803129.
- [9]. L. C. Pacheco-Londoño, W. Ortiz-Rivera, O. M. Primera-Pedrozo and S. P. Hernández-Rivera, *Vibrational spectroscopy standoff detection of explosives*. Analytical and Bioanalytical Chemistry, 2009. **395**(2): p. 323-335.
- [10]. A. Banas, K. Banas, M. Bahou, H. O. Moser, L. Wen, P. Yang, Z. J. Li, M. Cholewa, S. K. Lim, and Ch. H. Lim, *Post-blast detection of traces of explosives by means of Fourier transform infrared spectroscopy*, Vibrational Spectroscopy, 2009. **51**(2): p. 168–176.
- [11]. J. R. Castro-Suarez, L. C. Pacheco-Londoño, W. Ortiz-Rivera, M. Vélez-Reyes, M. Diem, and S. P. Hernandez-Rivera, *Open path FTIR detection of threat chemicals in air and on surfaces*. Proc. SPIE, 2011. **8012**: 801209.

- [12]. K. Banas, A. Banas, H. O. Moser, M. Bahou, W. Li, P. Yang, M. Cholewa and S. K. Lim, *Multivariate Analysis Techniques in the Forensics Investigation of the Postblast Residues by Means of Fourier Transform-Infrared Spectroscopy*. Analytical Chemistry, 2010. **82**(7): p. 3038–3044.
- [13]. C. W. Van Neste, L. R. Senesac and Thundat, *Standoff spectroscopy of surface adsorbed chemicals*. Analytical Chemistry, 2009. **81**(5): p. 1952–1956.
- [14]. J. Hildenbrand, J. Herbst, J. Wollenstein, A. Lambrecht, M. Razeghi, R. Sudharsanan and G. J. Brown, *Explosive detection using infrared laser spectroscopy*. Proc. SPIE, 2009. **7222**: 72220B.
- [15]. J.R. Castro, L. C. Pacheco, M. Vélez, M. Diem, T. J. Tague and S. P. Hernandez, *Open-Path FTIR Detection of Explosives on Metallic Surfaces. in Fourier Transforms: New Analytical Approaches and FTIR Strategies*. G.S. Nikolić, ed. InTech Open, Croatia, 2011.
- [16]. J. R. Castro-Suarez, L. C. Pacheco-Londoño, M. Vélez-Reyes, M. Diem, T. J. Tague and S. P. Hernandez-Rivera, *FT-IR Standoff Detection of Thermally Excited Emissions of Trinitrotoluene (TNT) Deposited on Aluminum Substrates*. Applied Spectroscopy, 2013. **67**(2): p. 181-186.
- [17]. H. Gunzler and H. U. Gremlich, *IR Spectroscopy: An introduction*, Wiley-VCH, Weinheim, Germany, 2002.
- [18]. G. W. Somsen, W. Morden and I. D. Wilson, *Planar chromatography coupled with spectroscopic techniques*. Journal of Chromatography A, 1995. **703**(1): p. 613–665.

- [19]. C. J. Percival and P. R. Griffiths, *Direct measurement of the infrared spectra of compounds separated by thin-layer chromatography*. Analytical Chemistry, 1975. **47**(1): p. 154-156.
- [20]. M. M. Gomez-Taylor, D. Kuehl and P. R. Griffiths, *Vibrational spectrometry of pesticides and related materials on thin layer chromatography adsorbents*. Applied Spectroscopy, 1976. **30**(4): p. 447- 452.
- [21]. M. M. Gomez-Taylor and P. R. Griffiths, *Improved Sensitivity for in Situ Infrared Identification of Species Separated by Thin-Layer Chromatography using Programmed Multiple Development*. Applied Spectroscopy, 1997. **31**(6): p. 528-530.
- [22]. M. P. Fuller and P. R. Griffiths, *Diffuse reflectance measurements by infrared Fourier transform spectrometry*. Analytical Chemistry, 1978. **50**(13): p. 1906-1910.
- [23]. G. E. Zuber, R. J. Warren, P. P. Begosh and E. L. O'Donnell, *Direct analysis of thin-layer chromatography spots by diffuse reflectance Fourier transform infrared spectrometry*. Analytical Chemistry, 1984. **56**(14): p. 2935-2939.
- [24]. A. Otto, U. Bode and H. M. Heise, *Experiences with infrared microsampling for thin-layer and high-performance liquid chromatography*. Fresenius Zeitschrift für analytische Chemie, 1988. **331**(3-4): p. 376-382.
- [25]. S. G. Bush and A. J. Breaux, *The application of diffuse and specular reflectance to TLC-FTIR and other microsampling applications*. Microchimica Acta, 1988. **94**(1-6): p. 17-20.
- [26]. Jr.B. T. Beauchemin and P. R. Brown, *Quantitative analysis of diazonaphthoquinones by thin-layer chromatographic/diffuse reflectance infrared Fourier-transform spectrometry*. Analytical Chemistry, 1989. **61**(6): p. 615-618.

- [27]. P.R. Brown and Jr, B.T. Beauchemin, *Thin-layer chromatographic-diffuse reflectance infrared Fourier transform spectroscopic analysis*. Journal of liquid chromatography, 1988. **11**(5): p. 1001-1014.
- [28]. N. D. Danielson, J. E. Katon, S. P. Bouffard and Z. Zhu, *Zirconium oxide stationary phase for thin-layer chromatography with diffuse reflectance Fourier transform infrared detection*. Analytical Chemistry, 1994. **64**(18): p. 2183-2186.
- [29]. S. P. Bouffard, J. E. Katon, A. J. Sommer and N. D. Danielson, *Development of microchannel thin-layer chromatography with infrared microspectroscopic detection*. Analytical Chemistry, 1994. **66**(13): p. 1937-1940.
- [30]. J. Faist, F. Capasso, D. L. Sivco, C. Sirtori, A. L. Hutchinson, A. Y. Cho, *Quantum Cascade Laser*. Science, 1994. **264**(5158): p. 553-556.
- [31]. J. Faist, F. Capasso, C. Sirtori, D. L. Sivco, J. N. Baillargeon, A. L. Hutchinson, S. G. Chu and A. Y. Cho, *High power mid-infrared ($\lambda \sim 5 \mu\text{m}$) quantum cascade lasers operating above room temperature*. Applied Physics Letters, 1996. **68**(26): p. 3680-3682,.
- [32]. M. B. Pushkarsky, I. G. Dunayevskiy, M. Prasanna, A. G. Tsekoun, R. Go and C. K. N. Patel, *High-sensitivity detection of TNT*. Proceedings of the National Academy of Sciences, 2006. **103**(52): p. 19630–19634.
- [33]. C.K.N. Patel, *Laser Based In-Situ and Standoff Detection of Chemical Warfare Agents and Explosives*. Proc. SPIE, 2009. **7484**: 748402.
- [34]. C. Bauer, U. Willer and W. Schade, *Use of quantum cascade lasers for detection of explosives: progress and challenges*. Optical Engineering, 2010. **49**(11): p. 111126-111127.

- [35]. L. C. Pacheco-Londoño, J. R. Castro-Suarez and S. P. Hernández-Rivera, *Detection of Nitroaromatic and Peroxide Explosives in Air Using Infrared Spectroscopy: QCL and FTIR*. *Advances in Optical Technologies*, 2013. **2013**: p. 1-8.
- [36]. J. R. Castro-Suarez, M. Hidalgo-Santiago, S. P. Hernández-Rivera, *Detection of Highly Energetic Materials on Non-Reflective Substrates Using Quantum Cascade Laser Spectroscopy*. *Applied spectroscopy*, 2015. **69**(9): p. 1023-1035.

VIII. CHAPTER 5

ACTIVE MODE REMOTE INFRARED SPECTROSCOPY DETECTION OF TRINITROTOLUENE AND PENTAERYTHRITOL TETRANITRATE ON ALUMINUM SUBSTRATES

OVERVIEW

Two remote infrared spectroscopy (RIRS) detection systems were assembled using an infrared telescope coupled to a Fourier transform infrared spectrometer, a cryo-cooled MCT detector, and a telescope-coupled mid-infrared excitation source. Samples of 2,4,6-trinitrotoluene (TNT) and pentaerythritol tetranitrate (PETN) deposited on aluminum plates were detected at several source-target distances by performing remote infrared detection measurements on the aluminum substrates in active mode. The samples tested were placed at various distances (1-30 m) for the standoff IR detection experiments. The effect of angle of collection of the reflected IR beams on S/N and vibrational band intensities were evaluated. All experiments were performed at ambient temperature. Several TNT and PETN surface concentrations were investigated. Partial least squares regression analysis was applied to spectra obtained. Overall, active mode RIRS detection was successful for quantifying highly energetic materials deposited on the aluminum plates with high confidence level up to source-target distances of 1-25 m.

5.1 INTRODUCTION

The detection and identification of high energetic material (HEM), commonly called explosives, is a subject that has become a heightened priority in recent years for homeland security and counter-terrorism applications [1-3]. Law-enforcement and forensic agencies have continued interest in promoting research and development activities for efficient sensing systems than help to detect explosives at a distance at public places such as airports, maritime facilities, railway and bus stations, large auditoriums, and stadiums. This way it is expected that damage from terrorists activities can be minimized or prevented in most cases [3].

Researches on development of sensors than to allow analytical procedures to enable faster, more sensitive, less expensive, and simpler means to detect trace detection of explosives has increased in recent years [4]. Modern detection systems are routinely used to prevent these events. These are based on ionization techniques accompanied with separation schemes, pyrolysis, gas phase reactions, interaction of highly HEM with radiation, colorimetric tests, immunochemical reactions between HEM and specific antibodies, etc. The techniques have shown be useful for explosive detection in different phases (solid, liquid and gas) on different substrates or complex matrixes (as soil, water, and air) [4-9]. However, in the greater part of the cases, they require some sort of sample preparation for subsequent chemical analysis.

Taking advantage that each chemical substance has its own distinctive fingerprint spectrum, vibrational techniques such as Raman spectroscopy (RS) and Fourier transform infrared spectroscopy (FT-IRS) have several advantages over other analytical techniques that make them ideal for the identification of a wide range of explosives and

related compounds. Some of these advantages are: the possibility analyzing samples in various physical states and mixtures, both techniques can be utilized with no or minimal sample preparation, minute explosive particulates can be readily analyzed if spectrometers include microscope-based systems, remote detection systems or portable spectrometers can be built, and sample analysis can be achieved in a short time (seconds) [3,7]. These techniques have been used to characterize, detect, quantify and discriminate HEM, biological and chemical agents (or their simulants), toxic industrial compounds, and other threat substances [10-13]. These techniques have the added advantage that they can be used in point detection and in hyperspectral imaging mode. Remote detection is the operational capability in which the instrumentation and operator remain separated from the sample by some distance (range) while measuring some property of the target [14]. Remote IR spectroscopy (RIRS) is an analytical method able to detect and to identify explosives at long distances are in great demand by security agencies in order to be able to anticipate the threat from a safe distance and to guarantee personal safety. In RIRS detection, infrared vibrational signatures can be obtained at distances of a few meters to several tens of meters between the target and operator. This modality of detection provides a way of performing real-time analysis, in which no sample preparation or operator contact is required, rapid cycle times are typical and enough chemical information of each HEM can be obtained to either identify, quantify or discriminate from interfering signals from other substances. These capabilities make RIRS a useful technique for sensing for HEM, and they further prevent or minimize the possible damage caused by terrorist action in the case that the energetic material sets off [13].

RIRS detection using FT-IR is the most versatile of the spectroscopy-based technologies because it can measure the presence of many chemicals deposited on substrates at trace level at a distance [15]. Important contributions to the development application are briefly discussed. Pacheco-Londoño et al. built an active IR standoff detection system by coupling a bench FT-IR interferometer to a gold mirror and detector assembly for detection of trace amounts of TNT and RDX explosives on reflective surfaces in the range of 1.0–3.7 m [16]. Suter et al. studied the spectral and angular dependence of scattered MIR light from surfaces coated with explosives residues (TNT, RDX, and Tetryl) at a 2 m distance [17]. An external cavity quantum cascade laser provided tunable illumination between 1250 and 1428 cm^{-1} was used. Kumar and collaborators measured the diffuse reflection spectrum of solid samples such as explosives (TNT, RDX, PETN), fertilizers (ammonium nitrate, urea), and paints (automotive and military grade) at a distance of 5 m using a mid-infrared supercontinuum light source with 3.9 W average output power [18].

In this report, FT-IR standoff detection experiments were performed. RIRS experiments were carried out in active mode using telescope-coupled MIR source. Effect of detector-target angle on IR the spectrum of PETN was evaluated. Analyses of data was based on multivariate partial least squares (PLS) regression calibrations. Statistical parameters such as the root mean square errors of cross-validations (RMSEVC) and coefficients of determination (R^2) were used as criteria to judge the quality of the data obtained in the IR detection methodology.

5.2 EXPERIMENTAL

5.2.1 Reagents

The reagents used included HEM and solvents. 2,4,6-Trinitrotoluene (TNT) was acquired from ChemService, Inc. (West Chester, PA) as crystalline solid (99%, min. purity; 30% water content). PETN was synthesized and purified in the laboratory according to the methods described by Ledgard [19]. Methanol (99.9%, HPLC grade), dichloromethane (CH_2Cl_2 , HPLC grade) and acetone (99.5%, GC grade) were purchased from Sigma-Aldrich Chemical Co. (Milwaukee, WI) and were used to deposit the explosives samples at different surface concentrations onto the aluminum (Al) plates used as substrates.

5.2.2 Sample Preparation

Sample preparation is an important step in remote detection experiments for detection of analytes present as trace residues deposited as contaminants on substrates. A sample-smearing technique was used to deposit HEM samples onto the metal substrates [13]. Aluminum plates of dimensions 1.0 ft. x 1.0 ft. (930 cm^2) were used as sample holders for the HEM targets. Acetone was used to clean the aluminum substrates. After cleaning, plates were allowed to dry before depositing the desired target HEM. A small amount of dichloromethane or methanol was used to dissolve the HEM samples to be deposited on the test substrates. Then, a Teflon stub $3 \text{ cm} \times 15 \text{ cm}$ was used to smear the samples on the Al plates. The amount of HEM that remained on the Teflon stub after sample smearing was negligible. The nominal surface concentrations obtained by the smearing technique used were: 50, 100, 200, 300 and $400 \mu\text{g}/\text{cm}^2$.

5.2.3 Experimental Setup

After dosing the Al plates with the desired nominal surface concentration, these were located at the target positions. Ambient temperature, plate temperature, and relative humidity were continuously monitored during the course of the experiments. Finally, RIRS detection experiments in active mode were carried out using two optical systems as is illustrated in Figure 5-1a and 5-1c. In the first system, a heated oxide source (globar) was coupled to a commercial MIR reflective telescope (Bruker Optics) as illustrated in Figure 5-1a. In the second optical system, the globar source was coupled to a home built a MIR refractive telescope as is shown in Figure 5-1c.

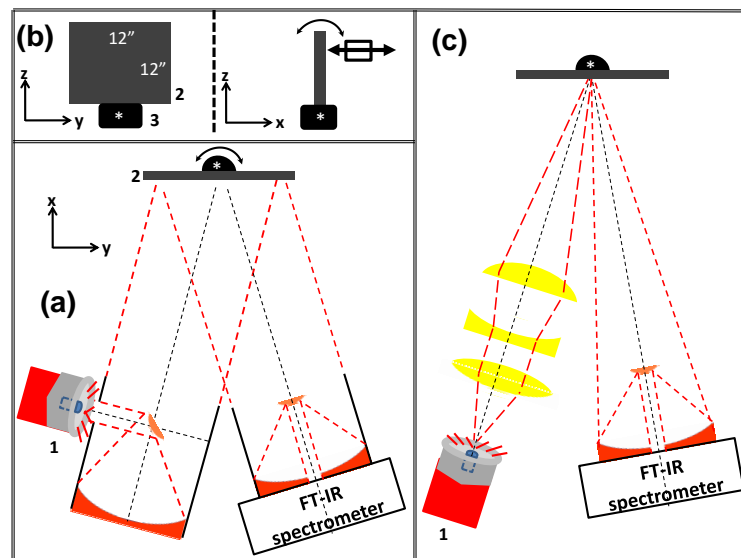


Figure 5-1. FT-IR interferometer configuration; (a) active mode setup for standoff measurements using reflective telescope: 1. IR source; 2. Al plate. (b) Plate mount; 3. Tilting mount. (c) Active mode setup for standoff measurements using refractive telescope.

In the remote sensing experiments, the IR beam from globar source was not modulated by the interferometer before interacting with the target and sat side-by-side to the MIR reflective collector telescope that was close coupled to the FT interferometer (Figure 5-

1a). The experiments were done in back-reflection mode. The FT-IR spectrometer used (Figure 5-1a and 5-1c) was an open path interferometer, model EM27 (Bruker Optics, Billerica, MA). The optical bench consisted of a compact, enclosed, and desiccated Michelson type interferometer equipped with ZnSe windows, an internal blackbody calibration source, a KBr beamsplitter, a very fast native focal ratio of $f/0.9$ and a field of view (FOV) of 30 mrad (1.7°). For optical system shown in Figure 5-1a, the transmitter source telescope had a diameter of 6 in., a focal ratio of $f/4$, and gold-coated mirrors with a FOV ≥ 7.5 mrad (0.43°). The receiver telescope was also 6 in. diam. and had an $f/3$ focal ratio and gold-coated mirrors with a FOV of 10 mrad (0.57°). In the second optical system (Figure 5-1c), the transmitter source telescope consisted of a set of three lenses of ZnSe. Lenses had a diameter of 4 in., a focal length (f) of 100 mm for bi-convex lens, f of -1000 mm for a plano-concave lens, and f of 1000 mm for plano-convex lens. The receiver telescope was the same as in the optical system 1. In these experimental setups, the targets were carefully aligned with the source and collector. To accomplish this, the metal plate was placed on a mount that allowed millimeter translations both horizontally and vertically, as illustrated in Figure 5-1b. The target-collector distances studied were 1, 4, 8, 12, 16, 20, 25 and 30 m. Ten spectra were acquired for each sample at 20 scans/spectrum and 4 cm^{-1} resolution. Spectra were recorded in the spectral range from 1400 to 750 cm^{-1} . The experiments were performed at ambient temperature ($\sim 25^\circ\text{C}$).

IR signals were detected using a MIR closed cycle (Stirling cooled) photoconductive MCT detector with $D^*_{\text{max}} \sim 4 \times 10^{10}\text{ cmHz}^{1/2}/\text{W}$. Background spectra of Al plates with no HEM deposited on them were run for every remote distance studied. Data analyses were based

on chemometrics multivariate analyses. In particular, PLS regression analysis was used to perform quantification studies of the HEM surface concentrations at all remote distances studied.

5.3 RESULTS AND DISCUSSION

5.3.1 HEM Standoff Detection

Signal to noise ratios (S/N) plotted as a function of the distance for active mode spectral measurements of TNT are shown in Figure 5-2, using optical system 1. Results for surface concentrations of $400 \mu\text{g}/\text{cm}^2$ deposited on Al plates are shown. The S/N initially decreased linearly with range (see Figure 5-2, black circles; slope: $-0.95 \pm 0.02 \text{ m}^{-1}$). However, when the remote detection distance was larger than 12 m the signal decreased at an even steeper slope ($-2.3 \pm 0.5 \text{ m}^{-1}$) reaching a S/N of ~ 3 at a distance of 24 m. The decrease of collected signal did not allow measuring the S/N for the entire distance range planned (to 60 m), making the measurements accurate up to 25-30 m. The two linear decreases in collected signal were calculated from fitting of the data and are shown as black and gray dotted lines in Figure 5-2. The difference in slope in the regions **I**: 4-12 m and **II**: 12-25 m suggested a fundamental reason for the behavior and led to measurements of the spot size of the MIR beam at the target plane. As shown in the graph, the spot diameter is smaller than the target size in region **I**; it is exactly equal to the target at 12 m; and is larger than the target in region **II**. A linear dependence of the spot diameter with the remote distance is also shown in Figure 5-2. When a MIR thermal source (globar) was used to accomplish these transreflectance measurements in active mode the peak intensities decreased as the distances increased. At distances larger than

25 m, it was not possible to visually detect some of the TNT vibrational signatures. This result was expected since as shown in Figure 5-2, the distance for the threshold S/N of 3 is 24 m in active mode. Furthermore, the density of infrared radiation that is transferred to the Al plates from the MIR source diminishes as a function of distance, leading to a smaller number of excited molecules at the target. Therefore, the detector could not register the transfection of the low-intensity vibrational signals.

The active mode MIR spectra for TNT deposited on Al plates at several distances and surface concentrations are shown in Figure 5(a), using experimental configuration illustrated in Figure 5-1(a). A reference spectrum for TNT is also included. The latter was obtained by preparing a pellet of 1 mg microcrystalline TNT in 100 mg KBr and measuring the absorption spectrum at the macro sample chamber of a bench top interferometer (IFS-66v, Bruker Optics, Billerica, MA). Solid black line labeled "Reference". Upon inspection of these spectra, it is evident that the most significant TNT vibrational signatures were detected in the remote sensed measurements. In particular, an intense vibrational band at about 908 cm^{-1} was tentatively assigned to the C-N stretching, a vibrational band at 938 cm^{-1} was assigned to the C-H out-of plane bend (ring) and the symmetric stretch band of the nitro groups appeared at 1350 cm^{-1} . These results are all due to conjugation of the nitro groups with the aromatic ring, which agree with result from Pacheco-Londoño et al. [16], Clarkson et al. [20] and Castro-Suarez et al. [21].

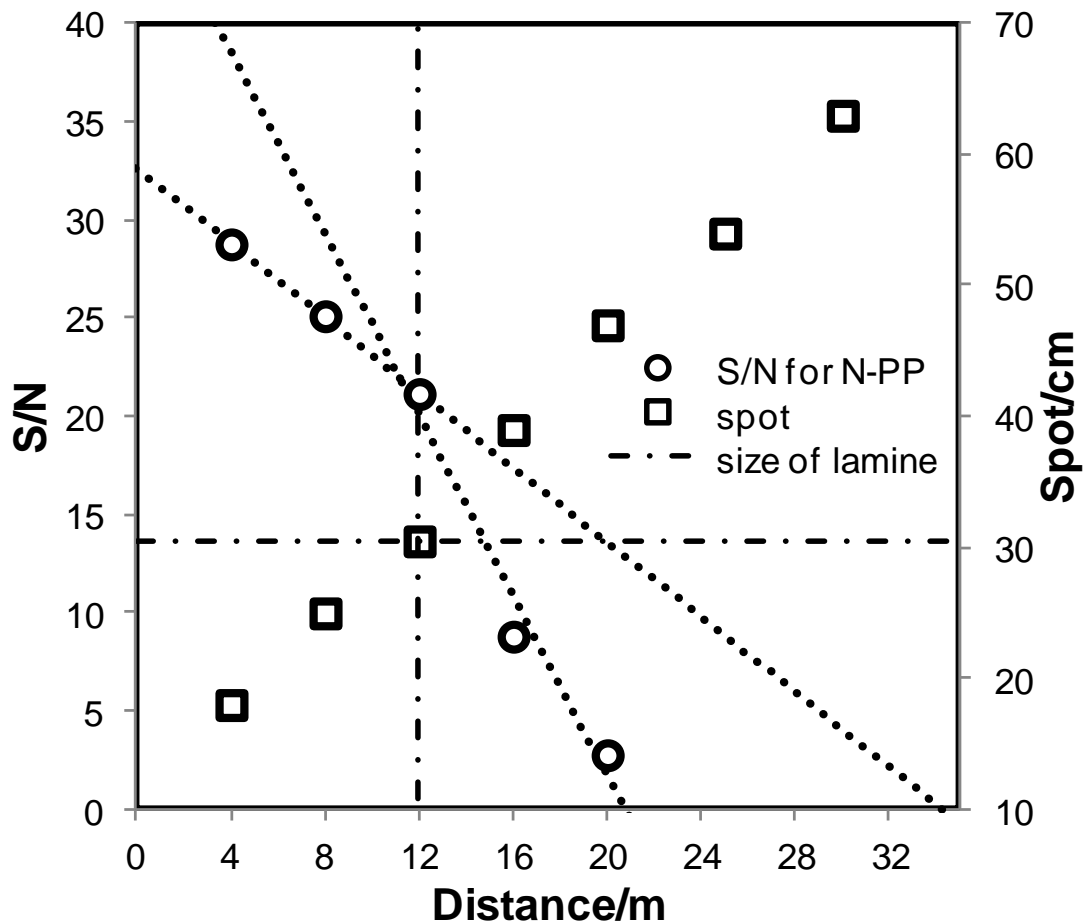


Figure 5-2. Ratio signal to noise (P-P; principal “y” axis) at various distances for active mode. IR beam spot size (secondary “y” axis) vs. range. Noise levels were measured at 830-870 cm^{-1} and peak heights were measured for signal at 790 cm^{-1} .

These spectra were not subjected to any pre-processing routine, such as offset correction, baseline correction, smoothing, or water vapor rotational lines removal. In other words, there was no common baseline for these spectra, and some spectra exhibited positive intensity ramps to higher wavenumber values. However, an increase in signal intensity as a function of the surface concentrations was also clearly shown without the use of chemometrics routines.

The spectral band shapes observed in remote detection mode, shown in Figure 5-3a, are superimposed on a ramp-shaped background, and the bands themselves exhibit strong reflective band profiles. Since these measurements were done on a reflective metal substrate, the distortion of the band profiles is expected; similar effects have been reported in DRIFT (diffuse reflection infrared Fourier Transform) spectroscopy [22] and in microscopically acquired infrared spectra of microspheres [23]. In both cases, the distortion of the absorptive line shapes is because within an absorption peak, the reflective index undergoes anomalous dispersion. In spectroscopic experiments carried out in reflectance mode, a mixing of the absorptive and dispersive line shapes can occur, resulting in bands that have a negative dips at the high wavenumber side of the peak. This will shift the peak maximum by up to 15 cm^{-1} toward lower values [24]. Moreover, mixing of absorptive and reflective line shapes can also be mediated by scattering effects, which could also produce significant band distortions [23]. A paper on line shape distortion effects in infrared spectroscopy by M. Miljković and et al. addresses the conditions under which mixing of reflective and absorptive band shapes will occur, and discusses the methods that have been developed to correct the spectral distortions [25]. In a recent paper by Castro-Suarez and et al. demonstrated that these spectra shown in Figure 5-3a have the appearance of “double pass” transmission-reflection (transflectance) spectra [21]. Transflection experiments are usually made by placing a thin target sample on a non-IR absorbing, reflective substrate such as a polished metal surface, focusing an IR beam onto a region of interest, and collecting the radiation that is reflected to the collection optics. The technique is termed transflection because most of the signal intensity

collected is a transmission signal as the beam passes through the sample, reflects off the substrate, passing through the sample again to the detector [24, 26].

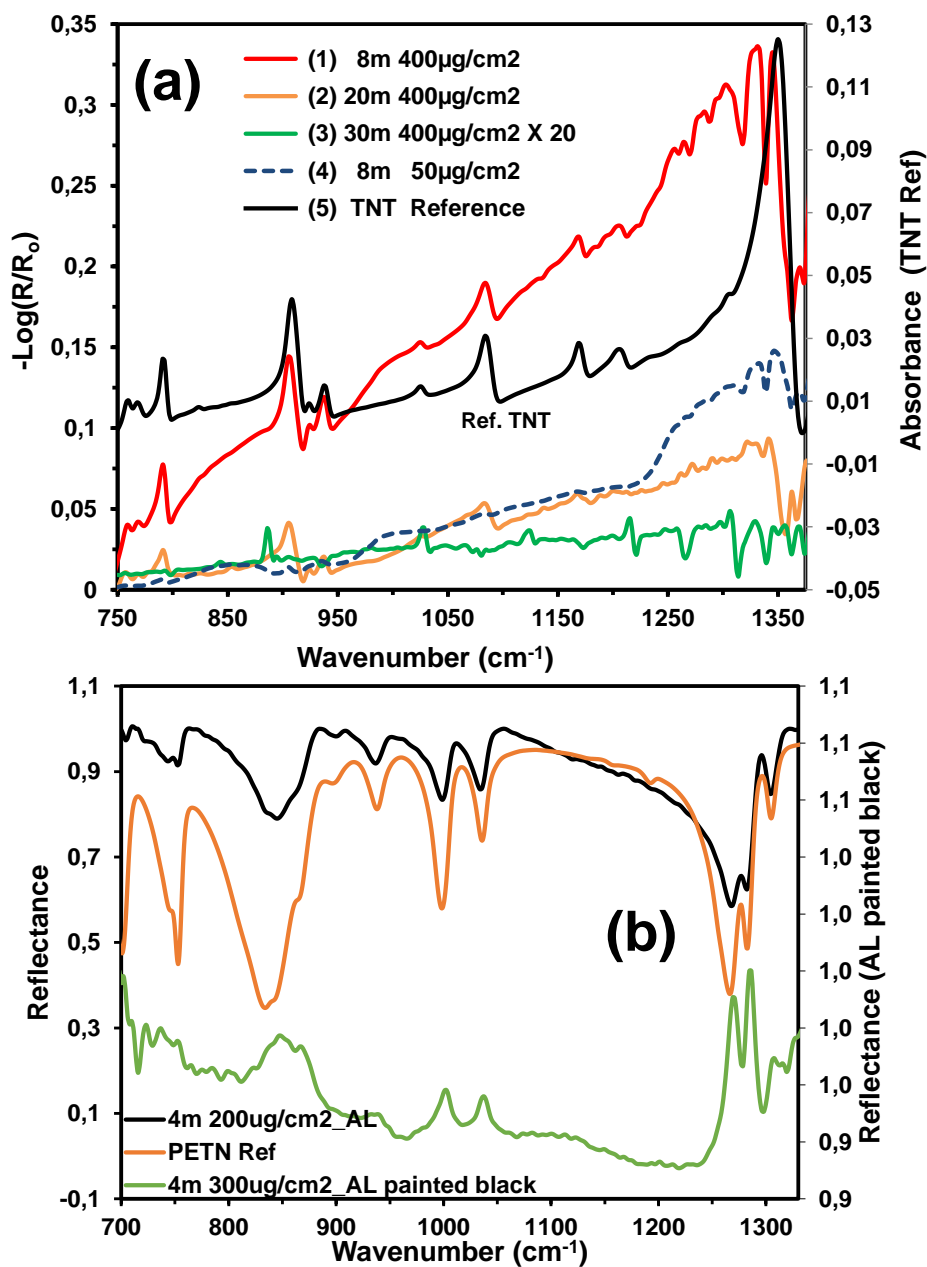


Figure 5-3. (a) Active mode standoff FT-IR spectra of TNT deposited on an Al plate measured at several distances: 8, 20, 30 m and surface concentrations: 400 $\mu\text{g}/\text{cm}^2$ and 50 $\mu\text{g}/\text{cm}^2$; (b) active mode standoff FT-IR spectra of PETN deposited on an Al plate and black painted Al measured at 4 m.

The active mode MIR spectra for PETN deposited on Al plates at several remote distances and surface concentrations are shown in Figure 5-3b, using the experimental setup illustrated in Figure 5-1c. This optical system was designed to overcome the limitations of the optical system illustrated in Figure 5-1a. Among the limitations of the telescope system previously used was the inability to focus at a certain distance, which did not allow having control of the size of the image that illuminates the target at the variable distance, as is shown in Figure 5-2. The size of the image increases as the distance increases when optical detection system shown Figure 5-1a is used, since it was designed for open path measurements. A reference spectrum for PETN is also included in Figure 5-3. These spectra contains the most significant vibrational bands detected in the remote sensed measurements. For PETN in Figure 5-3b, some of the important signatures have been tentatively assigned according to reported values. These correspond to 703 cm^{-1} (ON stretching + NO_2 rocking), 753 cm^{-1} (ONO_2 umbrella), 869 cm^{-1} (ON stretching), 939 cm^{-1} (CH_2 torsion), 1003 cm^{-1} (CO stretching), 1038 cm^{-1} (NO_2 rocking), 1272 cm^{-1} (ONO_2 rocking), 1285 cm^{-1} (NO_2 stretching) and 1306 cm^{-1} (NO_2 rocking) [27]. These spectra were not submitted to any pre-processing routines, such as offset correction, smoothing or water vapor rotational lines removal. In other words, there was no common baseline for these spectra, and some spectra exhibited positive intensity ramps to higher wavenumber values. However, an increase in signal intensity as a function of the surface concentrations showed clearly without the use of chemometrics routines.

Remote detection of PETN deposited on piece of black painted metal car chassis (Nissan Sentra 1985) is shown in Figure 5-3b (green spectrum). This spectrum has inverted peaks

when compared with spectrum taken from Al (black spectrum). Although both spectra were recorded in transflection mode, this shows the effect of the nature of substrate on the spectral profile of target, when active mode IRS is used for the remote measurements. In transflection experiments, as described above, the recorded spectra are a weighted sum of the transmission and reflection characteristics of the samples and substrates. In samples with high reflectivity substrates the weighting is such that the transmission signal dominates and the reflection signal is negligible, producing spectra closely resembling that of a transmission spectrum, as is the case for PETN on Al (black spectrum). However, if the transmission signal is weak or inexistent, the reflection signal will dominate, and a reflectance spectrum is obtained, this can be visualized in Figure 5-3b, green spectrum. Castro-Suarez, et al. discuss further the spectral profile of target on non-reflective substrates [21].

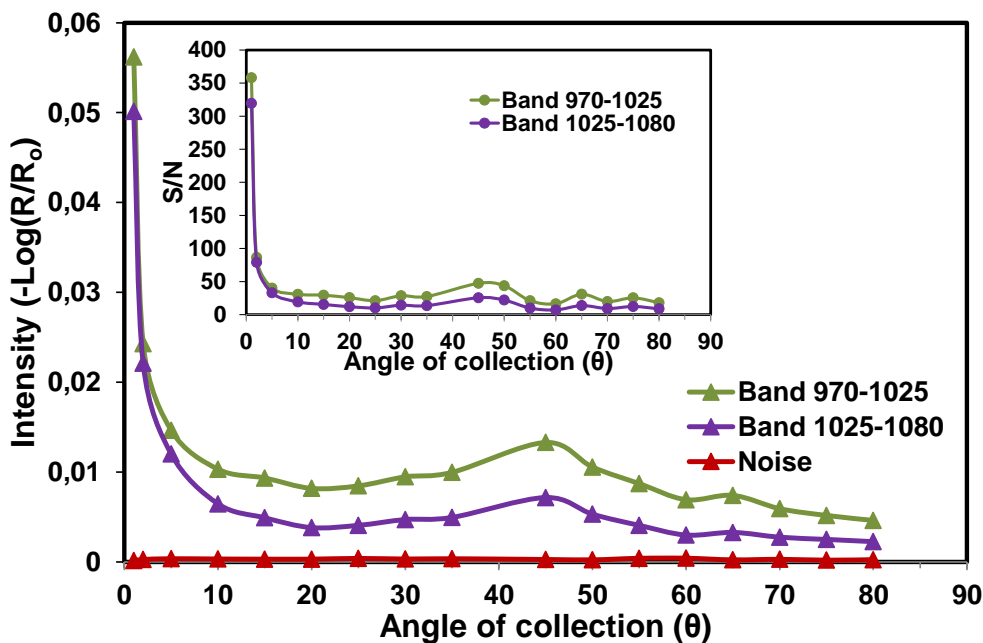


Figure 5-4. Vibrational bands intensity and S/N in different angle of collection for PETN ($200 \mu\text{g}/\text{cm}^2$).

In active mode RIRS detection of targets deposited on metal surfaces, the signal strength is highly dependent on the alignment between IR source-target-detector. Therefore, a study of the effect that had the angle of collection (θ) of the IR beams on the intensity of the vibrational signal was necessary. In this setup, θ is the angle between source/target and target/detector. The influence of the angle of collection on the signal to noise ratio (S/N) of two vibrational bands of PETN deposited on Al metal (at 200 $\mu\text{g}/\text{cm}^2$) is shown in Figure 5-4. The optical system illustrated in Figure 5-1c, detection was used at 1 m. Bands analyzed were those about 970-1025 cm^{-1} and 1025-1080 cm^{-1} . The band intensity was taken as the average height of 5 spectra. The noise intensity was taken as the average height of 5 spectra, both represented in units of $-\text{Log}(R/R_0)$ in the spectral range 1105-1130 cm^{-1} . The S/N was calculated as the peak-to-peak ratios (P-P) between band intensities and noise. The intensities of the bands and S/N were calculated by varying the angle of collection from 1° to 80°, as is illustrated in the Figure 5-4. The intensities of the two bands decreased to about 50% and 25%, when the collection was angle changed from 1° to 2°, and from 1° to 5°, respectively. For collection angles larger than or equal to 10° the intensity decreased drastically compared to that of 1°. For this angle, the decrease in intensity depended on the spectral band selected. For 1038 cm^{-1} band, reduces the intensity of 0.05 ($\theta = 1^\circ$) to ~ 0.004 ($\theta > 10^\circ$), the intensity decreases to 8% when compared to $\theta = 1^\circ$. However, for the 1003 cm^{-1} band intensity decreases of 0.056 ($\theta = 1^\circ$) to ~ 0.008 ($\theta > 10^\circ$), the intensity decreases to 14% when compared to $\theta = 1^\circ$. As shown in Figure 5-4, in collection angles 35 to 50 degree, both spectral bands showed an increase in intensity, this result is not yet well understood, despite that was reproducible in all experiments. The graph S/N vs. angle of collection, inserted into the Figure 5-4 has

a similar behavior to graph of intensity vs. angle of collection. At small angles ($\theta = 2^\circ$ or 5°), the S/N decreases drastically. However, even in $\theta = 80^\circ$, the values for the S/N is equal to eight, so the target characteristic spectral bands can still be detected, because it is five units higher than limit of detection S/N = 3.

5.3.2 HEM Quantification using PLS Regression

The partial least squares-1 (PLS-1) regression algorithm from Quant2™ software of OPUS™ (v. 6.0, Bruker Optics) was used to find the best correlation function between the spectral information and the surface concentrations [28]. Calibrations were performed using PLS-1 in which only one component can be analyzed separately, instead of simultaneously analyzing multiple components, as in the PLS-2 routine of chemometrics. PLS-1 regressions were used to generate chemometrics models for all of the remote distances studied. In addition, CV were made, and the root mean square errors of cross-validations (RMSECV) and coefficient of determination (R^2) were used as measures of the quality of the correlations obtained at the various remote distances studied.

Statistical parameters for the regression models based on PLS-1 were performed using the whole spectral region (from 700 to 1400 cm^{-1}), where the nitro symmetric stretch and aromatic C-H vibrations occur in these compounds. Ten replica spectra were used for each tested sample. In the models obtained, it was not necessary eliminate any spectrum. The method of leave-one-out cross-validation (LOOCV) was used, where each of the “n” calibration samples is left out, one at a time, and the resulting calibration models were used to evaluate the sample left out, which acts as an independent validation sample and

provides an independent prediction of each dependent variable. This process of leaving a sample out was repeated until all of the calibration samples had been left out.

Data preprocessing is an important step in performing chemometrics calibrations. To ensure reproducibility on the calibration samples, ten spectra of each sample (fixed surface concentration and remote distance) were acquired. The following data preprocessing steps were tested: vector normalization, first derivative, and second derivative. However, no preprocessing routine or combination of preprocessing routines of the data worked best. Therefore, data preprocessing steps were not applied for achieving the best possible values for RMSECV and R^2 in the spectral region from 700 to 1400 cm^{-1} other than applying mean centering to each spectrum [28]. Overall, the results indicate that the experimental setup used had good management of the external variables, such as humidity, temperature changes, and concentration of the samples deposited on the aluminum plates.

Figure 5-5a shows the results obtained for the CV carried out for TNT spectra measured using experimental setup shown in Figure 5-1a at distances of 20 m and for 25 m of in active mode, represented as black dots and unfilled squares, respectively. Table 5-1 shows the results of RMSECV and R^2 obtained in the PLS models generated. In these correlation charts, each point represents ten spectra with a fixed surface concentration (0, 50, 100, 200, 300, or 400 $\mu\text{g}/\text{cm}^2$). All the correlation charts of predicted surface concentration values vs. true surface concentration values for 4, 8, 12 and 16 m were similar to the correlation chart for 20 m remote distance (Figure 5-5a, black dots). However, as the remote distance increased beyond 20 m some of the spectral information fell below the quantification level causing the spectra for each sample to not to be identical

with each other (within experimental error) and making it difficult to predict the surface concentration (Figure 5-5a unfilled squares).

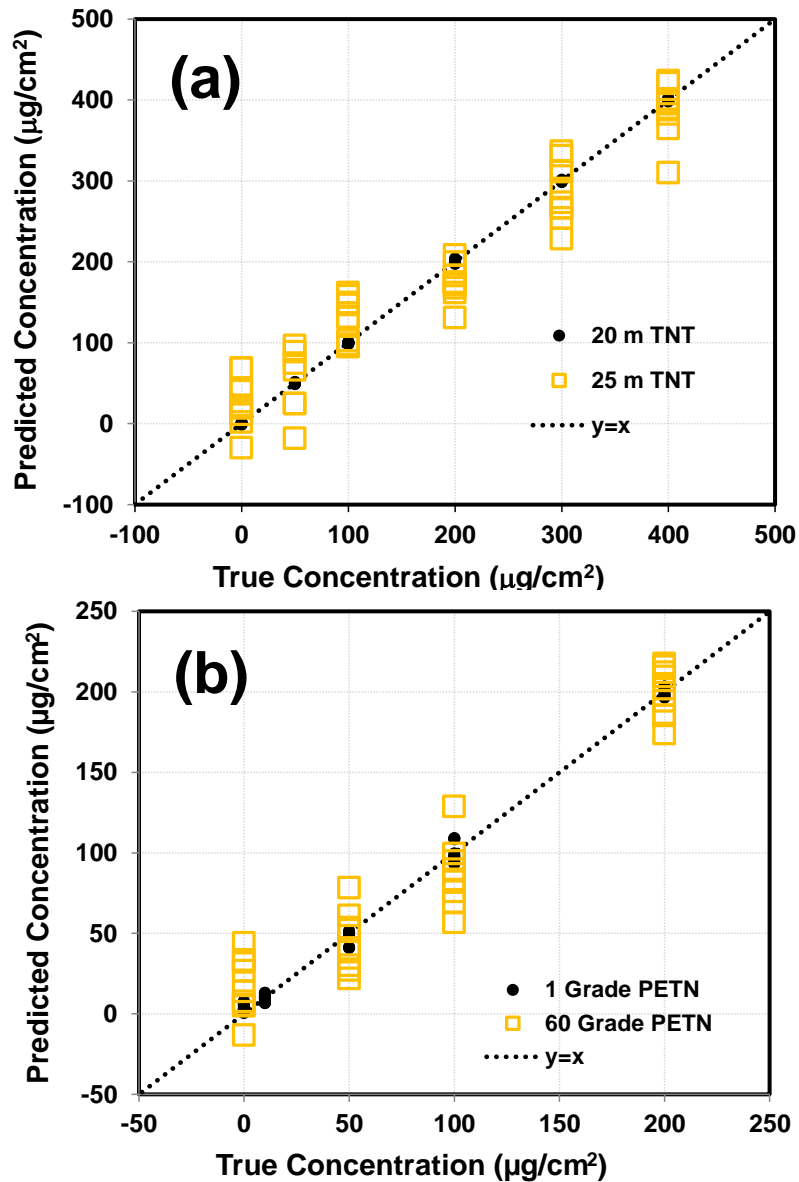


Figure 5-5. (a) Predicted vs. true coverage for TNT explosives on Al plates at different standoff distances: 20 m and 25 m. (b) Predicted vs. true coverage for PETN explosives on Al plates at different angle of collection: 1° and 60° .

Table 5-1. PLS calibration parameters for the different analyzed standoff distance.

Distance (m)	R ²	RMSECV	Rank	Spectral range (cm ⁻¹)	Preprocessing
4	1	0.457	8	1400-700	Mean centering
8	1	0.434	7	1400-700	Mean centering
12	1	0.676	8	1400-700	Mean centering
16	1	0.736	9	1400-700	Mean centering
20	0.9999	1.08	9	1400-700	Mean centering
25	0.9367	34.6	5	1400-700	Mean centering
30	0.8553	53.5	9	1400-700	Mean centering

Figure 5-5b shows the results obtained of cross-validations carried out for PETN spectra measured at SO distances of 1m in active mode for two angle of collection 1 and 60 grade (represented as black circles and empty squares respectively) using experimental setup shown in Figure 5-1c. Table 5-2 shows the results of RMSECV and R² obtained in the PLS models generated for angle of collection 1°, 20°, 40° and 60°. In these correlation charts, each point represents ten spectra with a fixed surface concentration (0, 10, 50, 100 or 200 µg/cm²). However, as the collection angle increased the IR vibrational bands intensity decrease drastically (as show above) causing the spectra for each sample to not to be identical with each other and making it difficult to predict the surface concentration (Figure 5-5b unfilled squares).

Table 5-2. PLS calibration parameters for the different analyzed angle of collection.

Collection Angle (Θ)	R ²	RMSECV	Rank	Spectral range (cm ⁻¹)	Preprocessing
1°	0.9963	4.26	7	1400-700	Mean centering
20°	0.9628	14.10	7	1400-700	Mean centering
40°	0.9802	10.30	7	1400-700	Mean centering
60°	0.9237	20.40	7	1400-700	Mean centering

Figure 5-6b shows the regression coefficient and loading (LV1) plot for the PLS model of PETN explosives detection and quantification on Al plates at 1 m standoff distance and angle of collection 1° . This regression coefficient spectrum in the spectral range from 750-1375 cm^{-1} contains the characteristic vibrational bands of PETN that are significant for predicting the detection/quantification of the HEM deposited at trace level on the Al substrates. Figure 5-6b also shows that the first loadings used in the PLS model, the variables with the largest statistical weights correspond to PETN characteristic bands illustrated in Figure 5-3b. The values obtained of RMSECV and R^2 for angle of collection 1° , 20° , 40° and 60° are as expected. As is shown in table 5-2, when Θ is equal to 40° is improved values RMSECV and R^2 , which is expected from the results shown in Figure 5-4. Taking into account the low values of RMSECV and high values of R^2 , high values S/N, these models are useful tools for determining the surface concentration of PETN in unknown samples.

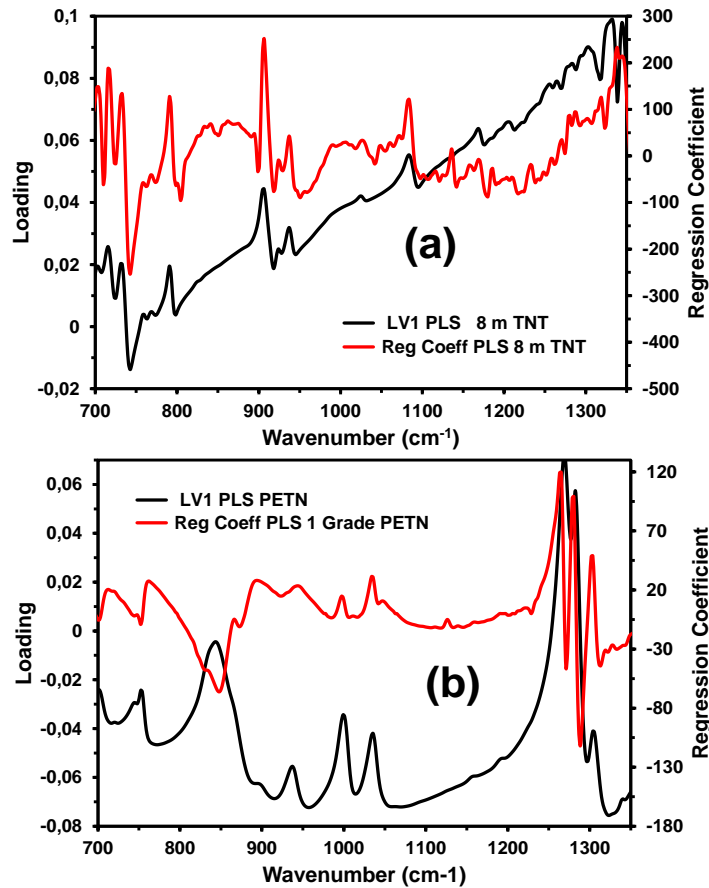


Figure 5-6. (a) Regression coefficient and loading plot for PLS model of detection of TNT explosives on Al plates at a remote distance 8 m; (b) Regression coefficient and loading plot for PLS model of detection of PETN explosives on Al plates at 1 m standoff distance and angle of collection 1° .

5.4 CONCLUSIONS

A remote detection technique based on an FT-IR spectrometer has been demonstrated and used to obtain spectral information of HEM samples deposited on Al plates. High spectral quality measurements were achieved by using MIR reflective and refractive telescopes coupled remote detection system. Detection in active mode proved to be useful for detecting TNT vibrational signatures in the range of 4-30 m (active mode). The remote detection system worked better for distances smaller than 24 m due to the

transmitter telescope characteristics in sensing de TNT. At 24 m the MIR beam size was as large as the target (30 cm) and S/N was 3, falling rapidly above 25 m using MIR reflective telescopes. However, it was necessary to align carefully the target with the detector to be able to measure with high accuracy at standoff distances of 25 – 30 m in TNT detection experiments. The optical system designed for detecting PETN vibrational bands in the range of 1 – 4 m by varying angle of collection from 1° to 80° performed as designed. Furthermore, excellent results for RMSECV and R² were obtained for models generated based on PLS CV for the active mode experiments.

5.5 ACKNOWLEDGMENTS

Support from the U.S. Department of Homeland Security under Award Number **2013-ST-061-ED0001** is acknowledged. However, the views and conclusions contained in this document are those of the authors and should not be considered as a representation of the official policies, either expressed or implied, of the U.S. Department of Homeland Security.

This contribution was supported by the U.S. Department of Defense, Proposal Number: 58949-PH-REP, Agreement Number: W911NF-11-1-0152. The authors also acknowledge contributions from Dr. Richard T. Hammond from Army Research Office, DoD.

5.6 REFERENCES

- [1]. H. Schubert and A. Rimski-Korsakov, *Stand-Off Detection of Suicide-Bombers and Mobile Subjects*, 2006. Springer, Dordrecht-The Netherlands.

- [2]. M. Marshall and J. C. Oxley, *Aspects of Explosives Detection*, 2009. Elsevier, Oxford.
- [3]. M. López-López and C. García-Ruiz, *Infrared and Raman spectroscopy techniques applied to identification of explosives*. TrAC Trends in Analytical Chemistry, 2014. **54**: p. 36-44.
- [4]. J. S. Caygill, F. Davis and S.P.J Higson, *Current trends in explosive detection techniques*. Talanta, 2012. **88**: p. 14-29.
- [5]. J. Yinon, *Field detection and monitoring of explosives*. TrAC Trends in Analytical Chemistry, 2002. **21**(4): p. 292-301.
- [6]. D. S. Moore, *Instrumentation for trace detection of high explosives*. Review of Scientific Instruments, 2004. **75**(8): p. 2499-2512.
- [7]. D. J. Klapac and G. Czarnopys, *Analysis and Detection of Explosives and Explosives Residues Review: 2010 to 2013*. In: N.N. Daéid, Ed. In 17th Interpol International Forensic Science Managers Symposium, Lyon 8 th-10 th October, 2013. **526**: p. 280-435.
- [8]. A. J. Bhandodkar, A.M. O'Mahony, J. Ramírez, I. A. Samek, S. M. Anderson, J. R. Windmiller and J. Wang, *Solid-state Forensic Finger sensor for integrated sampling and detection of gunshot residue and explosives: towards 'Lab-on-a-finger*. Analyst, 2013. **138**(18): p. 5288-5295.
- [9]. T. Caron, M. Guillemot, P. Montméat, F. Veignal, F. Perraut, P. Prené and F. Serein-Spirau, *Ultra trace detection of explosives in air: Development of a portable fluorescent detector*. Talanta, 2010. **81**(1): p. 543-548.

- [10]. J. L. Gottfried, *Discrimination of biological and chemical threat simulants in residue mixtures on multiple substrates*. Analytical and bioanalytical chemistry, 2011. **400**(10): p. 3289–3301.
- [11]. W. Ortiz-Rivera, L. C. Pacheco-Londoño, J. R. Castro-Suarez, H. Felix-Rivera, and S. P. Hernandez-Rivera, *Vibrational spectroscopy standoff detection of threat chemicals*. In SPIE Defense, Security, and Sensing, International Society for Optics and Photonics, 2011. **803129**: p. 803129-803129.
- [12]. J. Mass, A. Polo, O. Martínez, W. López, E. Zurek, M. Esmeral, J. Delgado, H. Alvarez, and L. García, *Identification of Explosive Substances Through Improved Signals Obtained by a Portable Raman Spectrometer*. Spectroscopy Letters, 2012. **45**(6): p. 413-419.
- [13]. J. R. Castro-Suarez, L. C. Pacheco-Londoño, M. Vélez-Reyes, M. Diem, T. J. Tague and S. P. Hernández-Rivera, *FT-IR Standoff Detection of Thermally Excited Emissions of Trinitrotoluene (TNT) Deposited on Aluminum Substrates*. Applied Spectroscopy, 2013. **67**(2): p. 181-186.
- [14]. J. E. Parmenter, Proceedings of the 38th Annual 2004 International Carnahan Conference on Security Technology, 2004. **355** IEEE: New York.
- [15]. P. R. Griffiths, L. Shao and A. B. Leytem, *Completely automated open-path FT-IR spectrometry*. Analytical and bioanalytical chemistry, 2009. **393**(1): p. 45-50.
- [16]. L. C. Pacheco-Londoño, W. Ortiz, O. M. Primera and S.P. Hernández-Rivera, *Vibrational spectroscopy standoff detection of explosives*. Analytical and bioanalytical chemistry, 2009. **395**(2): p. 323-335.

- [17]. J. D. Suter, B. Bernacki and M.C. Phillips, *Spectral and angular dependence of mid-infrared diffuse scattering from explosives residues for standoff detection using external cavity quantum cascade lasers*. Applied Physics B, 2012. **108**(4): p. 965-974.
- [18]. M. Kumar, M. N. Islam, F.L. Terry, M.J. Freeman, A. Chan, M. Neelakandan and T. Manzur, *Stand-off detection of solid targets with diffuse reflection spectroscopy using a high-power mid-infrared supercontinuum source*. Applied optics, 2012. **51**(15): p. 2794-2807.
- [19]. J. Ledgard, *The Preparatory Manual of Explosives*. 3rd Ed. 2007
- [20]. J. Clarkson, W. E. Smith, D. N. Batchelder, D. A. Smith and A. M. Coats, *A theoretical study of the structure and vibrations of 2, 4, 6-trinitrotoluene*. Journal of Molecular Structure, 2003. **648**(3): p. 203-214.
- [21]. J.R. Castro-Suarez, M. Hidalgo-Santiago and S.P. Hernández-Rivera, *Detection of highly energetic materials on non-reflective substrates using quantum cascade laser spectroscopy*. Applied Spectroscopy, 2015. **69**(9): p. 1023-1035.
- [22]. J. M. Chalmers and M. W. Mackenzie, *Some industrial applications of FT-IR diffuse reflectance spectroscopy*. Applied Spectroscopy, 1985. **39**(4): p. 634-641.
- [23]. P. Bassan, H. J. Byrne, F. Bonnier, J. Lee, P. Dumas and P. Gardner, *Resonant Mie scattering in infrared spectroscopy of biological materials—understanding the dispersion artifact*. Analyst, 2009. **134**(8): p. 1586-1593.
- [24]. P. Bassan, H. J. Byrne, J. Lee, F. Bonnier, C. Clarke, P. Dumas, E. Gazi, M. D. Brown, N. W. Clarke and P. Gardner, *Reflection contributions to the dispersion*

- artefact in FTIR spectra of single biological cells*. *Analyst*, 2009. **134**(6): p. 1171-1175.
- [25]. M. Miljković, B. Bird and M. Diem, *Line shape distortion effects in infrared spectroscopy*. *Analyst*, 2012. **137**(17): p. 3954-3964.
- [26]. J.M. Chalmers, *Mid-Infrared Spectroscopy: Anomalies, Artifacts and Common Errors*. In *Handbook of vibrational spectroscopy*, 2006. J.M. Chalmers and P.R. Griffiths, Eds. Chichester, John Wiley and Sons, vol. 3.
- [27]. W.F. Perger, J. Zhao, J.M. Winey, Y.M. Gupta. *First-Principles Study of Pentaerythritol Tetranitrate Single Crystals under High Pressure: Vibrational Properties*. *Chemical physics letters*, 2006. **428**(4): p. 394–399.
- [28]. K. Beebe, R. Pell and M. Beth, *Chemometrics: A Practical Guide*. 1998. Wiley & Sons, New York, NY.

IX. CHAPTER 6

DEVELOPMENT OF GC-MS ANALYSIS METHODS FOR EMERGENT GROUPS OF SYNTHETIC CANNABINOIDS FOUND IN VEGETATIVE SAMPLES

OVERVIEW

Three GC-MS analytical methods were developed and tested, using abuse-drugs standards, for synthetic cannabinoids (SC), THC, cocaine and heroin. Analytical procedure for extract synthetic cannabinoids from herbal mix seized in the black market by the Police Department of Puerto Rico, USA is shown. Different organic solvents were used for the extraction. Instrumental technique like GC was used for separation and purification of SC. Additional, electron impact-mass spectrometry was utilized as confirmatory method to identify the Synthetic Cannabinoids on the herbal sample. Two Synthetic Cannabinoids were found in real-world sample. The results show that analytical methods developed can be useful to identify Synthetic Cannabinoids rarely used such as PB-22 and 5F-PB-22 when are present in herbal mixture.

6.1 INTRODUCTION

Modern society has an urgent need to develop accurate and rapid methods necessary for chemical analysis of drugs of abuse. From the staff that combat drug trafficking and employees in charge of law enforcement, such as forensic science laboratories, police

officers, airport security officials, Drug Enforcing Agency (DEA) officers, and other government employees have implemented strategies to minimize the consumption and distribution of these illegal drugs.

The chemical analysis of street drugs has always been a topic of particular interest to forensic laboratories. These drugs have evolved over the past 30 years. From their original form of natural products with little or no chemical manipulation in their preparation, such as marijuana, opium, khat (cathinone), morphine, cocaine, etc. drugs of abuse developed into those where medium or high chemical skill are required for synthesis, such as heroin, amphetamines (and their derivatives), bath salts (such as synthetic cathinones), synthetic cannabinoids, etc. The latter, called designer drugs, or synthetic drugs, are easy to acquire by drug users, either because they can be camouflaged in complex matrices or because they are difficult to detect in the field. These drugs are often not identified by forensic science laboratories due to the absence of specific analytical procedures, probably due to the constant change in the chemical structure of these designer drugs [1,2].

Cannabinoids fall into three categories. The first one is *natural cannabinoids*: as the ones contained in cannabis plants, such as THC (Δ^9 -tetrahydrocannabinoid). The second group includes the natural cannabinoid, such as *endogenous cannabinoid* (EC), which is produced by the body itself and plays important physiological roles in regulating blood pressure, memory, thinking, concentration, movement, coordination, sensory and time perception, appetite, and pain. The last category is composed of the *synthetic cannabinoids* (SC), which are compounds produced in the laboratory, with the intention

to investigate endogenous cannabinoids, to create new alternatives for medical use, in a way to separate the desired analgesic effects from unwanted psychotropic effects [3,4].

An increasingly popular trend of recreational drug users is smoking blends of herbal products or incense mixed with one or more of the SC functionally, but not necessarily structurally related to THC [4,5]. The academic and / or pharmaceutical origin of these compounds is often reflected in the product name. The best-known class of these compounds is known as JWH-compounds, in honor of the organic chemistry professor John W. Huffman of Clemson University, South Carolina, who first synthesized these products in the 1990s. In a similar way AM (e.g. AM-630) refers to professor Alexandros Makriyannis from Northeastern University, Boston, MA and HU (e.g. HU-210) from the Hebrew University by Professor R. Mechoulam [6].

In general, these compounds are lipid soluble, non-polar molecules, which contain 20 to 26 atoms carbon [7]. Based on this chemical structure, SC can be divided into different classes [8]:

1. *classical cannabinoids*: structurally related to THC from Cannabis sativa, e.g. HU-210
2. *non-classical cannabinoids*: cyclohexylphenols or 3-arylcyclohexanols, e.g. CP-47.497)
3. *hybrid cannabinoids*: structural combinations of both classical and non-classical cannabinoids
4. *aminoalkylindoles*:
 - a. naphthoylindoles, e.g. JWH-018, and AM-1220
 - b. phenylacetylindoles, e.g. JWH-203, and RCS-8

- c. benzoylindoles, e.g. AM-694, WIN 48.098, and RCS-4
 - d. cyclopropoylindoles, e.g. UR-144, and XLR-11
 - e. naphthylmethylindoles, e.g. JWH-184)
 - f. adamantoylindoles, e.g. AB-001, and AM-1248
 - g. Indole carboxamides, e.g. APICA, STS-135;
5. *Eicosanoids*: endocannabinoids and synthetic analogs, e.g. AM-356;
6. *Others*:
- a. diarylpyrazoles,
 - b. naphthoylpyrroles, e.g. JWH-307
 - c. naphthylmethylindenes, e.g. JWH-176
 - d. indazole carboxamides, e.g. APINACA)

SC bind to the same cannabinoid receptors (CB) in brain and peripheral organs [9]. Unlike THC, which binds with almost equal affinity to CB1 and CB2 receptors, some of the new synthetic compounds exhibit more preference for CB1 receptors, which may produce more potent effects [4].

Little is known about the exact composition and properties of the plants used and in many cases the ingredients found in the lists of contents of packages of products do not include the whole content thereof [6]. Manufacturers of these mixtures make users believe that the mixture of plant material used causes the effects experienced. However, researches on plant materials have shown that most species of plants do not have psychoactive properties and therefore are only used to dilute added cannabinoids [10]. In addition, producers try to present their products as natural and safe to circumvent marijuana policies of governments. The United Nations Office on Drugs and Crime (UNODC)

concluded that producers respond very quickly to changes in legislation, making small changes to the new products launched at the markets [8].

SC products for sale on head shops, gas stations or via internet shops go through a variety of names. The most common in the United States are known as K2. Other common names are in the U.S. are: K2 Pink, K2 Strawberry, K2 Blueberry, K2 Sex, K2 Sex on the Mountain, K2 Blonde, K2 Ultra, K2 Citron, K2 Blue, Space, Spike, Mr. Blend Nice Guy (MNGB), Banana Cream Nuke, pep pourri, Pep spice, Voo Doo Remix, C4, and K1, K3, K4 and K20. other names are found, Gold, Yucatan Fire, Bonzai, Jamaika, Jamaican Gold Supreme, Aroma, Blaze, Blueberry Haze, Dank, Demon Passion Smoke, Genie, Hawaiian Hybrid, Magma, Ninja, Nitro, Ono Budz, Panama Red Ball, Puff, Sativah Herbal Smoke, Skunk, Spice, Ultra Chronic, Voodoo Spice and others. More than 140 different synthetic marihuana products have been identified to date [5, 11]. The materials are normally sold in metallic bags 2.5 in. x 2.5 in., with a zipper lock. The contents are typically 1.3 g of a mixture of dried and ground plant material (flowers, stems, leaves, etc.) often perfumed, aromatic odor [5].

In the last four years, there has been a steady increase in scientific publications of well-established research groups have invested efforts in the identification and quantification of SC. Some of the studies that have had great impact on the forensic community are highlighted next. In 2010, Uchiyama, et al. found several SC in 44 of 46 different types of herbal products that are currently distributed in the market for illegal drugs in Japan [12]; GC-MS analysis and liquid chromatography coupled to mass spectrometry (LC-MS) indicated that most of the herbal product contained two major SCs: (1RS, 3SR) 3-[2-hydroxy-4-(2-metilnonan-2-yl)-phenyl] cyclohexane-1-ol, commonly known as

cannabicyclohexanol, by Pfizer, Inc. and / or 1-naphthalenyl (1-pentyl-1H-indol-3-yl) methanone, called JWH-018. JWH-018 and cannabicyclohexanol Concentrations in the herbal products ranged from 1.1 to 16.9 mg/g and 2.0 to 35.9 mg/g, respectively, and showed considerable variation.

Furthermore, in 2012 Logan, et al. [5], used thin layer chromatography, GC-MS, high performance liquid chromatography (HPLC) to time of flight-mass spectrometry (HPLC-TOF-MS) for identification and quantification of these substances pharmacologically active in the forms of drugs of abuse. Using methods based on the instrumentation mentioned, they identified synthetic cannabinoids: JWH-018, JWH-019, JWH-073, JWH-081, JWH-200, JWH-210, JWH-250, CP47, 497 (C = 8) (cannabicyclohexanol) RCS-4, RCS-8 AM-2201 and AM-694 in several commercially available products. Other non-cannabinoids drugs including mitragyna, were also detected. Typical concentrations of drugs in the materials were in the range of 5-20 mg/g, or 0.5 to 2% by weight for each compound, although many products containing more than one drug.

In a recent paper, 2014, Veress and Nagy utilized several solvents (acetone, chloroform, methanol and n-hexane) for extraction of target compounds [13]. Subsequent IRS-attenuated total reflectance (ATR) analysis of evaporative residues of extracts were studied. The applicability of the elaborated procedure was demonstrated via analysis of real samples and has been found useful for the analysis of herbal mixtures containing AKB48, AB-PINACA, AB-FUBINACA, PB-22, AB-CHMINACA, 5F-PB-22, AM-2201.

In Puerto Rico, on August 4, 2012 the Articles 102 and 202 of Act No. 4 of June 23, 1971 known as the "Controlled Substances Act", were amended to define terms cannabinoids and SC and classify them as controlled substances. In this amendments, the sale of any

product or chemicals that contains cannabinoids or SC is prohibited, including AM-2201, AM-694, CB-25, CB-52, CP47-497, CP55-940, HU-210, HU-211, HU-308, HU-331, JWH-015, JWH-018, WIN55-212-3, JWH-019, JWH-073, JWH-081, JWH-133, JWH-200, JWH-203, JWH-210, JWH-250, JWH-251, JWH-398, RCS-4, RCS-8 and WIN55, 212-2 [14]. In this report, GC-MS analytical methodologies were developed using standards of SC. In addition, an analytical procedure for extracting, separating, and identifying 5F-PB-22 and PB-22 SC form herbal mixes seized in the black market by Police Department of PR, USA was developed. GC was used for the separation and purification of the SCs. Electron impact-mass spectrometry (EI-MS) was used to develop the confirming methodologies to identify the SCs in the herbal samples. The results show that analytical methods developed can be useful to identify SC rarely used, such as PB-22 and 5F-PB-22 when present in herbal mixture.

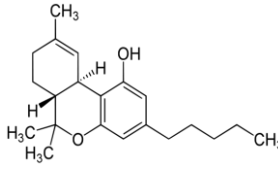
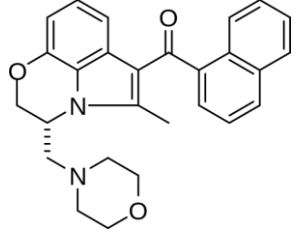
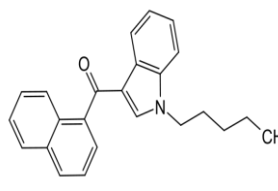
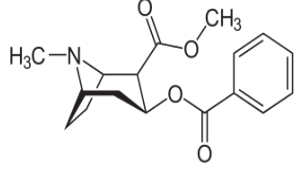
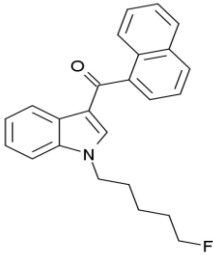
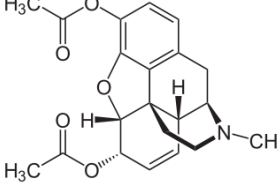
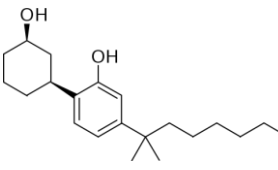
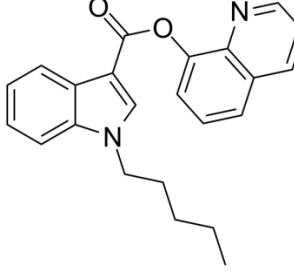
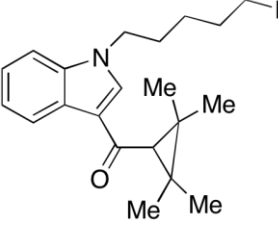
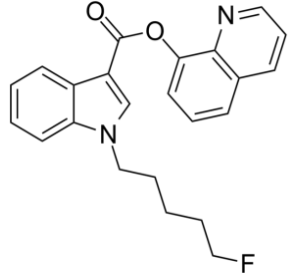
6.2 MATERIALS AND METHODS

6.2.1 Reagents and materials

The reagents and materials used in this study included SCs, and solvents. 5F-PB-22 and PB-22 were used as SC and were extracted from herbal blend donated by the Forensic Sciences Institute of Puerto Rico (FSI-PR), San Juan, PR, USA. Herbal mixtures with new psychoactive materials were seized in the black market of Puerto Rico by the Police Department and passed onto the FSI-PR. Standards of SCs donated by FSI-PR Ponce, PR, including compounds such as JWH-018, AM-2201, CP-47,497, WIN 55,212-2, and XLR-11 were used to develop chromatographic methods of analysis. THC, cocaine, and heroin donated by FSI-PR San Juan, PR also were used for developing the extraction,

GC analyses, and GC-MS analyses. Table 6-1 shows the chemical structures and IUPAC names of the different abuse drugs used in this research. Methanol (99.9%, HPLC grade), dichloromethane (CH_2Cl_2 , HPLC grade), acetone (99.5%, GC grade) were purchased from Sigma-Aldrich (Milwaukee, WI, USA) and were used as solvents to extract the SCs from vegetal sample.

Table 6-1. Chemical structures and IUPAC name of abuse drugs used

Abuse drugs standards and IUPAC name	Chemical structure	Abuse drugs standards and IUPAC name	Chemical structure
THC (Tetrahydrocannabinol) or (-)-(6a <i>R</i> ,10a <i>R</i>)-6,6,9-Trimethyl-3-pentyl-6a,7,8,10a-tetrahydro-6 <i>H</i> -benzo[<i>c</i>]chromen-1-ol		WIN55,212-2 (<i>R</i>)-(+)-[2,3-Dihydro-5-methyl-3-(4-morpholinyl)methyl]pyrrolo [1,2,3- <i>de</i>]-1,4-benzoxazin-6-yl]-1-naphthalenylmethanone	
JWH-018 Naphthalen-1-yl-(1-pentylindol-3-yl)methanone		Cocaine methyl (1 <i>R</i> ,2 <i>R</i> ,3 <i>S</i> ,5 <i>S</i>)-3-(benzoyloxy)-8-methyl-8-azabicyclo[3.2.1]octane-2-carboxylate	
AM-2201 1-[(5-Fluoropentyl)-1 <i>H</i> -indol-3-yl]-(naphthalen-1-yl)methanone		Heroin (5α,6α)-7,8-didehydro-4,5-epoxy-17-methylmorphinan-3,6-diol diacetate	
CP-47,497 2-[(1 <i>R</i> ,3 <i>S</i>)-3-hydroxycyclohexyl]-5-(2-methyloctan-2-yl)phenol		PB-22 1-Pentyl-1 <i>H</i> -indole-3-carboxylic acid 8-quinolinyl ester	
XLR-11 (1-(5-fluoropentyl)-1 <i>H</i> -indol-3-yl)(2,2,3,3-tetramethylcyclopropyl)methanone		5F-PB-22 1-pentylfluoro-1 <i>H</i> -indole-3-carboxylic acid 8-quinolinyl ester	

6.2.2 Sample preparation

The extraction of the target compounds in complex herbal matrices is a fundamental step in the analysis of SCs. This step allowed obtaining calibration models that provided good predictions for the validation samples. For extraction of SCs, a small amount (about 1 mg) of herbal mixture was placed in a test tube and 1 mL of organic solvent (such as acetone, dichloromethane, or methanol) was added to the test tube containing herbal mixture. This was followed by a stirring step. The stirring was done in two ways: manually for 30 s using the routine analytical procedure; and sonicated by 30-60 min using an ultrasonic bath. The supernatant was placed in a GC-MS vial and the organic solvent was evaporated (if methanol was not used for extraction) using a dry air flow. Finally, 0.5 mL of methanol was added to the vial and analyzed using GC-MS. Figure 6-1 shows an overview of the steps carried out for extraction, and GC-MS analysis of SCs.

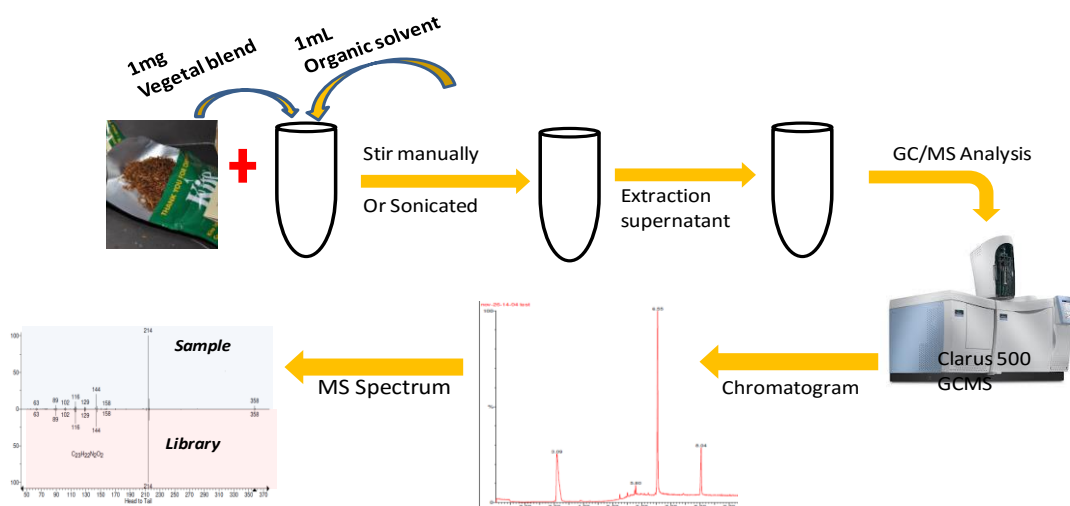


Figure 6-1. Experimental Setup for extraction and instrumental analysis of SCs present in vegetal blend.

6.2.3 GC-MS Analysis

Sample extracts and standards in methanol were analyzed by GC-MS using a Perkin-Elmer model Clarus 500™ GC/MS. The GC-MS analyses were carried out using one of the three methods developed and described in Table 6-2. Each MS spectrum of the chromatographic peaks was compared with those from NIST and Cayman libraries.

Table 6-2. GC-MS methods parameter used for analysis of SC present in blend vegetal

	Method 1	Method 2	Method 3
GC parameters			
Oven	T _{initial} : 180 °C for 1 min Ramp1: 30 °C/min to 250 °C, hold 1min Ramp2: 40 °C/min to 290 °C, hold 9.67 min	T _{initial} : 140 °C for 0.2 min Ramp1: 45 °C/min to 295 °C, hold 5.36 min	T _{initial} : 150 °C for 0.2 min Ramp1: 45 °C /min to 295 °C, hold 16.58 min
Column	J&W Scientific DB-5 MS, 15mx250µm	J&W Scientific DB-5 MS, 15mx250µm	J&W Scientific DB-5 MS, 15mx250µm
Injection Temp.	250 °C	250 °C	250 °C
Injection Vol.	0.5 µL	0.5 µL	0.5 µL
Split	50:1	50:1	50:1
Carrier Gas	He, 1 mL/min	He, 1 mL/min	He, 1 mL/min
MS parameters			
Ionization Mode	EI, 70 eV	EI, 70 eV	EI, 70 eV
Solvent Delay	1.00 min	0.5 min	0.5 min
Transfer Temp.	220 °C	220°C	220 °C
Source Temp	200 °C	200 °C	200 °C
Scan Mode	50 to 500 Da	50 to 500Da	50 to 500Da

6.3 RESULTS AND DISCUSSION

6.3.1 GC-MS Method Development

GC-MS based methods of fast and reliable chemical analysis of SCs present in herbal blends, obtained from the Puerto Rico black market were developed and tested. These methods are able to separate, identify, and quantify SCs and natural-abuse drugs commonly used such, as THC, cocaine and heroin in real samples. The methods were developed by taking into consideration that often the target substances are added in small amounts to the herbal mixes. Standards were chosen so as to have a wide variety of retention times (R_t ; low to high) in the GC analysis, allowing to obtain a more robust methodology for future SCs in herbal blends not included in our analytical methods. Figure 6-2 and 6-3 show chromatograms of SCs and THC standards using methods 1 and 2, respectively. Table 6-3 includes the R_t values obtained for SC and natural-abuse drugs standards, using analytical chromatographic method shown in Table 6-2. In general, the range of R_t values for the standards used employing methods 1 and 2 were between 3.61 min to 5.02 min, excluding WIN55,212-2 standard in both cases. When this standard for was analyzed using method 1 (a method routinely used by the FSI-PR lab for cannabinoids) no elution was observed. WIN55,212-2 was eluted in the next chromatographic run with an $R_t = 6.85$ min when running a blank sample consisting of methanol (see WIN55,212-2_b in Figure 6-2). Due to the high molecular weight of this compound and high R_t value for this suggested to modify method 1. The modification was done by adjusting the oven temperature parameters (see Table 6-2) and this new method was termed method 2. Since no elution was observed when analyzing for WIN55,212-2

using method 2, a further modification of the method was applied and designated as method 3.

All the standards used were analyzed with MS using the parameters shown in Table 6-2 for each analytical method. Mass spectra recorded agree with those from libraries of the instrument. Figure 6-5 and 6-6 shows mass spectra of standards used to develop the analytical methods. These MS spectra present fragmentation patterns characteristic of abuse drugs utilized. MS spectra showed no variability when the GC-MS analytical method was changed.

Table 6-3. Retention time for SC standards and other drugs standards using analytical methods shown in Table 6-2

Abuse drugs standards	Method 1 Retention Time (min)	Method 2 Retention Time (min)	Method 3 Retention Time (min)
THC	4.62	3.61	3.38
JWH-018	7.56	5.89	
AM-2201	8.39	6.56	
CP-47,497	5.01	3.80	
XLR-11	5.02	3.81	
WIN55,212-	6.85 ^a	8.11 ^a	13.66
cocaine	-	-	2.84
heroin	-	-	3.68

^a This SC was eluted in the next chromatographic run, corresponding to blank sample (methanol).

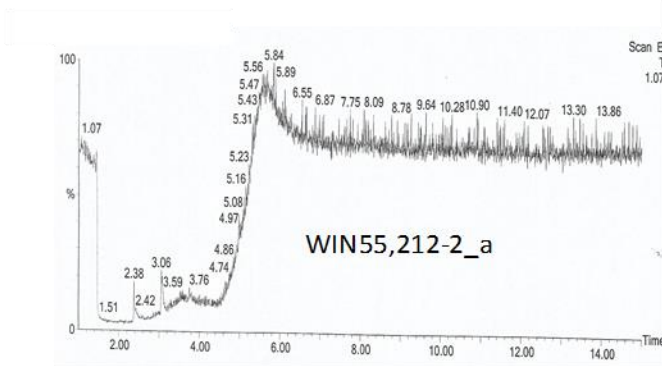
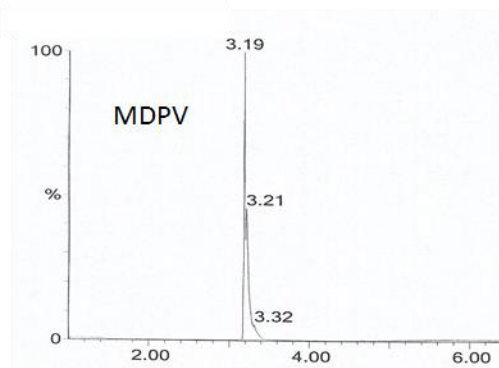
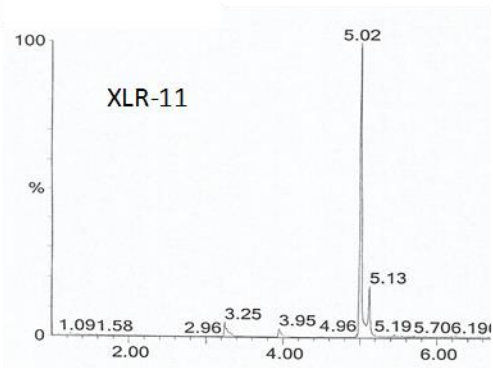
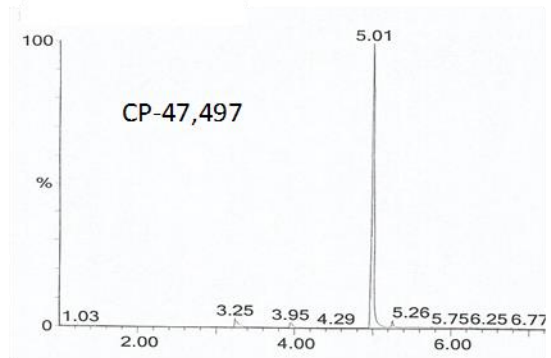
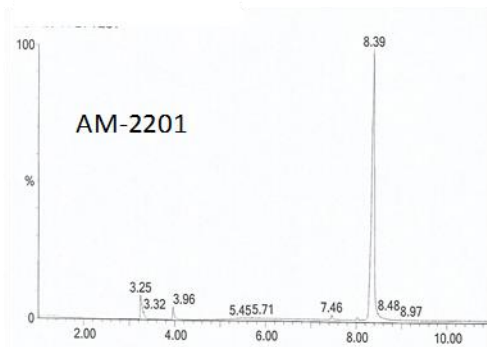
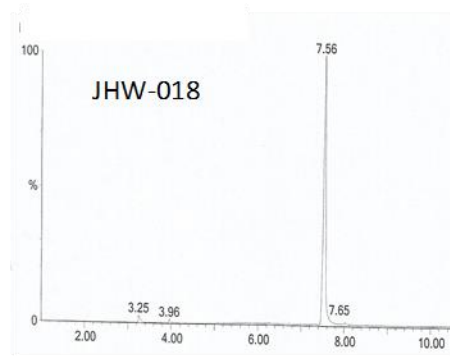
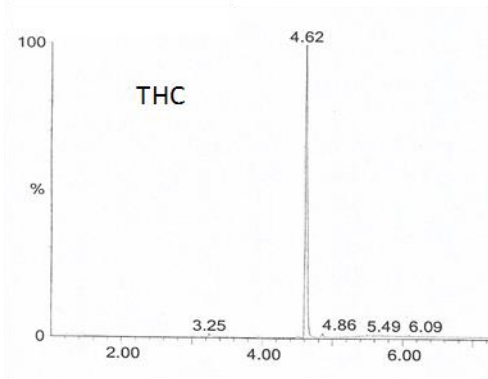


Figure 6-2. Chromatograms using method 1.

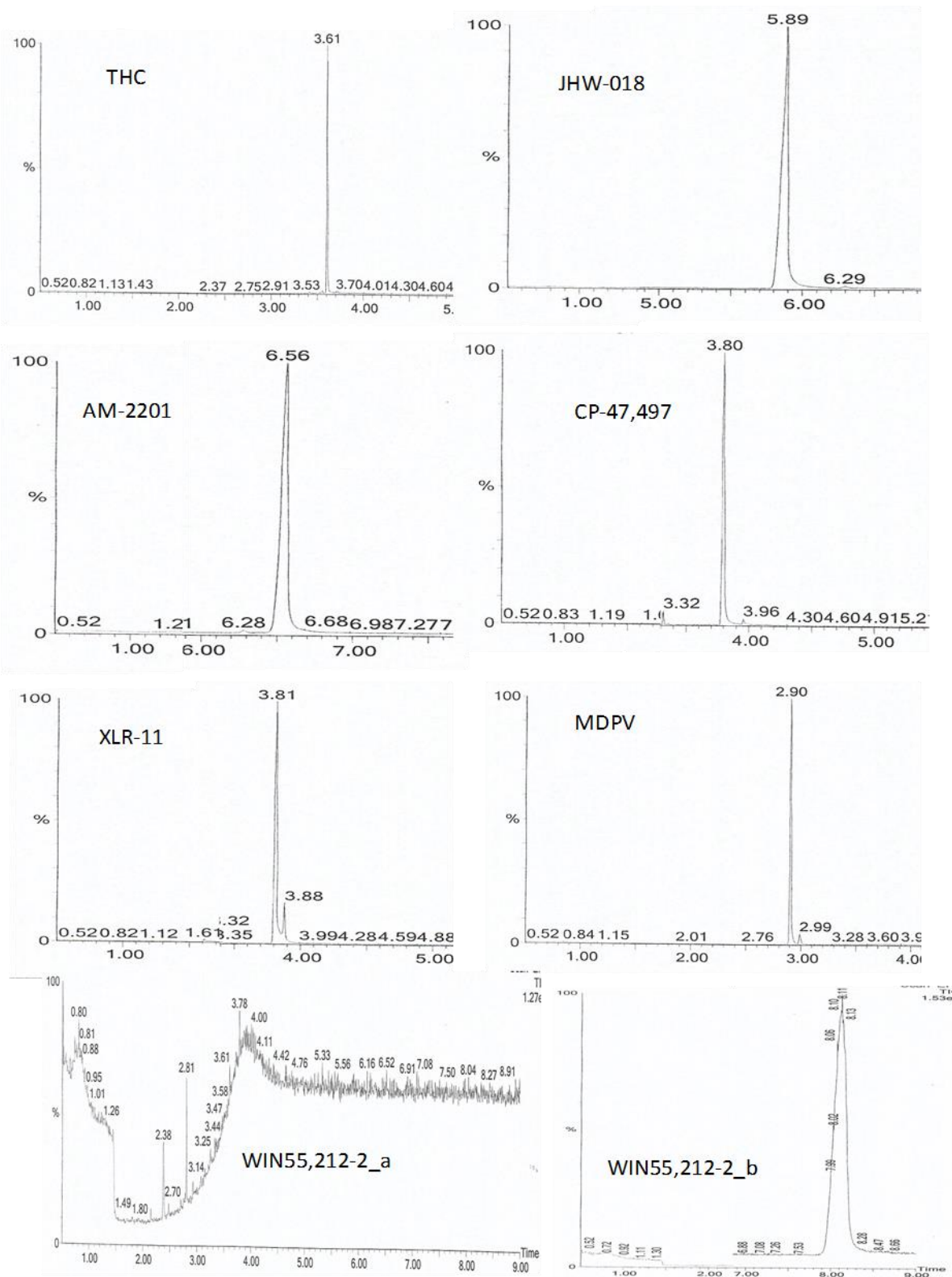


Figure 6-3. Chromatograms using method 2 described in Table 6-2.

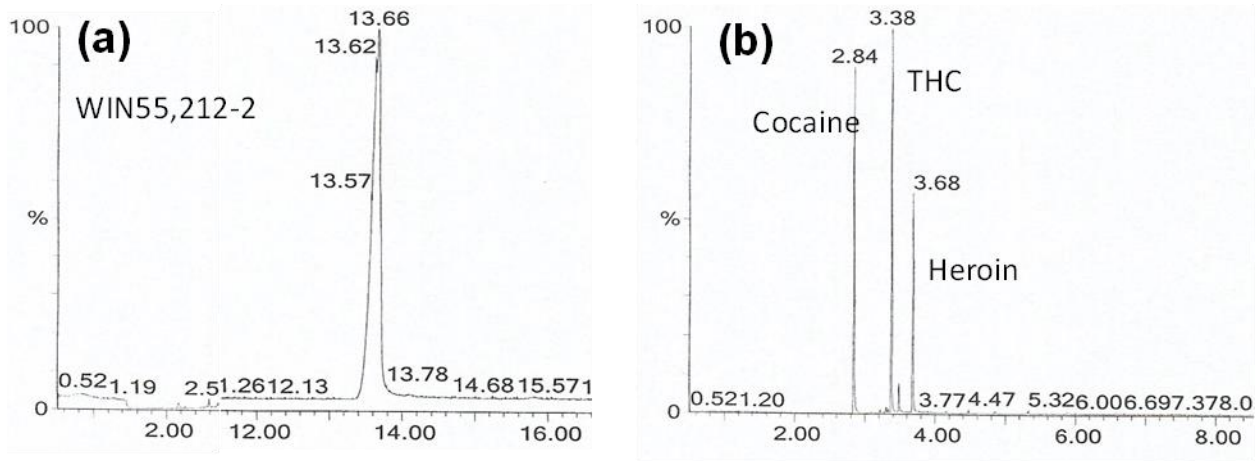


Figure 6-4. Chromatograms using method 3.

6.3.2 Vegetal samples analyses using GC-MS

Herbal blends containing psychoactive material, seized from the black market by the Police Department were analyzed using GC-MS methods. Real-world sample extracts were obtained using the procedures described in sample preparation section. Extracts were analyzed with methods presented in Table 6-2. Two samples of vegetal origin containing SCs were tested. Sample # 1 was analyzed using analytical methods 1, 2, and 3. Sample # 2 was analyzed using method 3 only. Figure 6-7 shows the GC-MS analysis from Sample # 1 using two organic solvents for the extraction, analyzed with analytical method 1. Figure 6-7a show chromatogram for acetone extract and Figure 6-7b show chromatogram for dichloromethane extract. Both samples were sonicated for 30 min. The mass spectra of each chromatographic peak in both samples (# 1 and # 2) were searched in the instrument-MS library in order to find substances of abuse such as SCs. When chromatographic peaks of acetone extract were explored (in MS library) a CS was detected in R_t equal to 8.04 min (see Figure 6-7a), according to mass spectrum from

library this CS corresponding to PB-22 (1-pentyl-8-quinolinyl ester-1H-indole-3-carboxylic acid). Comparing R_t of PB-22 with R_t of the standards using analytical method 1, we can infer that the structure of PB-22 should be similar to JWH-018 ($R_t = 7.56$) and MA-2201 ($R_t = 8.39$), PB-22 chemical structure is show in Table 6-1. Mass spectrum of PB-22 from vegetal sample-acetone extract compared with that from MS library is shown in Figure 6-7c. in the GC-MS analysis for dichloromethane extract, SCs no were detected (see Figure 6-7b), this suggest that the selection of a organic solvent adequate play a role important in the extraction process.

Figure 6-8 shows the GC-MS analysis from sample # 1 using acetone-organic solvents for the extraction with sonicated by 30-60min, and analyzed with analytical method 2. Figure 6-8a show chromatogram for acetone extract in which PB-22 with R_t equal to 6.98 min was detected and confirmed by MS library. It is expected the decrease of R_t for PB-22, and are in agreement with the results obtained when drug abuse standards are analyzed with the analytical method 2 compared to method 1. Mass spectrum of PB-22 from vegetal sample-acetone extract compared with that from MS library is shown in Figure 6-8b.

Figure 6-9 shows the GC chromatograms for Samples # 1 and # 2 analyzed with method 3, using two organic solvents for the extraction: methanol and acetone. Figure 6-9a shows the chromatogram for methanol extraction and Figure 6-9b shows the corresponding chromatogram for acetone extraction of Sample # 1. Figure 6-9c shows chromatogram for methanol extract and Figure 6-9d shows chromatogram for acetone extract of Sample # 2. All extracts were sonicated for 1 min.

The mass spectra of each chromatographic peak in the four chromatograms of Figure 6-9 were searched in the instrument-MS library in order to find substances of abuse like SCs. Two SCs were detected when chromatographic peaks were explored (in MS library). Peaks at $R_t = 6.32$ min were present in four chromatograms (see Figure 6-9), according to mass spectrum from library this CS corresponds to PB-22. The second SC was present in Sample #2 only. Peak at $R_t = 7.15$ min was present in Figure 6-9c and 9.D, according to mass spectrum from MS library corresponding to 5F-PB-22. 5F-PB-22 chemical structure is shown in Table 6-1. 5F-PB-22 and PB-22 mass spectra from vegetal sample extracts compared with that from MS library are shown in Figures 6-10a and 6-10b, respectively. It is important to note that methanol was used as solvent of extraction initially at IFS-PR lab using analytical method 1 with manual stirring (i.e. sonication was not carried out) and SCs were not detected. Thus it is suggested that the process of sonication plays an role important in the extraction process of SCs present in vegetal blends.

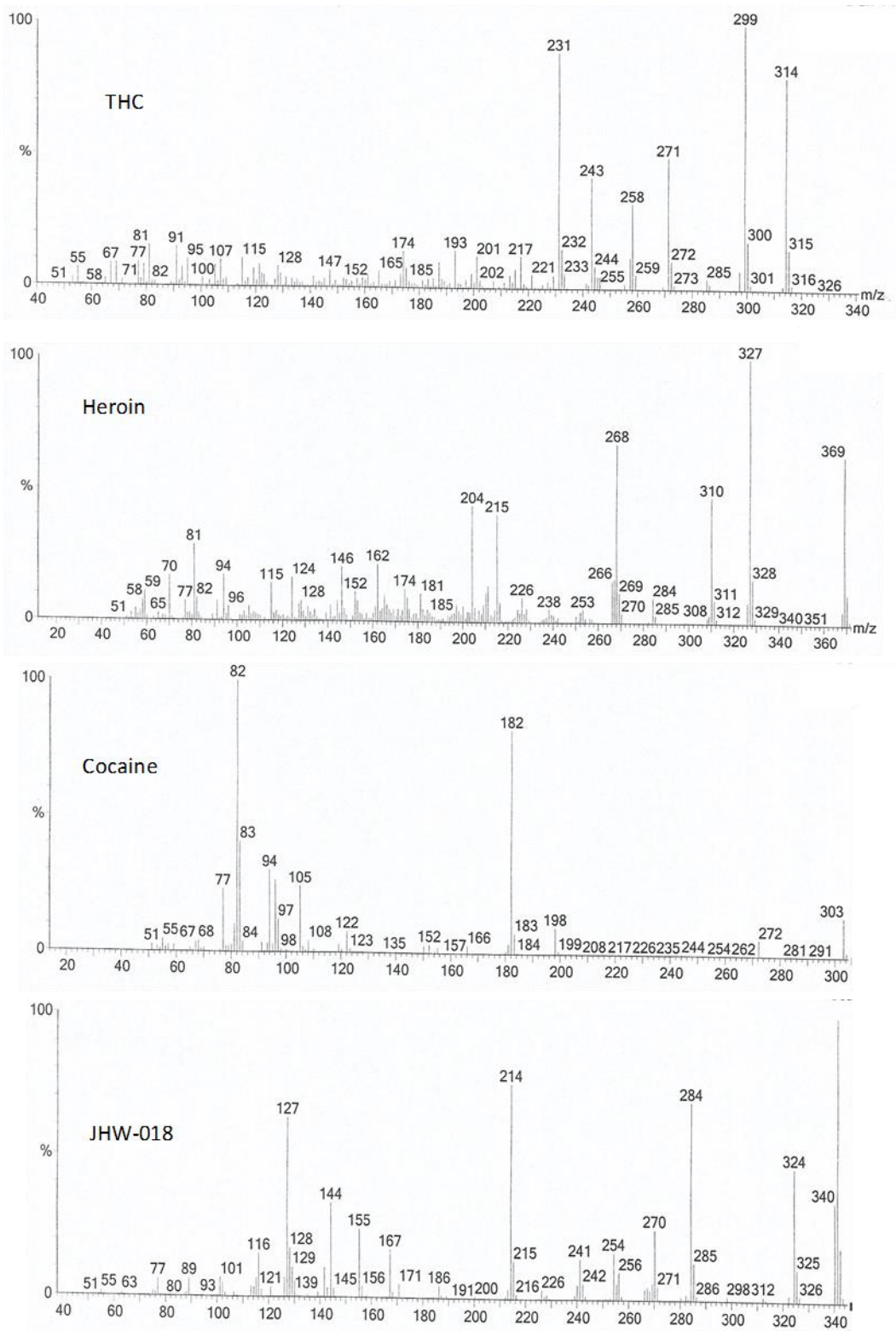


Figure 6-5. Mass spectra of THC, heroin, cocaine, and JHW-018 standards using method 1.

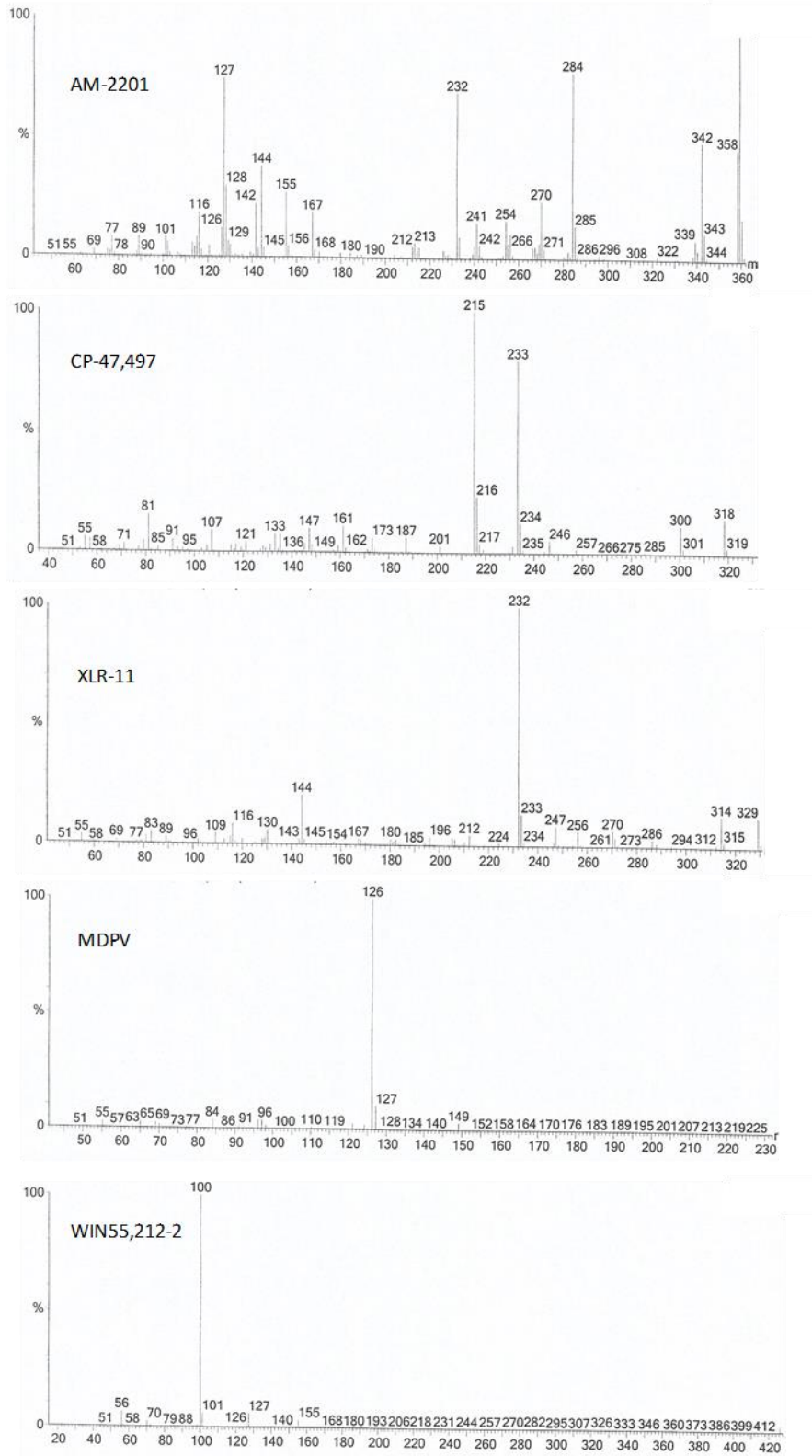


Figure 6-6. Mass Spectra of AM-2201, CP-47,797, XLR-11, MDPV and WIN55,212-2 standards using method 1..

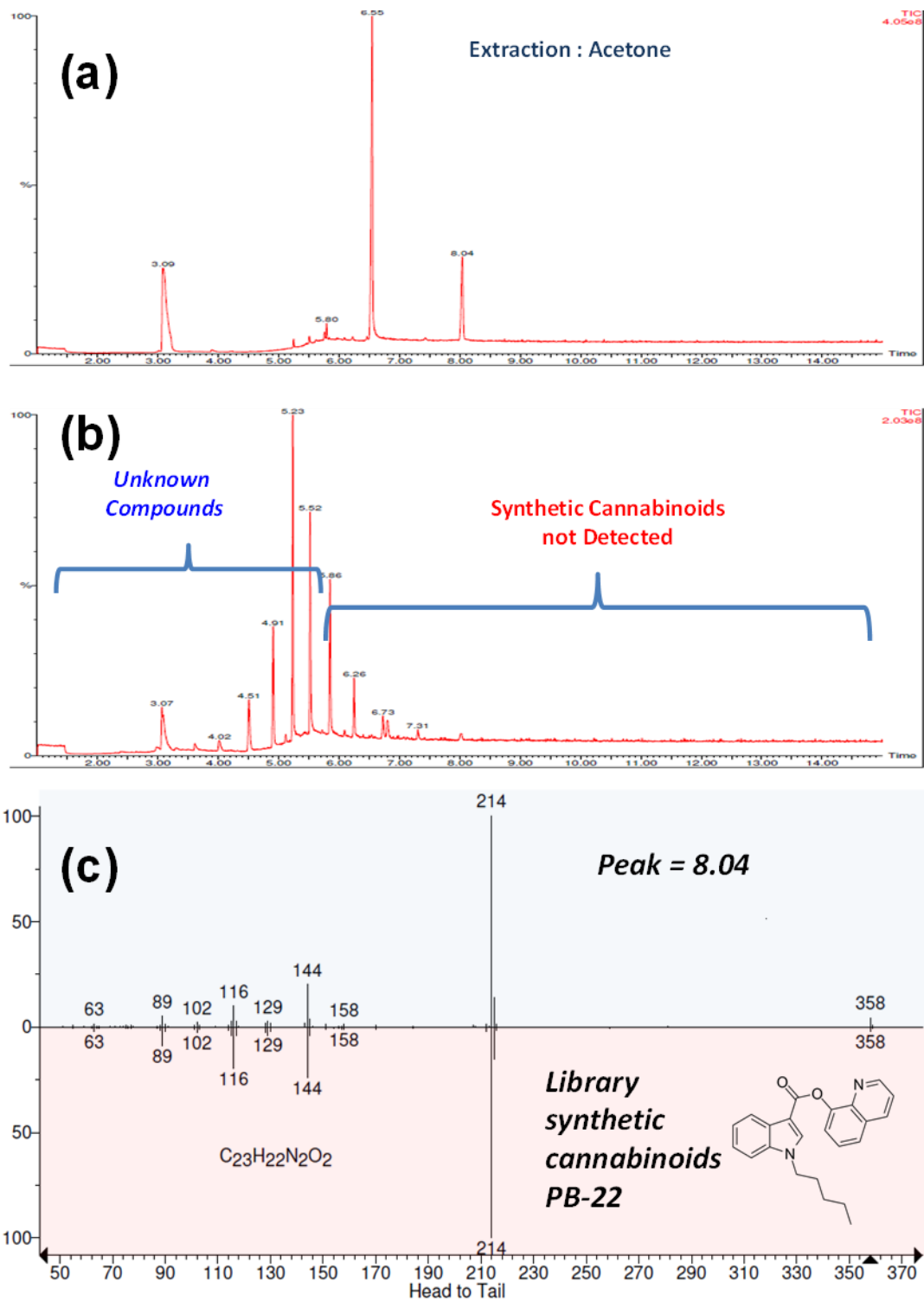


Figure 6-7. MS spectra and GC chromatograms from extract of Sample #1 using method 1. (a) Chromatogram of acetone extract; (b) chromatogram of dichloromethane extract; (c) mass spectrum of peak with $R_t = 8.04$ min.

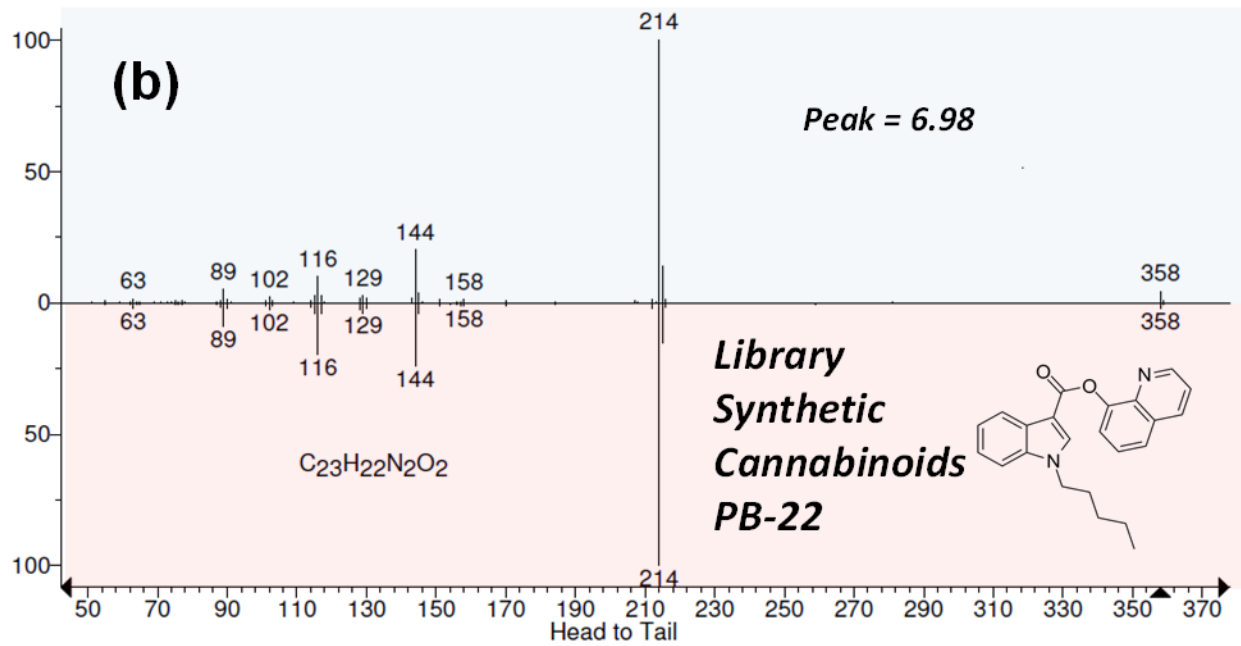
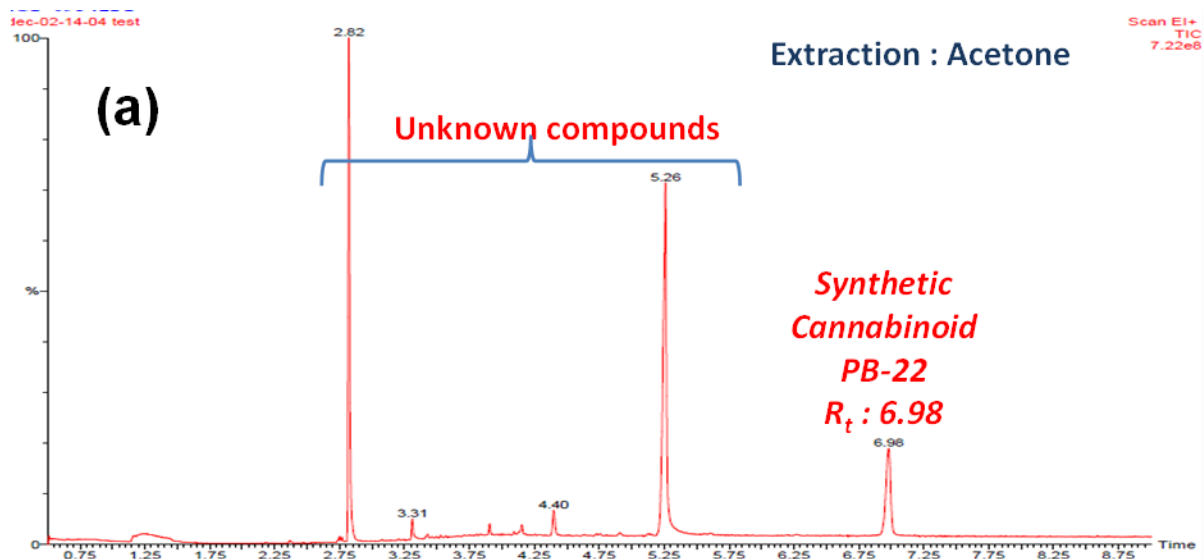
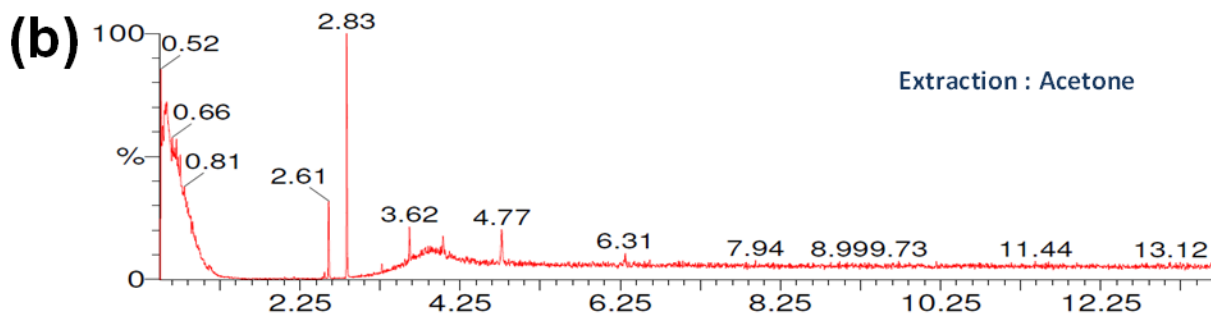
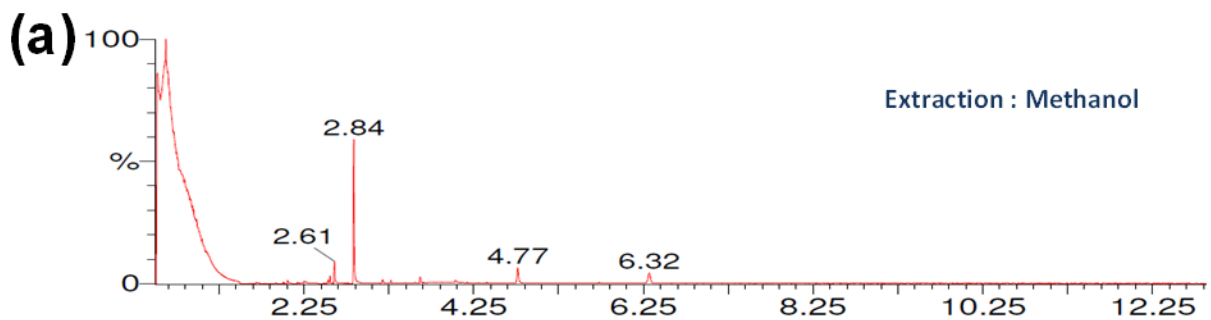


Figure 6-8. MS spectrum and GC Chromatograms from extract of sample #1 method 2. a) Chromatogram of acetone extract; (b) mass spectrum of peak with $R_t = 6.98$ min.

Sample 1



Sample 2

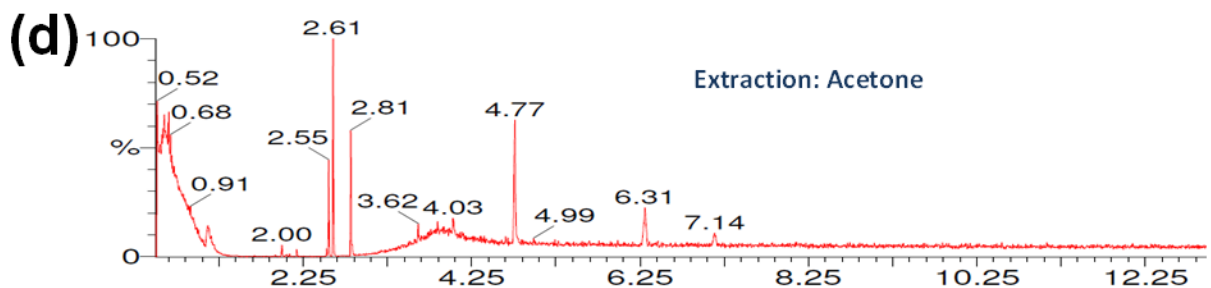
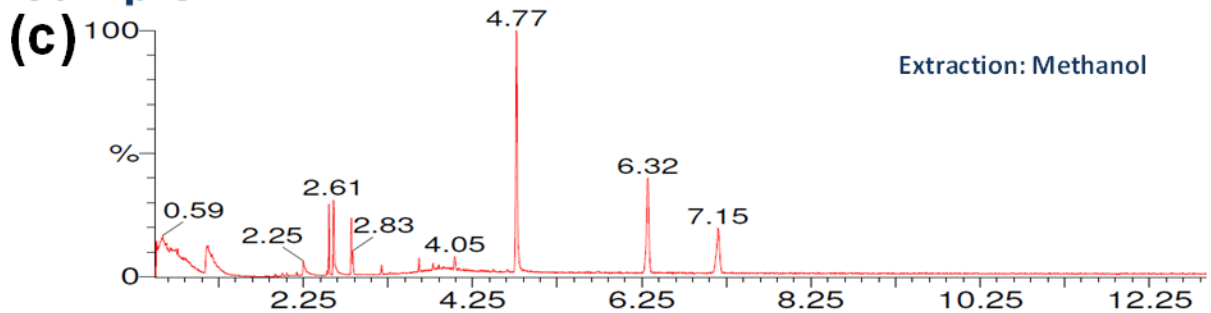


Figure 6-9. GC Chromatograms from extract of Samples 1 and 2 using method 3. Sample # 1: (a) methanol extract; (b) acetone extract. Sample # 2: (c) methanol extract; (d) acetone extract.

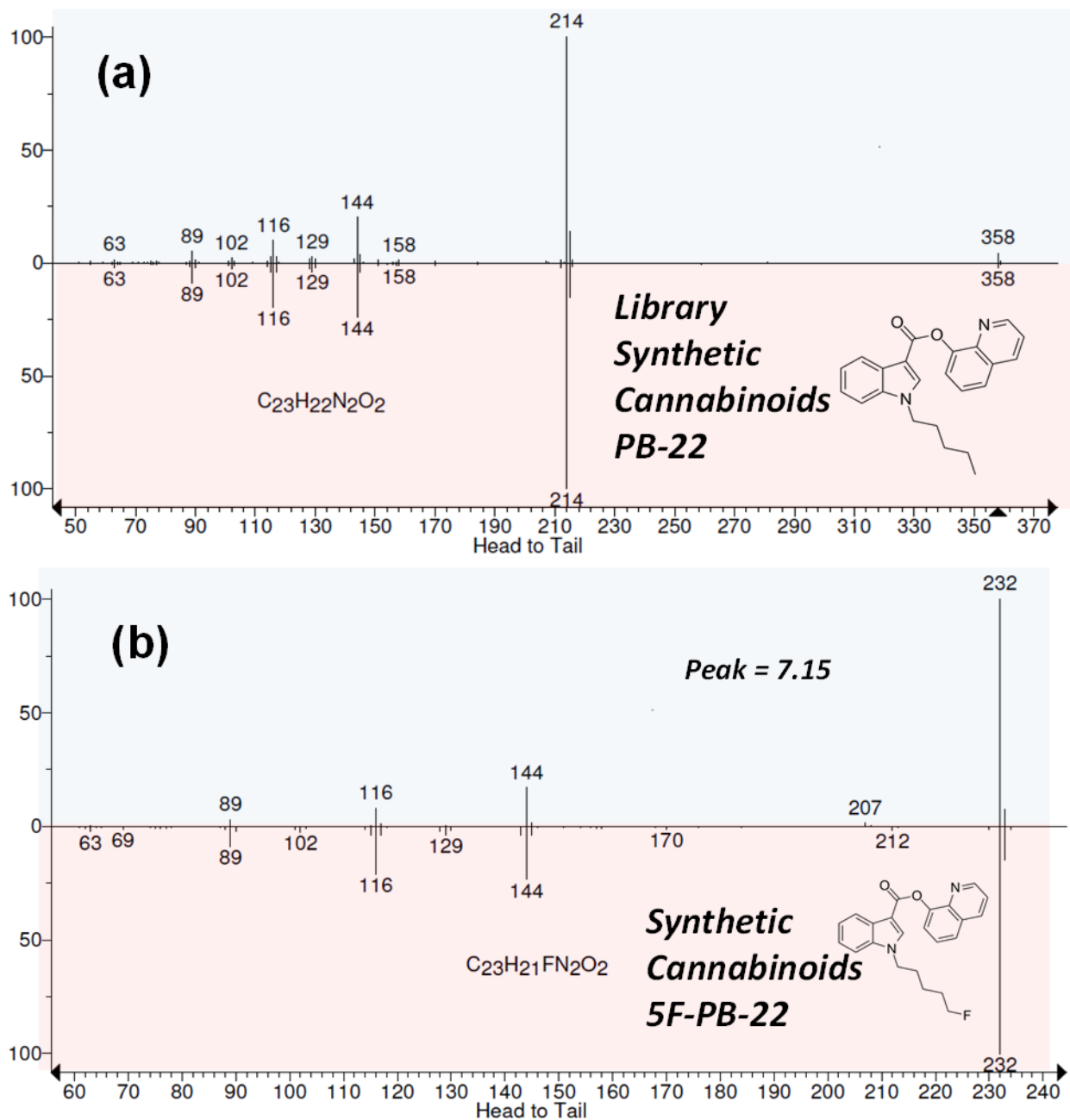


Figure 6-10. MS spectrum of SCs present in extracts of Samples 1 and 2 using analytical method 3. (a) Mass spectrum of characteristic peak with $R_t = 6.32$ min shown in Figures 6-9a to 6-9d; (b) Mass spectrum of characteristic peak with $R_t = 7.15$ min shown in Figure 6-9c to 6-9d.

6.4 CONCLUSIONS

GC-MS analytical methods for separation and detection of abuse drugs were developed. Three analytical methods were tested. However, GC-MS analytical method 3, proved to be the most appropriate to analyze the abuse drug standards available on this project, which were SCs like JWH-018, AM-2201, CP-47,497, WIN 55,212-2 and XLR-1, other standards include THC, Cocaine and Heroin. Using GC-MS method 3, lowest Rt was 2.84 min corresponding to cocaine and highest Rt was 13.66 min corresponding to WIN55, 212-2. Regarding the analysis of real-world samples, the following generalizations can be highlighted:

1. Real samples analyzed could have a co-eluting SC mixtures according to NIST and Cayman libraries.
2. These samples could contain co-elution of JWH-200, JWH-203, JWH-300, PB-22 and 5F-PB-22.
3. These samples could contain cocaine traces that can be confirmed by extraction of more samples.
4. At least four different SC and internal standard should be acquired to be validated with the GC/MS method developed.
5. Sample preparation process plays an important role in synthetic cannabinoid extraction for accurate detection.
 - Sonication process is necessary
 - Different organic solvent should be tested, according to herbal material
 - These recommendations shall be included in the analysis procedures to allow accurate detection of different drugs.

6. The developed GC/MS methods will assist the FSI-PR to pursue their mission as described in the organic agency law, tempering the analysis to account for new tendencies in drug abuse market.

6.5 FUTURE WORK

- Analyze standards of JWH-200, JWH-203, JWH-300, PB-22 and 5F-PB-22, with internal standard as SWGDRUG guides indicate.
- Re-analyze samples extracts with Cannabinoids standards to confirm their identities, as identified by NIST and Cayman library.
- Perform a publication of these findings in a scientific journal.

6.6 REFERENCES

- [1]. T. Marnell, *Drug identification bible*. 2011. Amera-Chem.
- [2]. Recommended methods for the Identification and Analysis of Synthetic Cannabinoid Receptor Agonists in Seized Materials - ST/NAR/48 by UNODC, 2014. http://www.unodc.org/documents/scientific/STNAR48_Synthetic_Cannabinoids_ENG.pdf, accessed on October 1, 2015.
- [3]. National Institute on Drug Abuse. Is Marijuana Medicine? Retrieved from <http://www.drugabuse.gov/publications/drugfacts/marijuana-medicine>, accessed on September 17, 2015.
- [4]. T. Tellioglu and F. Celebi, *Synthetic Marijuana: A Recent Turmoil in Substance Abuse*. *Bulletin of Clinical Psychopharmacology*, 2014. **24**(4): p. 396-404.

- [5]. B. K. Logan, L. E. Reinhold, A. Xu and F. X. Diamond, *Identification of synthetic cannabinoids in herbal incense blends in the United States*. Journal of forensic sciences, 2012. **57**(5): p. 1168-1180.
- [6]. De. B. Nik, K. Deventer, V. Stove, P. Van Eenoo, *Synthetic cannabinoids: general considerations*. Proceedings of the Belgian Royal Academies of Medicine, 2013. **2**: p. 209-225.
- [7]. S. Hudson, J. Ramsey, *The emergence, and analysis of synthetic cannabinoids*. Drug Testing and Analysis, 2011. **3**(7-8): p. 466-478.
- [8]. UNODC, Synthetic cannabinoids in herbal products. http://www.unodc.org/documents/scientific/Synthetic_Cannabinoids.pdf; accessed on October 7, 2015.
- [9]. J. Cohen, S. Morrison, J. Greenberg and M. Saidinejad, *Clinical presentation of intoxication due to synthetic cannabinoids*. Pediatrics, 2012. **129**(4): p. e1064-e1067.
- [10]. J. Ogata, N. Uchiyama, R. Kikura-Hanajiri and Y. Goda, *DNA sequence analyses of blended herbal products including synthetic cannabinoids as designer drugs*. Forensic science international, 2013. **227**(1): p. 33-41.
- [11]. Understanding the 'Spice' phenomenon: European Monitoring Centre for Drugs and Drug Addiction (EMCDDA); 2012. Available from: http://www.emcdda.europa.eu/attachements.cfm/att_80086_EN_Spice%20Themat ic%20paper%20—%20final%20version.pdf; accessed on October 1, 2015.

- [12]. N. Uchiyama, R. Kikura-Hanajiri, J. Ogata and Y. Goda, *Chemical analysis of synthetic cannabinoids as designer drugs in herbal products*. Forensic Science International, 2010. **198**(1): p. 31–38
- [13]. T. Veress and J. Nagy, *Fast and simple procedure for preliminary investigation of synthetic cannabinoids in plant matrix using infrared attenuated total reflectance spectroscopy*. European Journal of Forensic Sciences, 2015. **2**(1): p. 21-25.
- [14]. Act 154-2012. Government of Puerto Rico, United States. August 4, 2012.